Titre: Title:	Performance Evaluation of Cyclist's Position Using a Depth Camera-Based Motion Capture System
Auteur: Author:	Mojtaba Ghasemi
Date:	2021
Type:	Mémoire ou thèse / Dissertation or Thesis
Référence: Citation:	Ghasemi, M. (2021). Performance Evaluation of Cyclist's Position Using a Depth Camera-Based Motion Capture System [Thèse de doctorat, Polytechnique Montréal]. PolyPublie. https://publications.polymtl.ca/5605/

POLYTECHNIQUE MONTRÉAL
affiliée à l'Université de Montréal

Performance Evaluation of Cyclist's Position Using a Depth Camera-Based Motion Capture System

MOJTABA GHASEMI
Institut de génie biomédical

Thèse présentée en vue de l'obtention du diplôme de *Philosophiæ Doctor*

Génie biomédical

Février 2021

POLYTECHNIQUE MONTRÉAL
affiliée à l'Université de Montréal

Cette thèse intitulée :

Performance Evaluation of Cyclist's Position Using a Depth Camera-Based Motion Capture System

présentée par **Mojtaba GHASEMI**
en vue de l'obtention du diplôme de *Philosophiæ Doctor*
a été dûment acceptée par le jury d'examen constitué de :

Maxime RAISON, président
Delphine PÉRIÉ-CURNIER, membre et directrice de recherche
Daniel CURNIER, membre et codirecteur de recherche
Jean-Yves TRÉPANIER, membre et codirecteur de recherche
Philippe DIXON, membre
Nicola HAGEMEISTER, membre externe

DEDICATION

To my parents,
who have been my source of inspiration and strength,
for always loving and supporting me.

ACKNOWLEDGEMENTS

I would like to express my gratitude to my supervisors, Prof. Delphine Périé-Curnier, Prof. Daniel Curnier and Prof. Jean-Yves Trépanier, for their enthusiasm, continuous support and effort they exerted on this project.

I would like to thank Prof. Benjamin Pageaux, who helped me with the equipment and provided feedback on my research. I would also like to express my sincere thanks to Maxime Caru for his help during data collection and data analysis. Thanks to all of the participants who participated in the studies.

I thank with all my heart my loving parents, for all the enormous support and encouragement they have provided me not only during my PhD but throughout my life. Also, I would like to extend my most profound appreciation to my sister for providing me with motivation and guidance toward my schooling, and at the same time, pushing me to reach my goals. And finally, my girlfriend, for supporting and helping me through the difficult moments and all the challenges I faced.

RÉSUMÉ

L'optimisation de la posture d'un cycliste peut améliorer les performances et réduire la traînée aérodynamique. Les cyclistes visent à améliorer leurs performances en réduisant le temps et l'effort que leur demande la course cycliste. Toute modification de la position du cycliste pour améliorer la performance globale exige une compréhension fondamentale de ses caractéristiques, notamment aérodynamiques, physiologiques et biomécaniques, ce qui constitue la principale préoccupation de la recherche sur le cyclisme. Les méthodes actuelles font appel à des techniques coûteuses et compliquées, d'où la nécessité d'une approche fonctionnelle et abordable qui tienne compte de tous les paramètres concernés. Cette recherche vise à développer une application fonctionnelle permettant d'évaluer l'effet de la position et du guidon sur l'aérodynamique et les performances d'un cycliste.

La première partie de cette thèse porte sur le développement et la validation d'un ensemble d'outils paramétrés permettant de modéliser un mannequin numérique 3D représentant un cycliste professionnel à l'aide d'un système de capture de mouvement sans marqueur. De plus, la méthodologie développée a été appliquée pour analyser numériquement la traînée aérodynamique de différentes positions statiques de cyclisme en utilisant la dynamique des fluides numérique (CFD). Les résultats montrent que le système sans marqueur convient parfaitement à la modélisation et à l'étude de la dynamique des fluides numérique. Le cadre de modélisation paramétré combiné à la CFD s'avère un outil précieux pour évaluer avec précision la traînée associée aux différentes positions du cycliste.

La deuxième partie de cette thèse examine les effets de la modification de la position du guidon aérodynamique sur le schéma d'activation musculaire des extrémités inférieures et sur les variables cinématiques, attendu que tout ajustement de la position de cyclisme induit un changement dans la relation entre la posture du corps et la géométrie de la bicyclette, affectant la performance physique. L'électromyographie de surface et la cinématique articulaire du membre inférieur droit pendant le pédalage sur ergomètre ont été mesurées pour les cyclistes et triathlètes de compétition. Les expériences portent sur différentes positions du cycliste au cours d'épreuves contre-la-montre, dans le but de déterminer l'effet de la modification de la position de l'aéro-guidon lors de six exercices à charge constante sous-maximale. L'abaissement de la hauteur du guidon aérodynamique a révélé une amélioration des performances cyclistes grâce à la contribution plus importante de l'extenseur de la hanche et de l'angle d'extension de la hanche.

La méthodologie développée permet d'étudier les réponses physiologiques du cycliste et

d'effectuer une analyse aérodynamique détaillée lors de la modification de la position du guidon en contexte d'épreuves contre-la-montre, compte tenu de la contribution du cycliste à l'essentiel de la force de traînée du système cycliste-vélo. Les résultats suggèrent que par rapport à la position préférée lors du contre-la-montre, la zone frontale, le coefficient de traînée et la zone de traînée ont été réduits lors de l'abaissement de la position du guidon alors que toutes les variables physiologiques sont restées inchangées.

Cette thèse présente une approche unique permettant d'étudier la contribution des modifications d'ajustement du guidon sur les performances aérodynamiques et biomécaniques du vélo. Ce système de capture du mouvement sans marqueur, peu coûteux, conçu pour mesurer et analyser la cinématique du vélo, peut fournir des données fiables et applicables à une analyse aérodynamique et biomécanique plus poussée.

ABSTRACT

Optimizing the posture of a cyclist can ameliorate performance and reduce the aerodynamic drag. Cyclists aim to enhance performance decreasing the time and effort during the cycling race. Any modification of the cycling position to improve the overall performance demands a fundamental understanding of its characteristics, including aerodynamics, physiological and biomechanical features, which is the primary concern of cycling research. Current methods require costly and complicated techniques, and therefore, the necessity of a functional and affordable approach that considers all the involved parameters is apparent. This research aims to develop a feasible application for evaluating the effect of cycling position and aero handlebar on the aerodynamics and performance of a cyclist.

The first part of this thesis focuses on developing and validating a set of parameterized tools to model a 3D digital manikin of professional cyclists using a markerless motion capture system. Furthermore, the developed methodology has applied to numerically analyze the aerodynamic drag of different static cycling positions using computational fluid dynamics (CFD). Results show that the markerless system is fully capable of modeling and providing the requirement of CFD investigation. The parameterized modeling framework combined with CFD is found to be a valuable tool to accurately evaluate the drag of different cyclist positions.

The second part of this thesis explores changing the aero handlebar position on the lower extremities' muscle activation pattern and kinematic variables since any adjustment in the cycling position induces a change in the relation between body posture and bicycle geometry, affecting physical performance. The surface electromyography and joint-level kinematics of the right lower limb during cycling on an ergometer were measured for competitive road cyclists and triathletes. The experiments cover different time trial positions of the cyclist intending to determine the effect of alteration of aero handlebar position in six submaximal constant load exercises. Lowering the aero handlebar height showed improved cycling performance due to the more significant hip extensor contribution and extended hip angle.

The developed methodology is applied to investigate the cyclist's physiological responses and detailed aerodynamic analysis when altering the time trial handlebar position, considering the rider contributes most of the rider-bicycle system's drag force. Findings suggest that compared to the preferred time trial position, the frontal area, drag coefficient and drag area were reduced when lowering the handlebar position while all the physiological variables remained unchanged.

This thesis presents a unique approach to investigate the contribution of handlebar alterations on cycling aerodynamics and biomechanical performance. This low-cost markerless motion capture system for measuring and analyzing cycling kinematics can provide reliable and applicable data for further aerodynamics and biomechanical analysis.

TABLE OF CONTENTS

LIST OF TABLES

LIST OF FIGURES

LIST OF SYMBOLS AND ACRONYMS

A	Area
AC_D	Drag Area
BDC	Bottom Dead Center
BF	Biceps Femoris
BSP	Body Segment Parameters
C_D	Drag Coefficient
C_p	Pressure Coefficient
CAD	Computer-Aided Design
CFD	Computational Fluid Dynamics
CPET	Cardiopulmonary Exercise Test
DP	Dropped Position
DXA	Dual-energy X-ray Absorptiometry
EMG	Electromyography
FAPS	Fringe Acquisition and Processing Software
F_D	Drag Force
F_s	Safety Factor
FTAP	Flat Torso Angle Position
GCI	Grid Convergence Index
GET	Gas Exchange Threshold
GL	Gastrocnemius Lateralis
GM	Gastrocnemius Medialis
GMAX	Gluteus Maximus
HR	Heart Rate
iEMG	Integrated Electromyography
IMVC	Isometric Maximum Voluntary Contraction
$k-\omega$	k-omega Turbulence Model
LES	Large Eddy Simulation
MET	Metabolic Equivalent of Task
MPH	Mile per Second
MRI	Magnetic Resonance Imaging
MVC	Maximum Voluntary Contraction
p	Order of Accuracy
PPO	Peak Power Output

r	Grid Refinement Ratio
RANS	Reynolds-Averaged Navier-Stokes
RER	Rated Perceived Exertion
RF	Rectus Femoris
RMS	Root Mean Square
RMSE	Root Mean Square Error
ROM	Range of Motion
SDK	Software Development Toolkit
SENIM	Surface EMG for Non-Invasive Assessment of Muscles
SIMPLE	Semi Implicit Method for Pressure Linked Equations
SM	Semimembranosus
SST	Shear Stress Transport
ST	Semitendinosus
TA	Tibialis Anterior
TDC	Top Dead Center
TTP	Time Trial Position
U	Velocity
UP	Upright Position
VCO_2	CO_2 Consumption
VE	Minute Ventilation of Breathing
VL	Vatsus Lateralis
VM	Vatsus Medialis
VO_{2peak}	Maximal Oxygen Consumption
VT	Tidal Volume
ε	Relative Error
ρ	Air Density
3D	Three Dimensional

CHAPTER 1 INTRODUCTION

1.1 Motivation

Recent years have witnessed a remarkable expansion in the knowledge and application of biomedical and biomechanical concepts to cycling. Cycling is continuously pushing the bounds of new technology and researching every feasible method to increase speed, efficiency and performance. Therefore, new findings often prove to be invaluable to enhance cycling performance. For improvement of cycling performance, different aspects including the type of bicycle, the cyclist's training method and cycling techniques have changed substantially, to accommodate different uses such as commuting or racing. In order to provide resources for the potential improvements in the performance of cyclists, an assessment of various characteristics is critical (Coyle et al., 1991). Investigating the effects of each of these factors can shed light on the interaction of different involved variables and can be used as a valuable adjunct in predicting performance and quantifying other unknown or unmeasurable characteristics of the performance.

Chief among those parameters is aerodynamic analysis. It is well-known that approximately 90% of total resistance forces in cycling at speeds greater than 54 km/h (34 mph) influencing cycling performances is aerodynamic resistance (Belluye & Cid, 2001; Debraux et al., 2011; Defraeye, Blocken, Koninckx, Hespel, & Carmeliet, 2010a; Lukes et al., 2004; J. C. Martin et al., 2006), which is called aerodynamic drag. Researchers, coaches and cyclists have recognized the significance of decreasing aerodynamic drag in cycling for many years (Barry et al., 2015b; Blocken et al., 2013; Lukes et al., 2005). The accurate understanding of cycling aerodynamics, as well as the use of this understanding in the reduction of aerodynamic drag, could be adopted to maximize the cyclist's ability. Concerning the effects of aerodynamic drag, cycling race jersey (Chowdhury et al., 2010; Oggiano et al., 2009), bicycle design and shape including the wheels' (mainly the front wheels) aerodynamic resistance, bicycle frame and other components (Dal Monte et al., 1987), cyclist's helmet (M. Abdullah et al., 2017; Alam et al., 2014; Brownlie et al., 2010; Mustary et al., 2014) and cyclist's riding position (Defraeye, Blocken, Koninckx, Hespel, & Carmeliet, 2010a; Garcia-Lopez et al., 2008; Grappe et al., 1997; Jeukendrup & Martin, 2001; Jobson et al., 2008; Oggiano et al., 2009) have been investigated. The cyclist's riding position has been vastly investigated, and wind-tunnel based studies reveal that the majority of aerodynamic drag is due to rider and rider's posture (Alam et al., 2014; Chowdhury et al., 2010; C. Kyle & Weaver, 2004). Adjustments of cyclist postures are frequently used to enhance the position-related aerodynamics and, therefore,

the performance of professional cyclists (Barry et al., 2015b). Consequently, developing a conceivable, low-cost and efficient framework for evaluating and decreasing aerodynamic drag of different cyclist positions is crucial. Any attempt to discuss the aerodynamic analysis in the matter of assessing cycling performance should obtain affordable, reliable and repeatable high-resolution data.

To reduce aerodynamic drag, professional cyclists adopt different positions using different handlebar extensions (Oggiano et al., 2008). The alternation of posture results in changes in the sagittal torso angle (Chabroux et al., 2012; Oggiano et al., 2008), which is defined as the angle between the torso and the ground. García-López et al. (2008) showed that decreasing the torso angle position can drop the aerodynamic drag. Although reducing the torso angle decreases the aerodynamic drag effectively, it negatively affects the peak power output (PPO) (Jobson et al., 2008). This effect may be related to the fact that the cyclist's muscles are not working in their optimal range. In addition, studies have reported more significant muscular fatigue caused by the increased pressure on shoulder girdle, neck and arms, and increased value of activation of hip muscles (Gnehm et al., 1997; Grappe et al., 1997; Jobson et al., 2008). Therefore, previous investigations have emphasized the need to incorporate electromyography (EMG) of muscle activation in the cycling performance evaluation during posture adjustments (Amarantini & Martin, 2004). However, the relationship between EMG parameters and changes in the cyclist position during cycling is less clear (Davidson et al., 2016).

Determining how individual muscles contribute to observed motions is difficult because a muscle can accelerate joints that it does not span and body segments to which it does not attach (Seth et al., 2011). Hence, a detailed evaluation of kinematics of lower extremities, which influences the performance, must be examined during the cyclist position manipulations. Although various attempts have been made to measure kinematic parameters, synthesizing a detailed description of the elements of the kinematics of a cyclist while recording his movements in different positions are inconclusive. Furthermore, due to the very slight possibility of feasible and affordable measurements of aerodynamics, muscle activity and kinematics simultaneously, muscle pattern and kinematics evaluation of different cyclist position remains a major challenge.

1.2 Objectives of research

A thorough investigation into the interaction of aerodynamic and biomechanic parameters is needed for achieving a comprehensive understanding of cycling performance in different

cyclist positions. However, a significant difficulty associated with this evaluation is related to the availability, affordability and accuracy of the approach for this procedure. More particularly, the general research questions of this doctoral project are "*How to develop a more applicable and affordable method for the evaluation of performance analysis of cyclist position?*" and "*What are the outputs of the core muscles activities, joint level kinematics and aerodynamic analysis of the investigated cycling positions?*"

Answering these questions will enlighten the effect of various features on the performance while pedaling in different positions. In this context, we will need to establish a set of tools for data acquisition, simulation and data analysis. Consequently, the specific objectives and hypotheses underlying this project are:

1. Propose and validate a system for modeling cyclists in different positions. The assumption is that applying this method would ease the process of modeling and aerodynamic analysis by addressing the variability of changes in cycling positions.

2. Evaluate the muscle activation patterns of lower limb and joint kinematics of numerous positions. Thus, it is hypothesized that different positions will have distinct influences.

3. Develop and present an aerodynamic analysis of investigated cycling positions and compare them, which is relevant to the overall effort of improving the performance.

In this work, we present an approach that examines the altered cycling positions while measuring kinematics, muscle activation and aerodynamics. Outcomes will develop the quantitative knowledge of the biomechanical and aerodynamic limits of the cyclist, and the relationships between these parameters.

1.3 Overview of thesis

Following this introductory chapter, chapter 2 will present a critical review of the literature on the reported studies of cycling performance and the main concepts necessary to understand the project. The next three chapters are devoted to the original contributions of this thesis and correspond to the three articles. The developed method for modeling cyclists is presented in chapter 3. The technical features and materials of this technique are described here, in the first article. Chapter 4 includes the second article, which describes in detail the protocol and procedure of each experiment carried out and evaluates the muscle activation patterns and kinematic results of investigated cyclist positions. Chapter 5, the third article, contains the aerodynamic analysis of each position. Finally, Chapter 6 proposes a critical discussion of

the results obtained with the methods developed during this doctoral project. To conclude, this chapter presents the limitations of this research, possible improvement and prospectives for future work.

CHAPTER 2 LITERATURE REVIEW

This chapter presents a critical review of the literature related to the different methods we applied in this project. Section 2.1 covers an overview of the processes and procedures for modeling the cyclist concerning the performance and aerodynamic analysis, and the involved technical approaches. Section 2.2 follows on investigating the various cyclist's positions and cause-effect relationships of biomechanical parameters, including muscle activities and kinematics of lower extremity that affect the performance of the cyclist. Finally, section 2.3 offers a brief review of aerodynamic drag calculations for the specific investigated cyclist's positions.

2.1 Aerodynamic performance of cycling

Different methods, including field tests, wind-tunnel measurements and computational or numerical modeling, can be used to assess aerodynamic drag under actual conditions or in the laboratory (Barber et al., 2009; Blocken, 2014; Blocken & Toparlar, 2015). However, measurements of the flow field are less straightforward and more time-consuming compared to drag measurements. The drag coefficient (C_D) of cyclist, which is used to describe the overall shape, position and flow conditions related to the cyclist, can be connected to aerodynamic drag force (F_D) and the frontal area of cyclist (A) (Davies, 1980):

$$F_D = \frac{1}{2}\rho A C_D U^2 \tag{2.1}$$

Where ρ is the air density (kg/m^3) and (U) is the displacement velocity of cyclist (m/s). The density of air can be affected by air humidity but this effect is small and can be neglected (P. E. Di Prampero, 2000).

In general, there are substantial differences between these methods of evaluation for a given position since the anthropometric data of cyclists and experiment setup affect the measurements. Although field tests (linear regression analysis models, deceleration methods and traction resistance measurement methods) could be more practical with the possibility of applying various equipment, the reliability, sensitivity and accuracy of these methods are debatable (Candau et al., 1999; Capelli et al., 1993; Garcia-Lopez et al., 2008). Moreover, it is challenging to conduct measurement for various cyclist's positions since cyclists should keep the exact position during multiple laps and different speeds.

As a result, full scale and scaled-down wind-tunnel testing would be an alternative for the field tests, which allow a unique opportunity for the cyclists to provide instant feedback for aerodynamic drag decline. Nevertheless, wind-tunnel measurements are costly (Rutberg, 2008). Setting up the new field tests and remeasuring the parameters involved are often time-consuming and quite complicated (Crouch et al., 2014; Zaidi et al., 2010). Moreover, this method has extensive limitations regarding the flow around the bicycle setup while pedaling (Candau et al., 1999) caused by the complex nature of cycling aerodynamics and technical expertise required. Usually, the spatial resolution is also too limited to represent the complex flow field around the cyclist in detail, such as the locations of boundary-layer separation.

In addition to empirical examinations, numerical modeling is a relatively recent method to investigating aerodynamics in sports sciences (Gardan et al., 2017). Computational fluid dynamics (CFD) is one such method. CFD has been deemed to be a powerful and effective tool for simulating the aerodynamic analysis and complex flow field in different sports disciplines, such as swimming (Bixler et al., 2007; Bixler & Riewald, 2002; Gardano & Dabnichki, 2006; Lecrivain et al., 2008; Rouboa et al., 2006), bobsleighing (Barber et al., 2009), ski jumping (Dabnichki & Avital, 2006; Meile et al., 2006) and cycling aerodynamic investigations (Blocken et al., 2013; Defraeye, Blocken, Koninckx, Hespel, & Carmeliet, 2010a, 2010b; Hanna et al., 2002; Lukes et al., 2004). Previous areas where numerical analysis has been used in the aerodynamics of cycling are: the heat transfer of individual body segments (Blocken et al., 2013), shape of cyclist's helmet (M. Abdullah et al., 2017; Alam et al., 2014; Sims & Jenkins, 2011), to study bicycle aerodynamics (Barry et al., 2015b; Lukes et al., 2005), and performance of cyclist's riding position (Defraeye, Blocken, Koninckx, Hespel, & Carmeliet, 2010a; Defraeye et al., 2014; Griffith et al., 2014).

CFD can provide more relevant information with high sensitivity on cyclist position components to gain more insight into aerodynamic drag optimization. Conducting CFD simulations would obtain high-resolution data of the flow field together with drag information on cyclist posture and its aerodynamics, also allowing for a separate quantification of form drag and skin-friction drag, and thus, CFD applications have been increasingly proposed and used in cycling performance studies. Defraeye et al. (2010a) showed that CFD calculations of the aerodynamic drag are in close agreement with the wind-tunnel measurements. They reported a 6% difference between CFD results and values of drag by wind-tunnel.

Various CFD models can be applied in cycling analysis, including Reynolds-averaged Navier-Stokes (RANS) and large eddy simulation (LES). Although LES is a highly accurate simulation technique and is superior in predicting the flow, it is computationally more expensive with higher complexity than RANS (Blocken, 2018). Therefore, RANS simulation is consid-

ered to be a common and reasonable approach for cycling aerodynamic investigations.

2.2 Body segment measurement

It is well recognized that the accuracy of kinematics and kinetics derived from human motion data is dependant on the efficiency of estimating accurate body segment parameter (BSP) data such as segment positions, segment center of mass location and segment moments of inertia from anatomical reference points. Likewise, an essential step for CFD calculations is precisely capturing the geometry and constructing a 3D digital manikin model of the cyclist. Various procedures have been applied to obtain the specific body characteristics, anthropometric data and joints' positions of the cyclist, namely, mathematical models (Jensen, 1978; Sprigings et al., 1987), using data based on cadavers (Clauser et al., 1969; Dempster, 1955; Dempster & Gaughran, 1967), dual-energy X-ray absorptiometry (DXA) (Durkin et al., 2002), magnetic resonance imaging (MRI) (P. E. Martin et al., 1989; Pearsall et al., 1994), gamma-ray scanning (Casper et al., 1971), marker-based methods (Zhang et al., 2004), laser scanners (Ma et al., 2011) and depth measuring devices (Espitia-Contreras et al., 2014). Using the 3D laser scanner for different applications of CFD is favorable (Boehnen & Flynn, 2005). There are several technologies available for the 3D scanning of the cyclist's body surface. However, generating a single, closed 3D scanning from many different angles or several linked scanners is indispensable due to the intensive movement sensitivity of scanners and the time taken to complete multiple separate scans. Thus, a low-cost, user-friendly and applicable method of acquiring total body and segmental volumes is needed.

One method of obtaining personalized estimates of body segment measurements is the elliptical zone method. This strategy applies a geometric modeling method of estimating body segment volumes in which diameters of series of ellipses of the body segments are acquired by digitizing two photographs captured from the sagittal and coronal plane views of the body (Figure 2.1). Previous studies found that applying the elliptical zone method can provide the volumes of various segments and the whole body accurately (Sanders et al., 1991; Wicke & Lopers, 2003). Application of the technique is restricted by the accessibility of digitizing the body surface outlines as well as distinguishing the anatomical reference points, lines and joint centers of each segment compatible with the digitizing device.

In the face of challenges mentioned above, the Kinect sensor (Kinect, Microsoft Corp., USA) provides an opportunity to reconstruct the cyclist's body geometry, as well as joint motion kinematics. Kinect is a markerless, depth-measuring device that captures depth and color images simultaneously at a frame rate of about 30 Hz. This device is entirely operational for

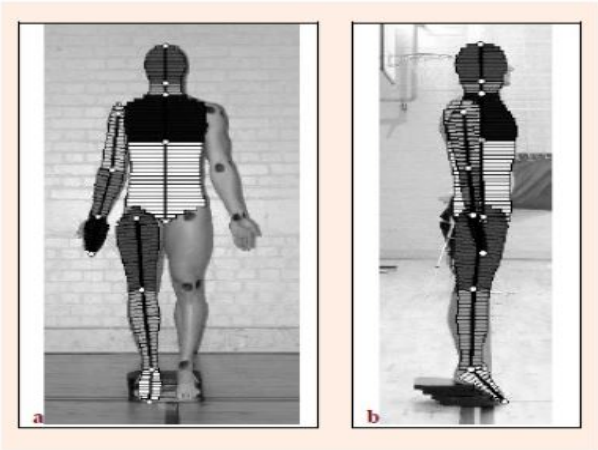

Figure 2.1 Illustration of body devided as ellipses: (Sanders et al., 2015): (a) coronal plane; (b) sagittal plane.

biomechanics and sports analysis (Berger et al., 2011; Chang et al., 2011; Fern'ndez-Baena et al., 2012). It could effectively scan the body surface to estimate body segment inertia parameters (Norton et al., 2002; Sheets et al., 2010), leading to an accurate estimation of the joint positions and anthropometry due to depth data captured and model the dynamics of action for motion analysis (Shotton et al., 2013; Ye et al., 2011). Despite marker-based methods, Kinect does not need a controlled and restricted environment, including lightening conditions and technical expertise, to obtain high-quality data (Bixler et al., 2007; Bixler & Riewald, 2002; Blocken & Toparlar, 2015; Defraeye et al., 2014; Garcia-Lopez et al., 2008). The advantage of using a Kinect sensor is that it allows 3D registration without a complicated setup of multiple cameras, without the need to attach markers to the subject, and can be purchased at a much lower cost than a traditional motion capture system. Figure 2.2 shows a comparison between the 3D scan of the torso segment obtained by a lser scanner and the Kinect-based scan.

Since Kinect is a recent development, limited information about the outcome quality and validity of raw measurement of its data capturing is available (Gabel et al., 2012; Galna et al., 2014; Taati et al., 2012). Clarkson et al. (Clarkson et al., 2013) conducted an applicable assessment of a four Kinect scanner system to scan and measure the circumference of a machined aluminum cylinder, representative of a large body segment. They validated the results by comparing them to the gold standard measurement, which showed ± 3.5 mm differences. Nevertheless, they concluded that Kinect could be used to scan and measure the human body for biomechanical applications. In another study that evaluated the reliability of

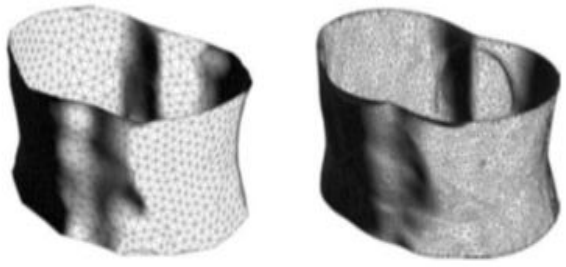

Figure 2.2 The 3D meshes of the scanned torso segment obtained by the Kinect (left) and the laser scanner (right) (Choppin & Wheat, 2013).

measuring anthropometric variables by Kinect, Katović et al. (Katović et al., 2016) measured the hight, left forearm length and left lower leg length of 25 participants. Based on their findings, the author concluded that there are no significant differences between the averaged digitally measured variables and classically measures ones.

2.3 Electromyography of muscle activity

In order to improve the cyclist's performance, it is significant to gain insight into the functioning of the muscles and muscle chain activation patterns in the lower extremities during riding. Analyzing the muscle activation patterns could provide details on how to train a particular muscle chain. Moreover, it has been proven that muscle activation can influence the physiological responses, plasma metabolic, kinetic and kinematic analyses both during and after exercise (Deschenes et al., 2000). The simplest and most often used method for measuring muscle activation is to extract the information from the electrical signal generated by the activated muscles, which is called electromyography (EMG) technique (Gregor et al., 1991). This diagnostic method can measure the electrical activity of muscles invasively, through wires or needles inserted directly into the muscle, or non-invasively, with the aids of electrodes placed over the skin surface overlying the investigated muscle (Cram, 2003; Mirka, 1991). Surface EMG obtains data from a large mass of muscle tissue through the superficial fibers, more than deep fibers, leading to the direct correlation to the mechanical outcome of different activities Frigo and Shiavi, 2004. Therefore, applying the surface EMG is preferred in healthy sedentary subjects and athletes. The amplitude of EMG signal is commonly defined with the root mean square value (RMS) (Duc et al., 2008; Laplaud et al., 2006) or integrated EMG (iEMG) values (Takaishi et al., 1998) from raw signals. However, the absolute value of EMG signal varies between different muscles and different cyclists caused by differences in physiological parameters and the inaccuracy associated with using various electrode

placement sites. To facilitate the quantification of EMG signals, it is necessary to use the EMG normalization procedures (Hsu et al., 2006). Previous researchers have documented that the EMG normalization should be reliable and repeatable, as well as being relevant to the given task (Knutson et al., 1994; J. F. Yang & Winter, 1984). The most prevalent method for normalization is the relative expression of the recorded EMG activity during the task, to the previously recorded isometric maximal voluntary contraction (IMVC) (Marsh & Martin, 1995). While pedaling, the extensor muscles of lower extremities are mainly active to extend the leg during the propulsive phase, whereas the hip flexor muscles become shorter (Brown et al., 1996; Chapman et al., 2008). The Propulsive phase of cycling stroke is referred to as the pedal position between 0° known as the top dead center (TDC) to 180°, also known as the bottom dead center (BDC), as shown in Figure 2.3. Muscle activation of a pedaling cycle is commonly defined by averaging the signals over several revolutions, as a percentage of the entire cycle duration. By defining the TDC and BDC, the comparison of cycling in different cadences is feasible.

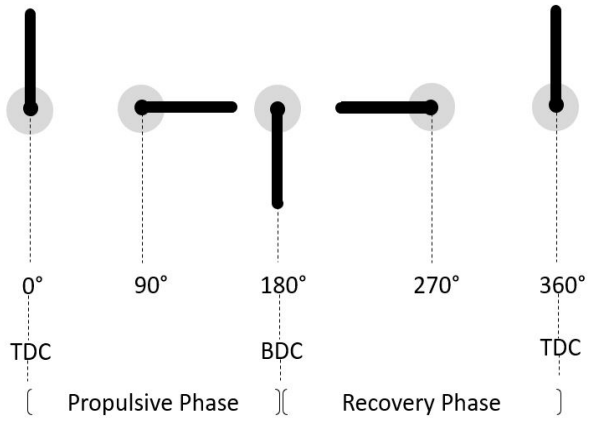

Figure 2.3 Pedaling phase during a single crank revolution. TDC: top dead center; BDC: bottom dead center.

Evaluation of muscle activation patterns during cycling has been carried out in many studies (M. Abdullah et al., 2017; Dorel et al., 2008; Ericson, 1986; Gregor et al., 1991; Hug, Decherchi, et al., 2004; Jorge & Hull, 1986). The first to use EMG for recording surface electromyograms during pedaling were Houtz and Fischer (Houtz & Fischer, 1959), who investigated all the main muscles of lower extremities, namely, gluteus maximus (GMax), rectus femoris (RF), vatsus lateralis (VL), vatsus medialis (VM), semimembranosus (SM), semitendinosus (ST), biceps femoris (BF, long head), gastrocnemius lateralis (GL) and gas-

trocnemius medialis (GM) and tibialis anterior (TA). Several studies recorded EMG activity of different cyclist's riding positions or seat heights (Chapman et al., 2008; Dedieu et al., 2020; Dorel et al., 2009; Duc et al., 2008; Sanderson & Amoroso, 2009); however, the lower limb muscle contribution to the cycling performance of alterations of aero handlebar position has not been quantified. It has been reported that the hip (GMax) and knee (VL and VM) monoarticular extensors activates at the beginning of the propulsion phase, while the knee (RF) biarticular flexor is activated at the end of recovery phase (270° to 360°) (Raasch & Zajac, 1999). Chapman et al. (2008) studied the EMG patterns of both standard upright position and time trial position (TTP) for the novice and elite cyclists as well as elite triathletes. They found that changing the body position did not affect the main bursts of muscle activity, although it did cause a more significant impact on muscle recruitment of triathletes compared to elite cyclists. TTP is used by cyclists to improve their performance and lower their trunk to reduce aerodynamic drag (Grappe et al., 1997; Lukes et al., 2005). Adjustments to aero handlebar positions, which may be the most important adjustments when fitting a bicycle (Lukes et al., 2005; Oggiano et al., 2008), allow this modified position of the upper body that is intended to decrease the frontal area and accordingly, increase the aerodynamic efficiency of the cyclist during competition. In another research, Duc et al. (2008) investigated the muscle activation of lower limb muscles in the standing and seated posture during the uphill cycling. Their results showed an increase in the mean and peak EMG activity and the timing of the knee and hip joint muscles, including GMax, VL and RF in standing pedaling compared to the seated position. Moreover, they observed a decline in the peak EMG activity of RF when the hand grip position moved from brake levers to the drops in the standing pedaling, which attributed to the increase of the trunk flexion. Furthermore, Dorel et al. (2009) related the reduced activation of GMax and increased activation of hip flexor RF in the positions with more elevated torso angles to the higher peak force in the propulsive phase. In a recent study, it was found that the changes in the saddle height influenced the duration and offset of VL, VM, RF and GM (Dedieu et al., 2020).

These results from previous investigations support the hypothesis that alteration of handlebar position can modify muscle coordination and EMG patterns. Amongst numerous upper body positions, modification of TTP and the aero handlebar position seems to be missing, though it would surely be of interest. Currently, no studies investigated the lower limb muscle contributions to different aero handlebar positions, which could provide more insight into optimizing the cycling performance.

2.4 Kinematics of cycling

Cyclist position and the configuration of the bicycle will affect joint kinematics and, therefore, the cycling performance (Chapman et al., 2008). Consequently, modifications in the riding position may induce significant changes in pedaling technique and the body segment kinematics since the orientation of upper body segments can impact the distal limb movements (Knox & Hodges, 2005; Massion et al., 2004). Furthermore, alteration of riding configuration could cause overuse injuries in the lower extremity (Ferrer-Roca et al., 2012). The leg experiences the extension during the propulsion as the pedal is moving from TDC to BDC, and it goes through flexion during the recovery phase as the pedal moves upward (Burke, 2003). Accordingly, any attempt to improve the performance of the cycling position should avoid over flexion and extension of the hip and knee joints. In order to capture the complexity of the body while pedaling, the consideration of kinematic relationships between segments is critical (Bartlett et al., 2007).

Previous studies on the correct positioning of the handlebars and the kinematics of the lower limb are formulated on the comfort of the cyclist and personal perspectives during the non-pedaling experiments (Silberman et al., 2005). With the advancement of technology, it is possible to analyze the dynamic bicycle configuration and its kinematic variables, which can be influenced by the workloads, cyclist's technique and position (Holliday et al., 2017). The motion of pedaling and the kinematics of the leg have been studied extensively (R. Bini et al., 2011; R. R. Bini et al., 2010; Chapman et al., 2008; Dedieu et al., 2020; Garcia-Lopez et al., 2008; J. C. Martin & Nichols, 2018).

Chapman et al. (2008) compared the leg and foot kinematics (i.e., peak range of motion, absolute range of motion and variability of movement patterns) between the upright position and the TTP for the elite and novice cyclists as well as elite triathletes. They did not find any significant differences between the measured parameters. In contrast, it has been reported that moving the saddle forward increased the knee and hip flexion angle (R. R. Bini et al., 2014; R. R. Bini et al., 2013) while the ankle mean angle and range of motion showed no considerable changes. Increasing the saddle height also affected the range of motion and the mean angle of the ankle, hip and knee joint significantly (Dedieu et al., 2020). Comparing the increased saddle height with a position of decreased saddle height, they observed that the mean angles inclined, whereas the range of motion declined.

Thus, to determine the performance of a cycling position, evaluating muscle recruitment of cycling without considering joint kinematics is insufficient. Although lower extremity joint kinematics during pedaling in TTPs has been described, the effect of alteration in handlebar

position, to produce different body positions during TTP has not been evaluated.

The kinematic data of body segments during cycling can be recorded using various systems. Whilst the marker-based systems provide highly accurate data, the expenses and extensive specialty for the installation make it less preferred to be used in the case of motion capturing applications (Rodrigues et al., 2019). Moreover, the need for reflective markers confronts an obstacle and restriction to use for human movement analysis. Using Kinect can facilitate recording 3D skeleton data using anatomic landmarks, with no movement limitation and faster set up (Choppin et al., 2014; Sheets et al., 2010).

Authors reported the root mean square errors (RMSEs) of 13.85° and 7.59° in abduction, 21.57° and 12.00° in flexion, and 0.12, 0.14 and 0.08 m for X, Y and Z center of mass positions, respectively, during the segment tracking of a manikin using Kinect (Choppin & Wheat, 2013). Figure 2.4 represents the tracking ability of Kinect, compared to a 12-camera motion analysis system (Choppin & Wheat, 2013). Methods to evaluate the application of Kinect in cycling kinematics, to enable changes aimed at improving performance, have not been experimentally assessed.

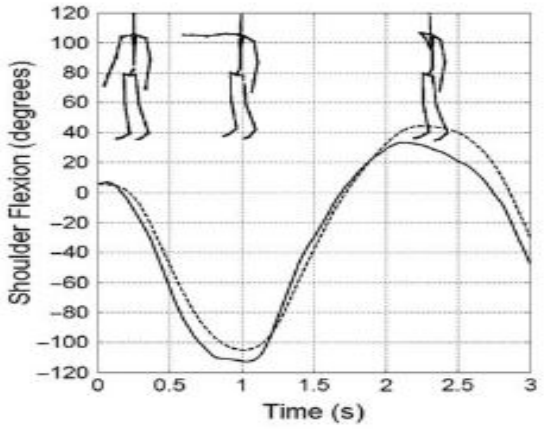

Figure 2.4 A comparison between the Kinect shoulder flexion segment angles (solid line) and a 12-camera system (dashed line) (Choppin & Wheat, 2013).

2.5 Changes in the time trial position

There are three main cycling positions: the upright position, with hands on the brake hoods of the handlebars; the dropped position, with hands on the drops or curved portion of the handlebars; the time trial position, with hands on the aero handlebars and elbows resting on

pads while hands extended to the end of the handlebar. The handlebar is one of the three points of contact between the rider and bike, along with the saddle and the pedals. Figure 2.5 depicts the three postures tested by Defraeye et al. (2010a). The aerodynamic drag can be reduced by adopting the riding position from upright to the time trial position. To reduce aerodynamic drag, cyclists alter their positions as low as possible by crouching forward and down and reducing the trunk angle, i.e., the angle between the horizontal and the trunk. This alteration results in adopting the time trial position, which targets to improve the optimal performance by reducing the frontal area (A) of the cyclist (Burke, 2003; Chabroux et al., 2012; Garcia-Lopez et al., 2008). However, lowering the position to reduce the aerodynamic drag could lead to contradicting effects in the biomechanical and physiological performance (Jeukendrup & Martin, 2001; Lukes et al., 2005). Table 2.1 shows a non-exhaustive summary of the reported drag area and the methodological details of previous studies for various positions.

Consequently, reduction in aerodynamic drag requires a vast significant understanding of the cycling position and its drag area (AC_D), which is the product of the drag coefficient (C_D) and the frontal area (A) (Chabroux et al., 2012). Despite numerous studies devoted to the aerodynamic performance of rider's position, limited information is available about the aerodynamics of realistic changes in the time trial position. Therefore, a detailed analysis considering the specific effects of different time trial positions is lacking.

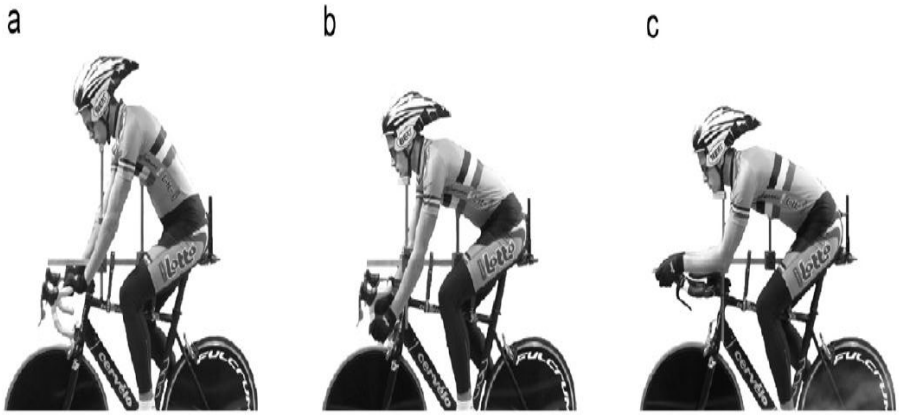

Figure 2.5 Three cyclist's positions tested by Defraeye et al. (Defraeye, Blocken, Koninckx, Hespel, & Carmeliet, 2010a): (a) upright position; (b) dropped position; (c) time trial position (TTP).

Jobson et al. (2008) tested nine competitive cyclists to evaluate the time trial position during laboratory cycling. Although they reported a significant difference between the power

output of different time trial positions, they concluded that body position does influence the ecological validity of laboratory-based pedaling. In an attempt of wind-tunnel experiments to provide aerodynamic reference values of cyclists with and without a helmet and for the time trial positions, authors showed that drag area increased 14% after lowering the handlebars and advancing the pads (Garcia-Lopez et al., 2008). They also reported that wearing the aero helmet did not change the aerodynamic drag. Therefore, a detailed analysis of various time trial positions and related modifications is necessary.

Table 2.1 Comparison of drag area measurements and other research details from previous studies of cyclist position.

Studies	Method	Wind speed U (m/s)	UP (m^2)	DP (m^2)	TTP (m^2)
di Prampero et al. (1979)	Field test	5-15		0.318	
Davies (1980)	Wind-tunnel	5-13	0.280		
Kyle and Burke (1984)	Wind-tunnel	9-15.5		0.320	
Dal Monte et al. (1987)	Wind-tunnel	15			0.246
Kyle (1991)	Wind-tunnel	13.3			0.221
Capelli et al. (1993)	Field test	8.6-14.5	0.255		
Zdravkovic et al. (1996)[a]	Wind-tunnel	8.2	0.260	0.230	0.170
Grappe et al. (1997)	Field test	5-13	0.299	0.276	0.262
Martin et al. (1998)	Wind-tunnel	13.4			0.269
Candau et al. (1999)	Field test	2.5-12.8	0.0.355		0.262
Padilla et al. (2000)	Wind-tunnel	13.9			0.244
Jeukendrup and Martin (2001)	Wind-tunnel	12.5	0.358	0.307	0.249
Martin et al. (2006)	Field test	7-12			0.258
Gibertini and Grassi (2008)	Wind-tunnel	13.9	0.282	0.275	0.223
Garcia-Lopez (2008)	Wind-tunnel	15			0.260
Defraeye et al. (2010a)[a]	Wind-tunnel	10	0.193	0.167	0.134
Defraeye et al. (2010a)[a]	CFD	10	0.219	0.172	0.142
Underwood et al. (2011)	Wind-tunnel	11.1			0.226
Blocken et al. (2013)[a]	Wind-tunnel	15	0.193	0.167	0.134
Blocken et al. (2013)[a]	CFD	15	0.213	0.173	0.135
Barry et al. (2015b)	Wind-tunnel	13.9			0.244
Barry et al. (2015a)	Wind-tunnel	18			0.214
Beaumont et al. (2018)[a]	CFD	15			0.138
Blocken et al. (2019)	CFD	15		0.277	0.236

UP, upright position; DP, dropped position; TTP, time trial position.
[a] Drag area for cyclist without bicycle.

CHAPTER 3 ARTICLE 1: FULLY PARAMETERIZED BODY ANTHROPOMETRY FOR THE AERODYNAMIC ANALYSIS OF CYCLIST POSITION USING THE CFD METHOD

This manuscript presents the development and validation of a framework for the aerodynamic analysis and performance evaluation of cyclists' positions. The parameterized elliptical zone method provided a comprehensive, feasible and affordable tool for modeling the cyclist manikin. This development consists of implementing the elliptical zone method for body segmentation, adopting the markerless motion capture system to acquire multiple anthropometric data and joint positions, generating the fully parameterized 3D body surface of cyclists as well as validation of the method and conducting CFD simulations. This manuscript is an essential contribution to this project as it establishes answers to its first objective.

My contribution to this manuscript included the development of the markerless motion capture system (70%), the development of the 3D generated digital manikin model (60%) and performing the CFD simulations of different cycling positions (80%). My contribution to the article includes the design of the paper and its redaction process.

This manuscript, "Fully parameterized body anthropometry for the aerodynamic analysis of cyclist position using the cfd method", has been submitted in Part P: Journal of Sports Engineering and Technology, manuscript number: JSET-20-0035, in April 2020 (Ghasemi, Curnier, Trépanier, et al., 2020).

Authors:

Mojtaba Ghasemi[1], Daniel Curnier[2], Jean-Yves Trépanier[1], Hadrien Koenig[1], Eddy Petro[1], Delphine Périé[1]

[1] Department of Mechanical Engineering, Polytechnique Montréal, Montréal, Canada
[2] Department of Kinesiology, Université de Montréal, Montréal, Canada

3.1 Abstract

The reduction in aerodynamic drag improves cycling performance. This reduction requires a considerable understanding of cyclist's characteristics and aerodynamics. However, current common methods require costly, time-consuming and complicated techniques. The aim of this study was to develop and validate a set of fully parameterized numerical tools allowing the investigation of the aerodynamic drag of the cyclist position. For this purpose, the body surface of professional cyclists was modeled using a markerless motion capture system (Microsoft KinectTM) and the elliptical zone method. The computational fluid dynamics (CFD) was conducted to provide a clear demonstration of this method. For CFD simulations, the virtual body surface of one cyclist was placed in the domain. The drag area of the cyclist was calculated. For the upright position (UP), dropped position (DP) and time trial position (TTP), the drag area was 0.197 m^2, 0.167 m^2 and 0.138 m^2, respectively. In addition, for the flat torso angle position (FTAP), the drag area was obtained 0.108 m^2. The comparison shows a close agreement with the previous studies. This study has shown that this markerless motion capture system combined with the fully parameterized modeling framework has a great potential for various biomechanical and sports-related research.

Keywords: CFD, parameterization, cycling, aerodynamics, body position

3.2 Introduction

Approximately 80-90% of the total resistive forces influencing cycling performances are aerodynamic resistances (Belluye & Cid, 2001; Candau et al., 1999; Debraux et al., 2011; Defraeye, Blocken, Koninckx, Hespel, & Carmeliet, 2010a; P. E. Di Prampero, 2000; Grappe et al., 1997; C. R. Kyle & Burke, 1984; C. Kyle & Weaver, 2004; Lukes et al., 2004; J. C. Martin et al., 2006; Millet & Candau, 2002; Padilla et al., 2000), called aerodynamic drag. Reduction in aerodynamic drag leads to improvement in cyclist's performance for the same power output. For instance, the power output required for the cyclist-bicycle system to overcome the aerodynamic drag is a third-order polynomial of the system velocity, so it is necessary to double the pedaling power for an increment of cycling velocity from 32.4 to 43.2 km/h (Grappe et al., 1997). Among these aerodynamic drag forces, about 60-70% appertains to the cyclist's body position (Gross et al., 1983; C. R. Kyle & Burke, 1984; C. Kyle & Weaver, 2004). Modifications of the cyclist positions are frequently used to ameliorate the position of professional cyclists (Barry et al., 2015a). Accordingly, reduction in aerodynamic drag requires a vast and significant understanding of the position of the cyclist's characteristics and its drag area (AC_D), which is the product of the drag coefficient (C_D) and the frontal area (A).

Aerodynamic drag could be inquired using field tests, wind-tunnel measurements, the particle image velocimetry (PIV) technique and computational fluid dynamics (CFD) approaches (Barber et al., 2009; Blocken, 2014; Blocken & Toparlar, 2015; Jux et al., 2018; Scarano et al., 2019; Spoelstra et al., 2019; Terra et al., 2016; Terra et al., 2018). CFD approaches can provide more appropriate details regarding cyclist position components (Blocken et al., 2013; Defraeye, Blocken, Koninckx, Hespel, & Carmeliet, 2010a, 2010b, 2011; Lukes et al., 2004) leading to more insights in terms of aerodynamic drag optimization due to certain reasons: (1) although the field test is more practical for the most appropriate conditions and equipment, its flow field are less adjustable and time-efficient as compared to CFD approaches; (2) full-size athlete wind-tunnel tests face some serious limitations caused by the complex nature of cycling aerodynamics, their extensive costs and the technical expertise required; (3) changing the flow field circumstances, setting up the new field tests and remeasuring the parameters involved are often time-consuming and quite complicated (Crouch et al., 2014; Defraeye, Blocken, Koninckx, Hespel, & Carmeliet, 2010a; Zaidi et al., 2010). Despite the promising potentials and prospects of CFD simulation, the adopted calculation always contains some uncertainties associated with the boundary conditions, turbulence modeling and geometry simplifications (Casey & Wintergerste, 2000). Hence, the CFD technique is an appropriate tool for investigating the cyclist position and its parametric optimization studies, which

must be carefully applied (Blocken & Toparlar, 2015; Defraeye, Blocken, Koninckx, Hespel, & Carmeliet, 2010a).

Conducting CFD simulation requires a digital manikin model of the cyclist for every obtained position. This digital model requires an accurate estimation of body segments parameters. Several methods have been developed to obtain the body segments parameters and joints' positions (Durkin et al., 2002; Ma et al., 2011; Pearsall et al., 1994). One technique of capturing individual estimates of these characteristics cost-effectively and non-invasively is modeling the segments as a series of ellipses of known depths and diameters (Jensen, 1978). This method, called the elliptical zone method, assumes that the body is composed of elliptical zones representing body shapes and segment densities. The reliability of the measurements depends on the accuracy of tracing the body surface outlines as well as distinguishing the anatomical reference points, lines and joint centers that define each body segment.

Using the markerless motion capture system (Kinect, Microsoft Corp., USA) is one of the best data collection methods that contains all the criteria relating to availability, expense, accuracy, flexibility and time-efficiency (Berger et al., 2011; Chang et al., 2011; Fern'ndez-Baena et al., 2012), and can be used to acquire the data required in the elliptical zone method. Kinect is a depth-measuring device that simultaneously captures color and depth data of thousands of points in a scene at 30 Hz. Kinect is entirely operational for biomechanics and sports analysis (Berger et al., 2011; Chang et al., 2011; Fern'ndez-Baena et al., 2012). It could effectively scan the body surface to estimate body segment inertial parameters (Norton et al., 2002; Sheets et al., 2010), leading to an accurate estimation of the joint positions and anthropometry due to the depth data captured (Shotton et al., 2013; Ye et al., 2011). For instance, the sagittal and frontal plane joint angles captured by the marker-based and Kinect-based motion capture system demonstrated a close agreement with each other by $< 0.5^{\circ}$ for a jig tool (Schmitz et al., 2014). Kinect is preferable compared to other methods, including marker-based methods due to some particular reasons: (1) Kinect does not influence the subject's position and movements caused by markers or other devices attached to the subjects; (2) Kinect reduces the cost and data collection time enormously (J. Han et al., 2013; Smisek et al., 2013), resulting in realistically accurate estimations of the extremities trajectories; (3) it prevents the displacement of joints and reference points caused by soft tissue movement in relation to the underlying bones and joints which could cause an alteration in the position of markers placed on the skin (Alexander & Andriacchi, 2001; Leardini et al., 2005). Kinect provides parameterizations for the effective modeling of plausible poses.

Therefore, this study aimed to develop and validate a set of tools, which are fully parameterized to body anthropometry and the position of the cyclist, allowing researchers to investigate

the aerodynamic drag of any cyclist position using the elliptical zone method with segment endpoints and body surface outlines being captured by a Kinect sensor. Our hypothesis is that applying this technique would enable us to conduct aerodynamic analysis by addressing the variability of different cyclist positions in reducing aerodynamic drag.

3.3 Methods

Five professional cyclists (age: 38.8 ± 6.2 years, height: 177.2 ± 5.8 cm, mass: 68.4 ± 5.6 kg) volunteered to participate (2 females, 3 males) and freely signed an informed consent form after the purpose and procedure of the study were clearly described to them. All participants were free of any musculoskeletal disorders, deformities and recent injuries. The host institution's ethical committee approved the study.

Participants were asked to stand still during the 1-minute acquisition. Photographs were taken from the front and right-side views where the Kinect was respectively perpendicular to the coronal and sagittal plane. Each participant's acquisition was made separately without altering the Kinect position or its distance from the participants. The Kinect was set on tripods at the height of 1.2 m with its axes parallel to the horizontal floor surface and at a distance of 2 m from where the participants were positioned. The integrated sensor software development toolkit (SDK, Microsoft Corp.) was used to detect the location of the joints of the participants. A circle of 12 cm in diameter was placed at the same depth as the subject to evaluate the value of the pixel to meter conversion factor. The segment measurement was conducted using the aforementioned calibration in the vertical and horizontal directions. The length and width of the segments were determined due to data processing (MATLAB, Math Works, USA). The obtained data were smoothed using the Sobel filter (cut-off frequency 10 Hz) to distinguish the segments' edges more accurately. The continuation of the segmentation and elimination of surrounding noise was conducted by dilatating the segmentation and smoothing body detection, respectively. Twenty coordinate points were determined to represent the whole-body segments (Figure 3.1).

The 3D body surfaces were modeled in CAD software (CATIA V5, Dassault-Systèms, France) for all participants using the data collected from the Kinect. The cyclist model was divided into two parts. The first part is an adaptable skeleton model based on the size, length and angles of the desired position. The second part is the body surface that represents the corpulence of the participants.

Only the degrees of freedom related to a conventional cyclist position movement were modeled

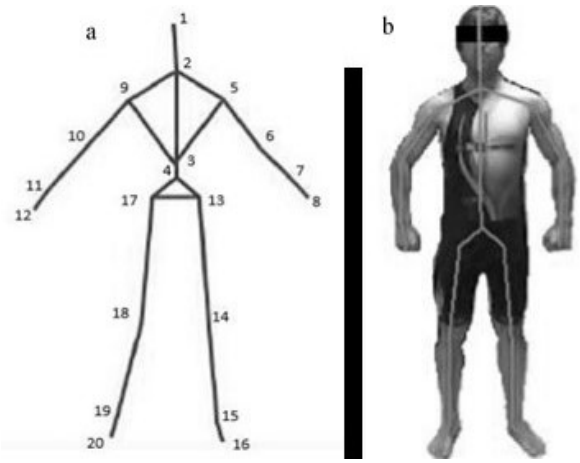

Figure 3.1 a) 20 points stick figure model and b) example of skeleton modeling for a single participant.

to avoid excessive complexity in the process of skeleton modeling. Therefore, all the lateral postures of the trunk and legs were fixed to keep body symmetry. Arm postures were identical for the same reason. A final angle was considered to model the inclination of the entire model in the sagittal plane. Six lengths (shank, thigh, forearm, arm, trunk, head) and two widths (hip, shoulder) were used to fully define the skeleton.

The surface of body segments around the skeleton was created using the elliptical zone method. The width of each segment was measured on the Kinect images (Table 3.1). A multi-section surface was created from the ellipses of each segment. The thigh and shank were constrained in a plane parallel to the sagittal plane and offset by the hip's width. The arm and forearm were constrained within the arm rotation plane that was defined by two intermediate planes representing the rotation degree of freedom of the shoulder joint. The arm was defined by its length and the 3 degrees of freedom of the shoulder (flexion, lateral rotation and abduction). The forearm was defined by its length and the elbow flexion angle. The trunk, neck and head were represented using the elliptical zone method. A cutting surface was assembled considering a 20 mm gap at the junction between the lower limbs and trunk, and a 10 mm gap between the shoulders and arms and also between arm and forearm to ensure continuity in the tangency of the entire surface (Figure 3.2). A fully parametrized cyclist surface is then obtained.

For the accuracy purpose, the surface of all participants was scanned using a non-contact laser scanner (InSpeck Inc., Canada) consisting of four optical 3D digitizers, a frame grabber for video signal acquisition and conversion, and a computer for data processing. The upper and lower geometries of each participant were required. Continuity was corrected in the presence

Table 3.1 Location of width measurement.

Segment	Arm	Forearm	Hand	Thigh	Shank	Trunk
Percentage of measuring (%)	50	33.33	50	30	15	50
	100	100	-	60	33.33	100
	-	-	-	90	90	-

The percentage represents the location of the measurement where 0% and 100% indicates the proximal and the distal end of segments respectively.

of strong color gradient on the subject by using InSpeck fringe acquisition and processing software (FAPS). Once the acquisitions of the four scanners were processed, the four point clouds were merged to build the surface model. Subsequently, the differences between the resulted parameterized model, which was created using the elliptical zone method, and the scanned surface model, which were in an identical position, were calculated using CAD software.

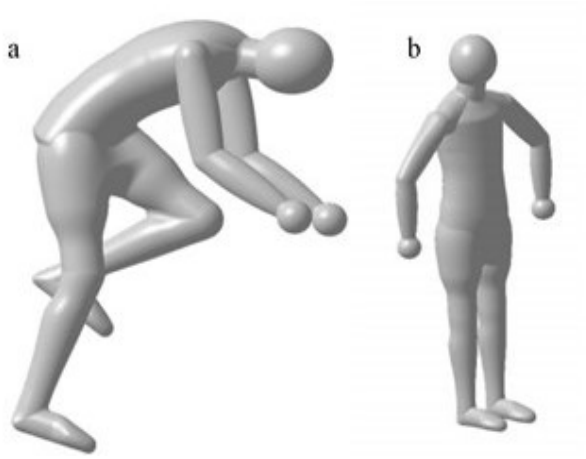

Figure 3.2 Defining the geometry of cyclist indicated for the (a) cycling position and (b) standing position.

The CFD simulations were performed with the ANSYS Fluent 16.1© to obtain the drag area of a cyclist in four different positions; namely, the upright position (UP), dropped position (DP), time trial position (TTP) and flat (0°) torso angle position (FTAP). These positions, which are categorized based on the torso angle relative to the ground and shoulder angle, are generally adopted by cyclists in different types of competitions to improve their performance as much as possible. The dimensionless coefficient C_D can be related to drag force F_D (N) and the frontal area A (m^2) as demonstrated below, where ρ is the density of air (kg/m^3) and U is the approach-flow wind velocity (m/s) (Equation 3.1).

$$F_D = 0.5\rho A C_D U^2 \tag{3.1}$$

Reporting the drag area (AC_D) is preferable to C_D since it does not require a precise determination of the frontal area (A). A virtual body surface of an individual cyclist was placed in a trapezoid-shaped domain (Figure 3.3). This form allowed a unique flow condition to be applied. In addition, each of the faces was not parallel to the flow direction, which improved the computing performance. Note that to minimize computation time, only the cyclist's body has been considered without including the bicycle (Blocken et al., 2013). The roughness of the cyclist's surface caused by the participants' jersey has not been considered. The distance between the virtual cyclist and the outlet of the domain was 11 m. The sides and upper surfaces of the field were defined as symmetric walls. No-slip boundary conditions were applied on the ground. The inlet and outlet boundary conditions were imposed as inlet velocity (a uniform velocity of 10 m/s) and free outflow condition (ambient static pressure), respectively. In this study, no-wind conditions were considered.

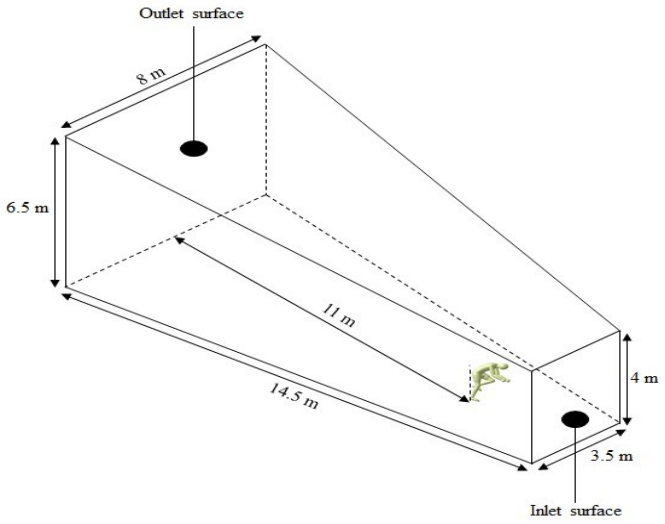

Figure 3.3 Computational domain of CFD simulations; Simulations were performed with a uniform velocity of 10 m/s.

The simulation of the non-pedaling (static-legs) cyclist model was conducted with the assumption that the flow topology of a cyclist is consistent across a static leg and rotating leg at the related phase of leg rotation. Crouch et al. (2016) showed a slight variation in the wake flow structure and the aerodynamic performance of a pedaling cyclist as compared to a non-pedaling cyclist with the pedals in the same position, confirming our assumption

regarding the non-pedaling cyclist.

For the CFD simulations, a steady Reynolds-averaged Navier-Stokes (RANS) with the standard k-ε turbulence model was chosen. This model is extensively considered to perform well due to computational stability reasons related to the large size of the computational domain and is often applied in sports science studies in case of a fully turbulent flow in the whole fluid domain such as swimming and cycling studies (Blocken et al., 2013; Fintelman et al., 2014; Zaidi et al., 2010).

We compared our obtained drag area against other studies (Blocken et al., 2013; Defraeye, Blocken, Koninckx, Hespel, & Carmeliet, 2010a; Gibertini & Grassi, 2008). Given almost the same computational domain and initial conditions, the values were compared to assess the accuracy and reliability of our results. The simulated cyclist positions were also modeled with the same condition and torso angle.

3.4 Results

The comparison between the Kinect-based model and the InSpeck-based model for the five participants showed that the maximum difference in upper and lower extremities was 36.4 ± 10.4 mm and 30.2 ± 7.8 mm, respectively. These differences ranged between 2.1% and 1.7% when reported relative to participants' height, which was considered insignificant. The largest maximum difference was in the chest, shoulder and knee (Figure 3.4).

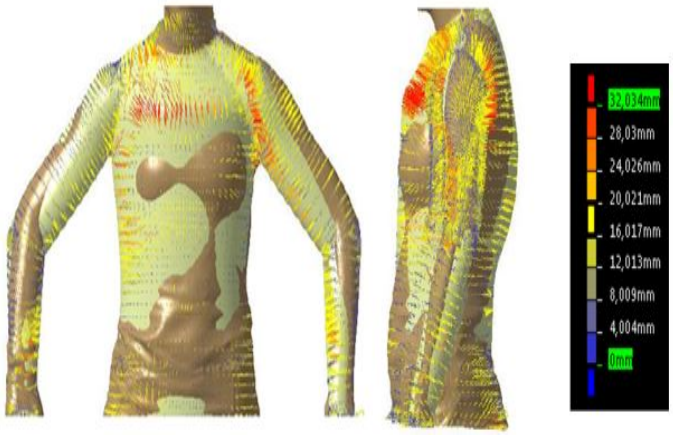

Figure 3.4 The overlapped (mm) between CAD modeled surface coverage and Inspeck non-contact laser scanner.

The CFD results were presented along with data from other studies (Blocken et al., 2013;

Fintelman et al., 2014; Zaidi et al., 2010) (Table 3.2). The drag areas of the cyclist obtained from our CFD simulations are in good agreement with their results for a cyclist without bicycle. The results showed that the drag area of UP is higher than in other positions (Table 3.2). As compared to UP, the drag area decreased -15.2% in DP, -29.9% in TTP and -45.2% in FTAP. This decline is in agreement with the experimental results (-13.5% in DP vs UP; -30.6% in TTP vs UP) and CFD calculation (-18.3% in DP vs UP; -31.5% in TTP vs UP) of reference research (Defraeye, Blocken, Koninckx, Hespel, & Carmeliet, 2010a). Moreover, it can be seen that the frontal area of UP is higher than the frontal area of other positions (+18.0% vs DP; +35.3% vs TTP; +70.4% vs FTAP). The frontal areas were slightly higher in our study, caused by differences in the anthropometric data of participants (0.46 m^2, 0.39 m^2 and 0.34 m^2 for the UP, DP and TTP against 0.41 m^2, 0.37 m^2 and 0.34 m^2 obtained by Defraeye et al. (2010a)). The FTAP had the least frontal area (0.27 m^2), contributing to the minimization of the aerodynamic drag forces and the least drag area (0.108 m^2).

For UP, DP and TTP, a relatively low drag area was calculated compared to the values in a previous study (Defraeye, Blocken, Koninckx, Hespel, & Carmeliet, 2010a). FTAP showed the least value of drag area conforming to the frontal area. The drag area for UP was less than twice the drag area of FTAP.

The contour patterns colored by velocity for UP, DP, TTP and FTAP positions (Figure 3.5) showed that the flow behavior is different for each cyclist position. Comparing the flow pattern reveals that increasing the torso angle could induce a higher drag force as expected. In addition, changing the arm angle (angle between arm and forearm) and its position affects the drag area and flow pattern enormously.

3.5 Discussion

We have presented a fully parameterized and low-cost framework to generate a 3D virtual human body based on anthropometric data. Parameterized modeling provides a possible and efficient solution to generate different size models at runtime and post-processing. An established set of parameterized models has high applicable value for the CFD simulations and other analysis on segments of the body. Using the Kinect sensor to capture the anthropometric data of cyclists combined with the CAD software parametric surface modeling provided the opportunity to conduct CFD simulations to determine the drag area in different cyclist positions. This method affords enough scope to define the proper and accurate edges of body surface modeling. In addition, the implementation of many movements and postures

Table 3.2 Drag area AC_D (m^2) deduced from CFD (RANS) at 10 m/s and frontal area A (m^2) of cyclist position for the UP, DP, TTP and FTAP.

Studies	UP		DP		TTP		FTAP	
	AC_D (m^2)	A (m^2)	AC_D (m^2)	A (m^2)	AC_D (m^2)	A (m^2)	AC_D (m^2)	A (m^2)
Defraeye et al. (2010a) (ref.) Wind-tunnel[a]	0.193	0.41	0.167	0.37	0.134	0.34		
Defraeye et al. (2010a) (ref.) CFD[a]	0.219	0.41	0.179	0.37	0.150	0.34		
Gibertini and Grassi (2008) Wind-tunnel[b]	0.282	0.40	0.275	0.36	0.223	0.30		
Blocken et al. (2013) CFD[a]	0.213		0.173		0.135			
Current research CFD[a]	0.197	0.46	0.167	0.39	0.138	0.34	0.108	0.27
Deviation (%) from (ref.) Wind-tunnel*	2.0		0.0		2.9			
Deviation (%) from (ref.) CFD*	11.1		7.2		8.7			

Abbreviations: AC_D, drag area; A, frontal area; UP, upright position; DP, dropped position; TTP, time trial position; FTAP, flat (0°) torso angle position.

[a] Drag area for the cyclist.

[b] Drag area for the cyclist with bicycle.

* $\frac{AC_{D,Ref} - AC_D}{AC_{D,Ref}} \times 100$

are inconvenient or impossible for the participants of human movements' experiments, which could be prevented by using this approach, i.e., measuring the anthropometric data using the Kinect and modeling the body surface with the specified postures in CAD software using the elliptical zone method. Since the surface modeling and extraction of numerous human bodies is time-consuming and costly, this method would ease the process. Accordingly, changing the position and modeling various positions in CFD simulations requires only a re-generation of the mesh. It should be noted that the absolute results of CFD simulation were not our primary objective. It was conducted to provide a clear demonstration of the elliptical zone method and outline the potentials of the markerless motion capture system. The markerless motion capture system combined with the fully parameterized modeling framework can contribute to the conclusive and comparable relative comparison of various cycling positions.

The drag area increased by increasing the torso angle and the frontal area accordingly. The reason for the consideration of the UP, DP and TTP positions was to depict an adequate image for the effect of the torso angle on the obtained position and its drag area. Moreover,

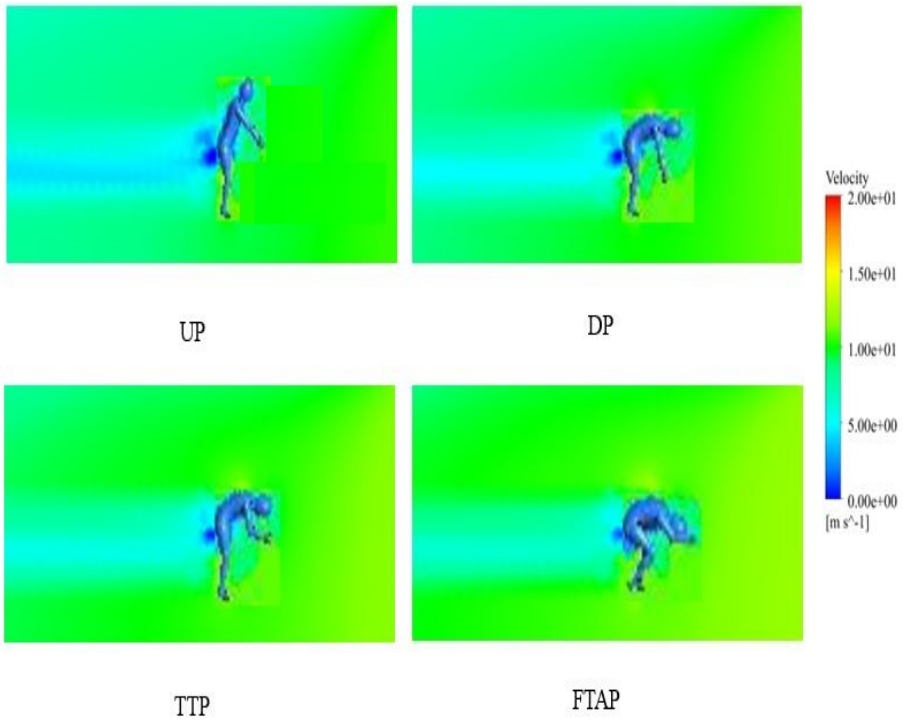

Figure 3.5 Contour pattern colored by velocity (m/s) for the individual cyclist at the speed of 10 m/s and for UP, DP, TTP and FTAP positions.

these investigated positions were used in previous studies (Defraeye, Blocken, Koninckx, Hespel, & Carmeliet, 2010a, 2010b). Because of different methodological approaches and experiment features in the literature, such as the various anthropometric characteristics, the comparison of the findings of the literature to our results was difficult. However, the comparison between our results and the ones obtained by Defraeye et al. (2010a) with the same uniform inlet velocity (10 m/s) showed a close agreement. Although our model was a simplification of the cyclist, it has reflected the critical aspect of different cyclist positions. Nevertheless, wind-tunnel experiments on a full-scale cyclist should be executed in terms of proper validation and verifications.

The deviations could be related to the body geometry (i.e., anthropometric parameters) of the 3D parameterized model used in our simulations that does not precisely match the model and geometry used in their numerical model, including the frontal area. We did not represent the aero helmet for the created model, while they considered the aero-helmet in both experimental setups and CFD simulations. Several studies were carried out on the effect of the aero-helmet, which confirmed the reduction trace in comparison to no helmet (M. N. Abdullah et al., 2015; Alam et al., 2010; Chowdhury & Alam, 2014; Mustary et al., 2014).

Alam et al. (2010) and Chowdhury et al. (2014) have shown that using the aero helmet contributes about 2-8% of the aerodynamic drag for velocities more than 30 km/h. For all the cyclists' riding positions, we have modeled the head position in the head-down position, while Defraeye et al. (2010a) have tested the head in the head-up position (the helmet is aligned laterally and level with the torso). In the head-down position, cyclists frequently look down toward their gears to rest their necks. This position, which is adopted by elite cyclists, helps cyclists to reduce their frontal profile and drag area as much as possible (Beaumont et al., 2018). Using CAD software to create the body surface would include some construction constraints mainly on straight lines and ellipses in different parts of the body such as the abdomen, chest and hands. These constraints caused the largest deviation percentage in TTP, where the position and exact shape of hands with their distance from each other on the handlebar are vital (Chabroux et al., 2012).

The FTAP position and its frontal area also confirmed the effect of torso angle on drag area. Garcia-Lopez et al. (2008) also reported a significant positive correlation indicating the decrease of drag area by a decline in torso angle, which is similar to our results. Considering the aerodynamic aspects, an individual could conclude that this position is the most effective cyclist position. However, the power output, physiological responses and metabolic variables are impaired at the small torso angle (Dorel et al., 2009; Gnehm et al., 1997) that depicts the importance of a trade-off for the cyclist position.

Regarding the Kinect acquisition accuracy, the differences between the Kinect-based model and the InSpeck-based model are acceptable considering the length and width of body segments (Yu et al., 2003; Yu et al., 2010). One should consider that the first generation of Kinect has been used in this research, while using the second version will improve the accuracy and resolution (Xu & McGorry, 2015; L. Yang et al., 2015). Previous studies have revealed that using more than one Kinect simultaneously can improve the accuracy through specific approaches, such as the multi-Kinect trilateration approach (L. Yang et al., 2015). Furthermore, applying various algorithms to reduce the noise of depth data and captured photos would simplify the reconstruction, allowing surfaces to converge quicker and with more details (Chen et al., 2016; Nguyen et al., 2012).

CFD simulations can be improved using a more accurate method. The RANS modeling technique is the most common and appropriate method for the investigation of aerodynamics regarding the time and cost of calculation. However, the RANS model cannot model the actual flow conditions completely analogously. It still models and simplifies the actual turbulent flow conditions.

Improving the segmentation algorithm as well as the integration of the Kinect-based captur-

ing measures with kinetics and kinematics could provide profound details regarding output performances of the core muscles of the body and joint mechanics levels, leading to valuable details about improving the manufacturing procedures, cyclists' training and cycling performances. It is recommended to conduct further more detailed CFD analysis to explain the wake structure and flow patterns around the cyclist in different cycling positions so that this approach's potential is more thoroughly explored. Moreover, modeling different positions and comparing their aerodynamic results coupled with the metabolic variables and physiological responses of cycling during those positions will enable us to identify the most applicable optimized position.

3.6 Acknowledgments

None.

CHAPTER 4 ARTICLE 2: THE EFFECT OF DIFFERENT AERO HANDLEBAR POSITIONS ON MUSCLE ACTIVITY AND KINEMATICS OF LOWER LIMB

This manuscript is allocated to developing an application of the Kinect-based motion capture method to determine the influence of changing the time trial handlebar position on the lower extremities' kinematic variables in conjunction with the lower limb muscle functioning and physiological responses of competitive time trial cyclists and triathletes in submaximal constant load exercises. The foundation of this manuscript, coupled with chapter 3, is a substantial contribution as it fulfills this study's second objective.

My contribution to this article included the design and development of experimental approaches and protocols (80%), carrying out the experiments (80%), collecting the muscle activation and kinematic data and physiological parameters (90%), analyzing the data and its statistical interpreting (100%), the design and redaction of the manuscript.

This manuscript, "The effect of different aero handlebar positions on muscle activity and kinematics of lower limb", has been submitted in the Journal of Sports Sciences in October 2020 (Ghasemi, Curnier, Caru, Pageaux, et al., 2020).

Authors:

Mojtaba Ghasemi[1], Daniel Curnier[2,3], Maxime Caru[2,3], Benjamin Pageaux[2,4], Jean-Yves Trépanier[1], Delphine Périé[1]

[1] Department of Mechanical Engineering, Polytechnique Montreal, Montreal, Canada
[2] School of Kinesiology and Physical Activity Sciences, Faculty of Medicine, University of Montreal, Montreal, Canada
[3] Research Center, Sainte-Justine University Health Center, Montreal, Canada
[4] Centre de recherche de l'institut universitaire de gériatrie de Montréal (CRIUGM), Montreal, Canada

4.1 Abstract

Using aero handlebars allows cyclists to adopt a decreased aerodynamic resistance position optimized for time trial competition. This study deals with the effects on muscle activity and kinematic variables when altering the aero handlebar position. Seven male participants cycled at 75% gas exchange threshold using six different aero handlebar positions: handlebar at the preferred time trial position (TTP), TTP 30° up, TTP 30° and 5 cm up, TTP 5 cm down, TTP 5 cm up and TTP 5 cm forward. Electromyography and kinematic data were continuously collected. The data showed a significant increase ($P < 0.01$) in gluteus maximus and decrease ($P < 0.05$) in vastus lateralis activity level in TTP 5 cm down as compared to TTP 5 cm up. The peak of ankle and knee angles of TTP 5 cm up and preferred TTP were higher ($P < 0.05$), compared to TTP 5 cm down, whereas the peak value of the hip angle of TTP 5 cm down was higher ($P < 0.05$) than TTP 5 cm up. Future studies should test whether lowering the handlebar position and associated changes in lower limbs muscle activation and kinematics could positively impact cycling time trial performance.

Keywords: movement analysis, electromyography, body position, performance, cycling

4.2 Abbreviations

ANOVA	Analysis of variance
CPET	Cardiopulmonary exercise test
EMG	Electromyography
GET	Gas exchange threshold
GMax	Gluteus maximus
MVC	Maximum voluntary contraction
RF	Rectus femoris
RMS	Root mean square
ROM	Range of motion
SD	Standard deviation
SDK	Software development toolkit
TTP	Time trial position
VCO_2	CO_2 Consumption
VE	Minute ventilation of breathing
VL	Vastus lateralis
VM	Vastus medialis
VO_{2peak}	Maximal oxygen consumption

4.3 Introduction

Reduction in aerodynamic drag, which is the dominant resistive force influencing the performance and efficiency of competitive cyclists and triathletes (Debraux et al., 2011; C. Kyle & Weaver, 2004; J. C. Martin et al., 2006), is closely related to the cyclist's body position. To minimize drag, the cyclist position should be as low as possible while simultaneously keeping the physiological responses and metabolic variables unimpaired during cycling (Fintelman et al., 2014). The time trial position (TTP) is adopted by cyclists to improve their optimal performance and lower their torso angle to reduce the frontal area (Grappe et al., 1997; Lukes et al., 2005). Adjustments to aero handlebar positions, which may be the most important adjustments when fitting a bicycle (C. Kyle, 1989; Lukes et al., 2005; Oggiano et al., 2008), allow this modified position of the upper body that is intended to decrease the frontal area and accordingly, increase the aerodynamic efficiency of the cyclist during competition. For instance, applying wind tunnel tests, Oggiano et al. (2008) found that changes in handlebar position had a greater reduction in aerodynamic drag compared to changes in seat position.

A number of studies have been carried out to compare the electromyography (EMG) and kinematics of standard cycling positions such as the dropped, upright and aero positions. It has been reported that the riding posture affects the quadriceps femoris muscle activation during cycle exercise (Hug & Dorel, 2009). Savelberg et al. (2003) showed that a 20° forward and backward trunk angle position influenced the EMG patterns compared to a vertical upright cycling position. Dorel et al. (2009) showed that riding in TTP notably affected the EMG activity of lower limb muscles crossing hip and knee joints. They reported expanded muscle activation in the gluteus maximus (GMax) in TTP compared to upright and dropped positions. Fintelman et al. (2016) examined the muscle activation of trained cyclists in a TTP at different torso angles and observed that the vastus lateralis (VL) and GMax were affected by torso angle altering while the rectus femoris (RF) remained unchanged. Chapman et al. (2008) found no leg kinematics changes when cycling in a dropped position compared with an upright position. However, Heil et al. (1997) observed an increase in the ankle, knee and hip kinematic parameters during cycling at different seat angles.

Thus, although riding in TTP has been shown to affect muscle activation, no information is available about the effect of aero handlebar position changes during TTP on muscle recruitment and joint kinematics. To the best knowledge of the authors, no published study has investigated the alteration of aero handlebar positions in TTPs and its effects on muscle activation and joint kinematics, simultaneously.

In this study, we (1) describe the muscle activation patterns of lower limb muscles and joint

kinematics, corresponding to alterations of aero handlebar positioning during TTP cycling and (2)investigate whether an aero handlebar position has advantages over others. This information has the potential to profoundly affect the assessment technique for performance optimisation and coaching perspectives. It was hypothesised that altering the handlebar position influences the lower limb joint kinematics and muscle activity.

4.4 Methods

4.4.1 Participants

Seven male competitive but non-elite cyclists and triathletes voluntarily participated in this investigation, and all were free of any recent or previous musculoskeletal disorders, deformities as well as known respiratory, cardiovascular and metabolic disease. Characteristics of participants are fully described in Table 4.2. Briefly, the participants can be included in the performance level 3-4 in the classification of subject groups in sport science research (de Pauw et al., 2013).

The experimental protocols, including any possible risks, discomforts and benefits associated with the study, were clearly explained and written informed consent was obtained from all participants before participation. The study was approved by the Ethical Committee of Polytechnique Montréal on human research (reference no CER-1819-30) and conducted in line with the Declaration of Helsinki.

4.4.2 Experimental protocols

The testing protocol consisted of two sessions conducted in the following order: (1) collecting data on the anthropometric measurements and incremental cardiopulmonary exercise test on ergocycle performed until exhaustion to establish the individual exercise intensities used in the tests performed in the subsequent visit; (2) experimental session of cycling in constant load exercise tests in six random TTPs while the kinematic and surface EMG were continuously measured during this protocol. Participants were instructed to refrain from caffeine and alcohol consumption, smoking and high-intensity training ($\geq$ 7.5 METS or anaerobic intervals or strength training) for the week before and between testing. All the experiments were conducted at $\sim$ 25°C. Aero handlebars were mounted on the ergometer during both sessions.

4.4.3 Cardiopulmonary exercise test

During the first session, participants were asked to configure their preferred TTP and adjust the handlebar height, stem length and vertical and horizontal saddle positions on the cycle ergometer – this was referred to as their "preferred" position. The preferred settings were recorded and replicated during subsequent testing sessions using a goniometer to measure all the angles and video recording to check the exact participants' preferred settings. Each participant performed a maximal cardiopulmonary exercise test (CPET) on a cycle ergometer (Excalibur Sport, Lode BV, Groningen, Netherlands) in order to assess their peak oxygen consumption ($\dot{V}O_{2peak}$). $\dot{V}O_{2peak}$ measurements were computed with a breath-by-breath system (Ultima CardiO2®, MGC Diagnostics, Saint Paul, MN, USA). The gas analyzers were calibrated with calibration gas (25% O_2 and balance N_2 and 16% O_2, 5% CO_2 and balance N_2) and air volume [3 L syringe (Roxon)] at the beginning of each session.

The protocol began with a five minute unloaded warm-up. After a two minute resting period on the cycle ergometer, a standard incremental procedure at a pedaling cadence of 60–90 rpm was started at 75 W for three minutes. The ramp increase was 20 W/min until the participant's voluntary exhaustion, despite strong verbal encouragement. The participants had to reach two out of four of the following criteria in order to establish the $\dot{V}O_{2peak}$: (1) A plateau in $\dot{V}O_{2peak}$ despite an increased workload; (2) a respiratory exchange ratio value > 1.15; (3) a rated perceived exertion > 7 (Borg Scale CR10, (Borg, 1998)); and (4) heart rate $\geq 85\%$ of the predicted value using the equation (208-[0.7×age]) as indicated by Tanaka et al. (2001). The participants were then monitored for an additional 6 minutes of passive recovery.

4.4.4 Submaximal constant load exercise tests

In the second session, six submaximal constant-load exercise conditions at 75% of the determined gas exchange threshold (GET) were investigated. This intensity-duration was chosen close to that reported in previous investigations (Grappe et al., 1998; Origenes et al., 1993), without the risk of early fatigue (Blake et al., 2012; Tordi et al., 2003). To obtain the moderate-intensity workloads (75% of GET), the GET was visually determined by two of the laboratory team members as the point during incremental exercises at which ($\dot{V}E/\dot{V}O_2$) ratio increased without any change in the ventilatory equivalent for CO_2 ($\dot{V}E/\dot{V}CO_2$). The protocol of constant load exercise tests consisted of six blocks of six minutes at a power corresponding to 75% of GET. Participants were tested in a randomized order, under six time trial body positions: (1) handlebar 30° up from the preferred position (TTP 30° up);

(2) handlebar 30° and 5 cm up from the preferred position (TTP 30° and 5 cm up); (3) handlebar 5 cm down from the preferred position (TTP 5 cm down); (4) handlebar 5 cm up from the preferred position (TTP 5 cm up); (5) preferred TTP; (6) handlebar 5 cm forward from the preferred position (TTP 5 cm forward), as shown in Figure 4.1. The angle between the upper arms and the torso was constant across all trials and based on the participants' preferred TTPs. Participants performed a five-minute warm-up at a preferred pedaling rate. Each position was tested for six minutes followed by six minutes of passive recovery to avoid fatigue throughout the session. Participants were asked to maintain the constant preferred pedaling rates, chosen at the end of the warm-up period, throughout the session, while the kinematic variables and surface EMG were collected continuously during each ride. This sequence was followed until all six conditions were tested. All the adjustments to the aero handlebars was performed during the rest, and the angles were measured using a goniometer.

4.4.5 Electromyography (EMG)

Surface EMG activity during cycling was continuously recorded for the following four muscles of the right lower limb: gluteus maximus (GMax), rectus femoris (RF), vastus medialis (VM) and vastus lateralis (VL). These lower limb muscles were selected based on their major contribution to produce pedaling movement and power generation in cycling (Chin et al., 2011; Hug, Bendahan, et al., 2004; Li, 2004; MacIntosh et al., 2000) and their possible differences among different racing body positions (Dorel et al., 2009). Four disposable bipolar EMG electrodes (Covidien Kendall) were positioned longitudinally over each muscle belly, according to the recommendations by Surface EMG for Non-Invasive Assessment of Muscles (SENIAM) (Hermens et al., 2000), with an interelectrode distance of 20 mm. The reference electrode was placed at the knee. Before electrode application, all sites were prepared by shaving, abrading and cleaning the skin with alcohol swabs to minimize impedance. The wires connected to the electrodes were well-secured to the leg with adhesive tape to minimize any movement artifacts during the exercise.

Raw EMG signals were recorded by an eight-channel PowerLab (ADInstruments, Australia) running LabChart 8 software (ADInstruments), with a bandpass filter at 6-500 Hz and a sampling rate of 2000 Hz. To diminish movement artifacts, a high-pass filter (5th order zero-phase lag Butterworth) at 10 Hz was further applied on the EMG. Maximum voluntary contraction (MVC) of each muscle group was performed before each participant commenced the pedaling trials. MVCs were performed against gravity and manual resistance in standardised testing positions, using a short-seated position for RF, VM and VL and a prone position with the knee flexed for GMax. Participants performed three repetitions of five

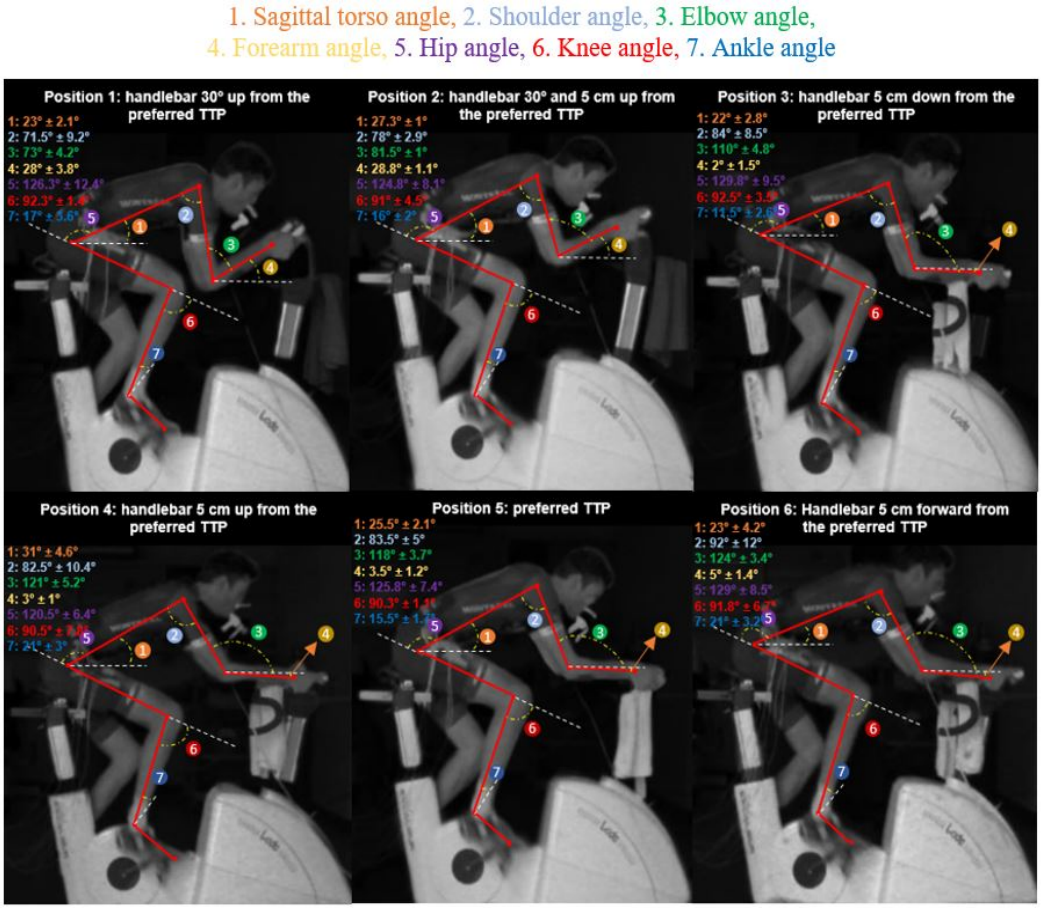

Figure 4.1 The six cyclist positions with definition and values (mean ± SD) of (1) sagittal torso angle; (2) shoulder angle; (3) elbow angle; (4) forearm angle; (5) hip angle; (6) knee angle; (7) ankle angle. Position 1, time trial position (TTP) 30° up; Position 2, TTP 30° and 5 cm up; Position 3, TTP 5 cm down; Position 4, TTP 5 cm up; Position 5, preferred TTP; Position 6, TTP 5 cm forward.

seconds for each assessment, with at least 30 seconds of rest between repetitions to reduce the likelihood of fatigue. The maximum EMG root mean square (RMS) value of each muscle was determined as the average of the three highest values from the MVC trials. These values were then used to normalize subsequent EMG data.

Using the rectified and smoothed data, the timing of EMG onset and offset thresholds were determined as 20% of the maximum EMG value obtained in each trial (Li & Caldwell, 1998). Raw EMG data of every muscle of every participant was rectified, and RMS envelope with a window of 25 ms was applied. The RMS value of each muscle was normalized to the maximum values of the MVC trials. The processed RMS signals were then analysed by creating the ensemble averages over 10 consecutive crank revolutions during the last two minutes of each

effort, to provide a reasonable and enough interval for an individual to reach a steady state. The RMS of all participants was plotted against the crank angle as it rotated from the highest pedal position, top dead center, to the lowest, bottom dead center and then back to top dead center to complete a 360° crank cycle.

4.4.6 Kinematic evaluation

Right lower limb kinematics were measured using the markerless motion capture system (Kinect, Microsoft Corp., USA) during submaximal cycling. Data were collected at 30 Hz from the right-side view where the Kinect was perpendicular to the sagittal plane. The kinematic and EMG data were synchronized using signals sent via the ADInstruments software (LabChart 8, Australia). The acquisition of each participant was done separately, without altering the Kinect position or its distance from the cycle ergometer. The position of the Kinect and cycle ergometer was marked on the floor with taped to secure reproducibility between sessions. The Kinect was set on tripods at a height of 1.2 m with its axes parallel to the horizontal floor surface, at a distance of 2 m from where the ergometer was positioned. The integrated sensor software development toolkit (SDK, Microsoft Corp.) was used to detect the location of the joints of the participants. Data were smoothed using the Sobel filter, with a cut-off frequency at 10 Hz. The positions of lower limb joints at each frame were determined through data processing (MATLAB, Math Works, USA).

The positions of the hip, knee, ankle and toe (fifth metatarsal head) were derived from the Kinect measurements. The joint positions were used to calculate the ankle, knee and hip joint angles and joint angular velocity, after which the mean joint angle, angular velocity and range of motion at the hip, knee and ankle were computed. Mean joint angles and angular velocities were an average over 10 consecutive crank revolutions during the last two minutes of each effort, and the range of motion was defined as the difference between maximum and minimum joint angle displacement values. These parameters were used to illustrate the overall excursion of the right leg throughout a complete cycling pattern.

4.4.7 Statistical analysis

Statistical analyses were conducted using the statistical package SPSS Version 26.0 (SPSS Inc., Chicago, IL). All variables were reported as mean ± standard deviation (SD). To confirm the assumption of normally distributed data sets and sphericity, the Shapiro–Wilk and Mauchly tests were conducted, respectively. The Greenhouse-Geisser correction factor was applied when sphericity was violated. Repeated measures of analyses of variance (ANOVA)

were performed on all kinematic and muscle activation parameters to test the effect of the six TTPs. In the case of a significant main effect, Bonferroni post-hoc tests were used to determine the sources. Statistical significance was set at $P < 0.05$. The effect size is reported as partial eta squared (η_p^2) and Cohen's d for pairwise comparisons where $d \geq 0.80$ was considered large (Lakens, 2013).

4.5 Results

4.5.1 Participants

A total of seven male competitive cyclists and triathletes whose characteristics are provided in Table 4.2, were included in our study. All participants who were included in our analyses had completed the maximal CPET.

Table 4.2 Characteristics of participants (mean ± SD, N = 7).

Variables	Mean ± SD
Age (years)	29.6 ± 7.5
Body mass (kg)	73.6 ± 4.6
Stature (cm)	182.9 ± 7.4
Peak oxygen consumption ($mL.kg^{-1}.min^{-1}$)	61.4 ± 11.3
Peak power output (W)	357.9 ± 53.5
Oxygen consumption at GET ($mL.kg^{-1}.min^{-1}$)	47.4 ± 7.3
Power output at GET (W)	246.4 ± 36.3
Power output at 75% of GET (W)	184.6 ± 27.2
Peak respiratory exchange ratio	1.42 ± 0.1
Rating of perceived exertion at CPET exhaustion	10.0 ± 0.0
Peak heart rate (bpm)	183.6 ± 12.4
Average weekly cycling distance (km/week)	286 ± 74
Years of racing (years)	5.6 ± 2.4

4.5.2 Electromyography (EMG)

Figure 4.2 presents muscle activity patterns of all the six trial conditions (seven participants per condition), with ensemble linear envelopes of the RMS EMG data for each of the four investigated muscles.

The mean normalized RMS EMG measured during the entire crank rotation for each individual, as well as all the muscles (sum RMS EMG), are represented in Figure 4.3. There was a significant interaction between the handlebar positions and GMax activation ($P =$

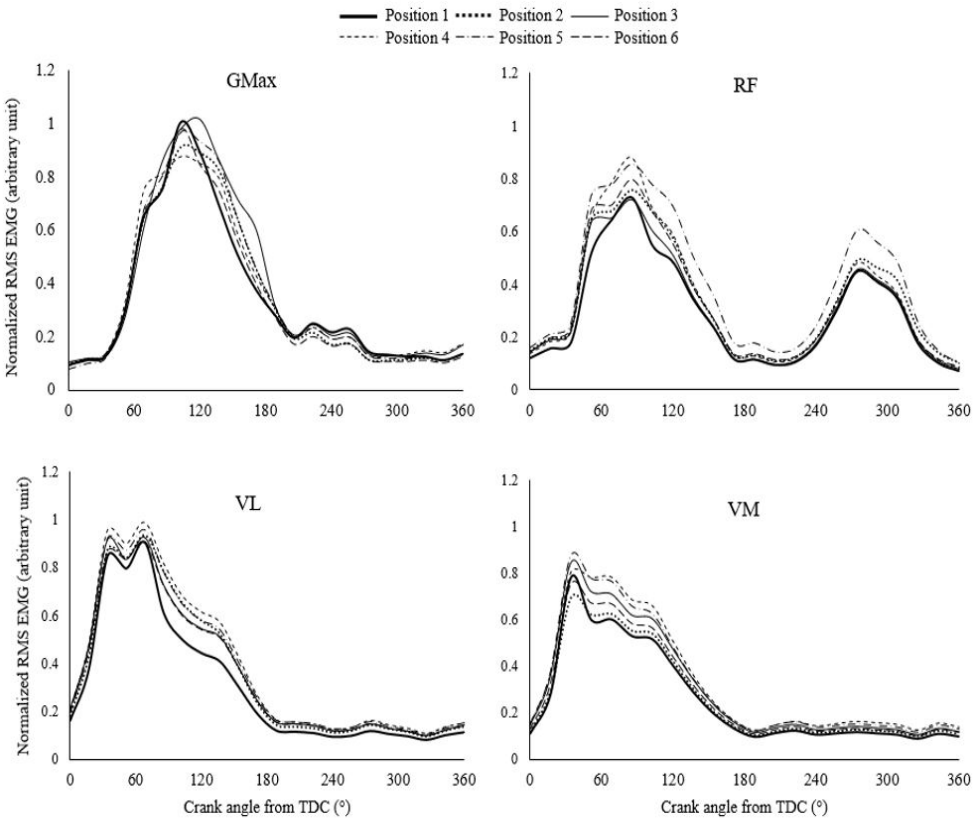

Figure 4.2 Ensemble curves of normalized electromyography (EMG) root mean square (RMS) linear envelope across 10 consecutive pedaling cycles for gluteus maximus (GMax), rectus femoris (RF), vastus lateralis (VL) and vastus medialis (VM) for all time trial body positions. Position 1, time trial position (TTP) 30° up; Position 2, TTP 30° and 5 cm up; Position 3, TTP 5 cm down; Position 4, TTP 5 cm up; Position 5, preferred TTP; Position 6, TTP 5 cm forward. Pedaling cycle rotated from the highest pedal position TDC (top dead center, 0°) to the lowest pedal position BDC (bottom dead center, 180°) and back to TDC to complete a 360° crank cycle.

0.004, $\eta_p^2 = 0.370$), RF activation ($P = 0.041$, $\eta_p^2 = 0.221$) and VL activation ($P = 0.012$, $\eta_p^2 = 0.322$). There was no significant interaction between the handlebar positions and muscle activity for VM ($P = 0.294$, $\eta_p^2 = 0.151$). TTP 5 cm down, Preferred TTP and TTP 5 cm forward induced greater ($P = 0.011$, d =0.846; $P = 0.042$, $d = 0.698$; $P = 0.013$, $d = 1.377$, respectively) muscle activity than TTP 30° and 5 cm up for GMax. Furthermore, GMax activity was significantly greater ($P = 0.007$, $d = 1.011$) for TTP 5 cm down as compared to TTP 5 cm up, and the mean value of the RMS EMG of RF was greater ($P = 0.032$, $d = 0.973$) in preferred TTP, as compared to TTP 30° and 5 cm up. A significantly greater mean value of RMS EMG was observed in TTP 5 cm up than TTP 5 cm down ($P = 0.035$, $d = 0.880$) for VL. No significant difference in VM was found between the six TTPs. The

sum RMS EMG mean values was greater in positions preferred TTP and TTP 5 cm down, compared to other positions. However, the only significant change was that it was higher (P = 0.019, d = 0.823) in preferred TTP than TTP 30° and 5 cm up.

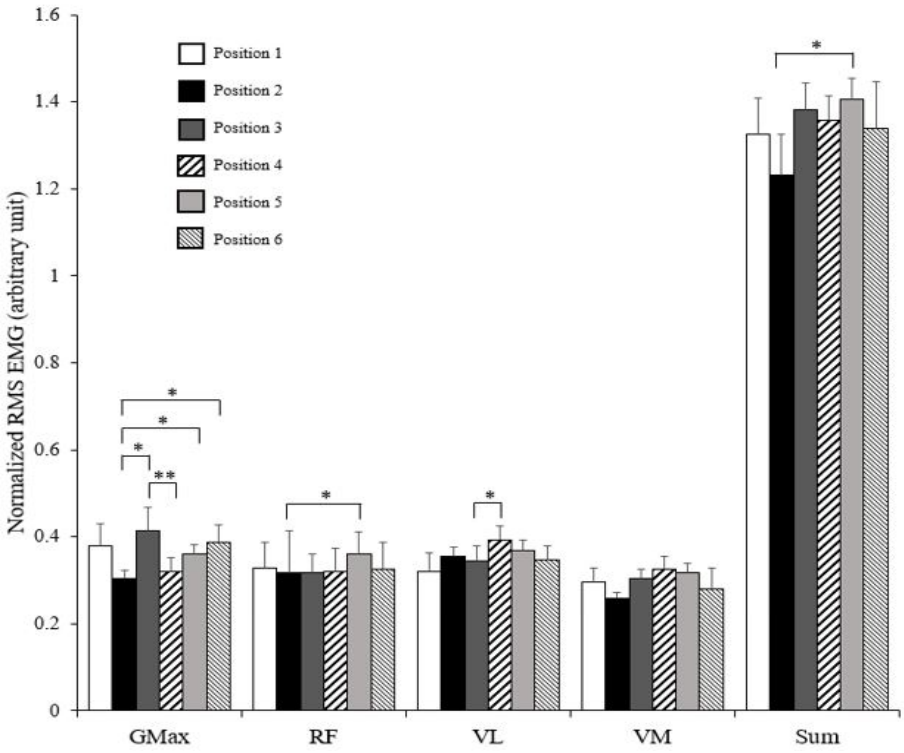

Figure 4.3 Mean (±SD) values of the normalized RMS muscle activity of individual muscles and cumulative summation (sum) of muscle activity for the complete cycle (0 to 360°) for the six body positions. $^{*}P < 0.05$ and $^{**}P < 0.01$ significant difference between conditions. GMax, gluteus maximus; RF, rectus femoris; VL, vastus lateralis; VM, vastus medialis. Position 1, time trial position (TTP) 30° up; Position 2, TTP 30° and 5 cm up; Position 3, TTP 5 cm down; Position 4, TTP 5 cm up; Position 5, preferred TTP; Position 6, TTP 5 cm forward.

Figure 4.4 depicts the mean values of the onsets, offsets and duration of the EMG burst. Regarding onset, there was a significant interaction in GMax (P = 0.006, η_p^2 = 0.492), and a non-significant interaction in RF (P = 0.446, η_p^2 = 0.138), VL (P = 0.459, η_p^2 = 0.140) and VM (P = 0.625, η_p^2 = 0.119). The onset of the GMax burst appeared significantly later during the pedal cycle when lowering the handlebar. The onset in TTP 5 cm down occurred significantly later, compared to the TTP 5 cm up and TTP 30º and 5 cm up (P = 0.003, d = 0.922; P = 0.033, d = 0.711, respectively). Moreover, the onset in TTP 5 cm forward (P = 0.036, d = 0.676) occurred significantly later, compared to TTP 5 cm up. Additionally,

significant differences in offset between the handlebar positions were observed for VL ($P = 0.008$, $\eta_p^2 = 0.421$) and VM ($P = 0.042$, $\eta_p^2 = 0.234$). The offset of VL and VM activation occurred later in TTP 5 cm down ($P = 0.005$, $d = 1.242$; $P = 0.046$, $d = 0.650$, respectively), compared to TTP 5 cm up. However, no significant interaction was detected in GMax ($P = 0.310$, $\eta_p^2 = 0.142$) and RF ($P = 0.157$, $\eta_p^2 = 0.181$).

Results showed that the duration of the GMax muscle activation was significantly shorter ($P = 0.038$, $d = 0.963$) in TTP 5 cm down than TTP 5 cm up. No statistically significant interaction between the cycling conditions and duration of muscle activity in RF ($P = 0.492$, $\eta_p^2 = 0.154$), VL ($P = 0.224$, $\eta_p^2 = 0.154$) and VM ($P = 0.324$, $\eta_p^2 = 0.126$).

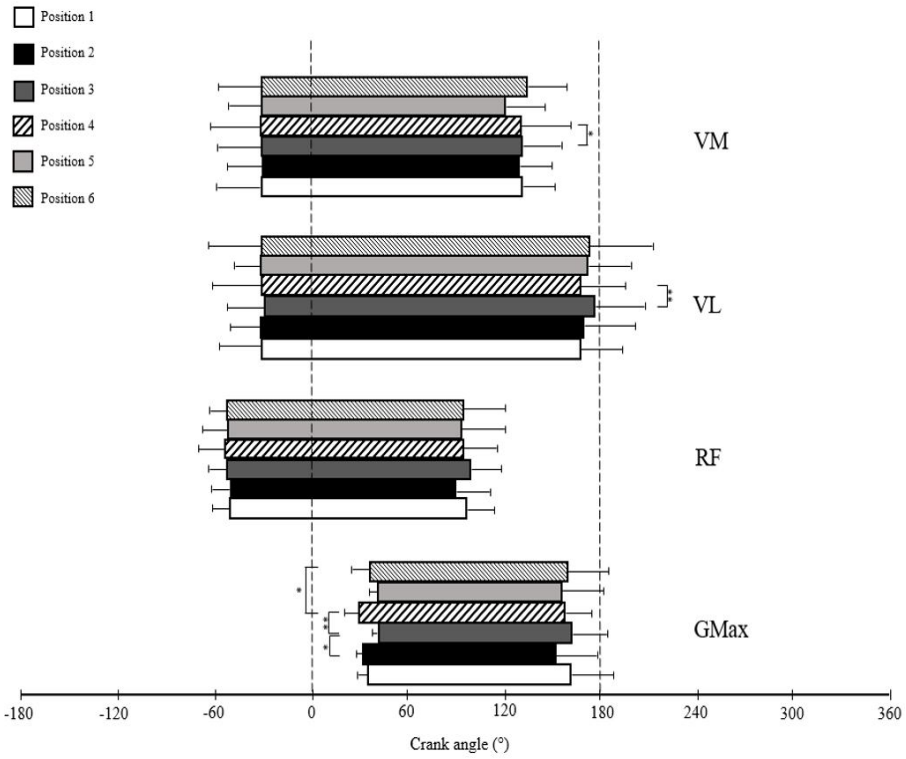

Figure 4.4 Mean onset, offset and duration (mean ± SD) of EMG linear envelopes, based upon crank angle from top dead center (TDC) among the different cycling positions. $^{*}P < 0.05$ and $^{**}P < 0.01$ significant difference between conditions. GMax, gluteus maximus; RF, rectus femoris; VL, vastus lateralis; VM, vastus medialis. Position 1, time trial position (TTP) 30° up; Position 2, TTP 30° and 5 cm up; Position 3, TTP 5 cm down; Position 4, TTP 5 cm up; Position 5, preferred TTP; Position 6, TTP 5 cm forward.

4.5.3 Kinematics

The markerless motion capture system performed very well during the submaximal tests. A sample size of 18 angle and ROM values, with three joint measurements per handlebar position, allows estimating the differences of kinematic parameters. The Bland-Altman graphs in Figure 4.5 show that the plotted differences lie within the 95% confidence interval, which indicates a good agreement between the measurements of all the positions.

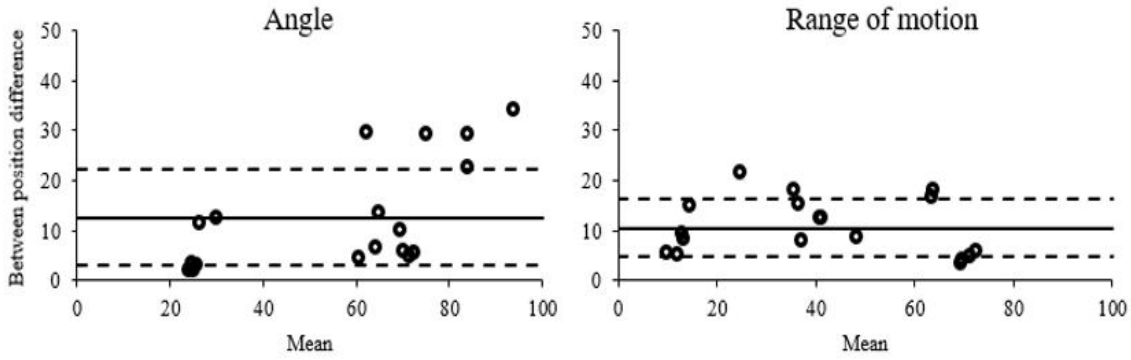

Figure 4.5 Bland-Altman plots for selected kinematic parameters: angle (deg); and range of motion. The upper and lower dashed lines represent the 95% confidence interval, while the solid line represents the mean difference between positions.

Joint kinematics were compared for the six TTPs using the peak values of angles and angular velocities and the range of motion (ROM) for each lower joint (Table 2). Statistically significant differences in the joint peak angle between handlebar positions were observed for the ankle ($P = 0.039$, $\eta_p^2 = 0.247$), knee ($P = 0.044$, $\eta_p^2 = 0.164$) and hip ($P = 0.021$, $\eta_p^2 = 0.346$). Further analysis showed that the peak angle of the ankle in TTP 5 cm up and preferred TTP were higher ($P = 0.016$, $d = 1.892$; $P = 0.017$, $d = 1.232$, respectively), compared to TTP 5 cm down. Knee peak angle was significantly increased at TTP 5 cm up compared to TTP 5 cm down ($P = 0.047$, $d = 0.888$). A higher range of hip peak angle value was observed in TTP 30^o up, TTP 5 cm down and TTP 5 cm forward (P =0.031, $d = 0.717$; $P = 0.018$, $d = 0.910$; $P = 0.014$, $d = 1.289$, respectively) than in TTP 5 cm up.

Significant differences between the joint ROM were only found for the ankle (P =0.028, $\eta_p^2 = 0.252$). Ankle ROM in TTP 5 cm up was higher than in TTP 30^o up ($P = 0.035$, $d = 0.844$) and TTP 5 cm down ($P = 0.026$, $d = 1.071$). No significant differences were observed in ROM for the knee (P =0.495, $\eta_p^2 = 0.111$) and hip (P =0.469, $\eta_p^2 = 0.115$).

There was a significant difference in the peak angular velocity for the ankle (P =0.027, η_p^2

Table 4.3 Comparison of kinematic variables across positions.

Kinematic Variables		Position 1	Position 2	Position 3	Position 4	Position 5	Position 6
Sagittal torso angle (°)		23.0 ± 2.1	27.3 ± 1.0	22.0 ± 2.8	31.0 ± 4.6	25.5 ± 2.1	23.0 ± 4.2
Shoulder angle (°)		71.5 ± 9.2	78.0 ± 2.9	84.0 ± 8.5	82.5 ± 10.4	83.5 ± 5.0	92.0 ± 12.0
Elbow angle (°)		73.0 ± 4.2	81.5 ± 1.0	110.0 ± 4.8	121.0 ± 5.2	118.0 ± 3.7	124.0 ± 3.4
Peak angle (°)	Ankle	30.3 ± 14.8	34.1 ± 7.3	28.4 ± 6.3	39.6 ± 2.6*	35.5 ± 4.9*	30.4 ± 3.3
	Knee	98.3 ± 8.3	95.6 ± 20.6	92.8 ± 11.6	104.2 ± 4.8*	103.7 ± 7.2	103.5 ± 6.2
	Hip	101.8 ± 26.2†	96.1 ± 28.1	115.6 ± 31.0	84.5 ± 27.8*	97.0 ± 8.7	104.8 ± 18.9†
Range of motion (°)	Ankle	14.8 ± 5.3†	13.6 ± 10.9	16.1 ± 5.0	12.0 ± 21.5*	13.0 ± 9.1	14.4 ± 8.3
	Knee	71.4 ± 4.7	73.5 ± 16.7	74.1 ± 17.8	72.6 ± 5.7	70.0 ± 4.0	69.7 ± 3.4
	Hip	40.9 ± 12.4	41.4 ± 12.3	35.9 ± 18.1	36.8 ± 15.2	48.6 ± 8.6	37.2 ± 7.7
Peak angular velocity (deg/s)	Ankle	73.3 ± 35.9	108.2 ± 85.4	62.9 ± 26.9	120.9 ± 46.8*	100.0 ± 58.2	72.9 ± 29.4†
	Knee	315.7 ± 23.2	294.5 ± 65.6	287.9 ± 62.7	328.5 ± 38.2	306.0 ± 12.6	326.9 ± 30.8
	Hip	221.4 ± 86.4	190.0 ± 27.9	235.9 ± 92.7	176.0 ± 70.7*	190.0 ± 53.3	212.2 ± 39.1†

Values are means ± SD. *Significantly different from TTP 5 cm down ($P < 0.05$). † Significantly different from TTP 5 cm up ($P < 0.05$). Position 1, TTP 30° up; Position 2, TTP 30° and 5 cm up; Position 3, TTP 5 cm down; Position 4, TTP 5 cm up; Position 5, preferred TTP; Position 6, TTP 5 cm forward.

= 0.189) and hip (P =0.024, η_p^2 = 0.292) between cycling conditions, whereas no significant results were observed for the knee (P =0.408, η_p^2 = 0.127). The ankle and hip showed a significantly higher angular velocity (P = 0.043, d = 0.825; P = 0.015, d = 1.245) in TTP 5 cm up compared to TTP 5 cm down and TTP 5 cm forward. Additionally, Figure 4.6 represents ensemble mean joint angles and joint velocities for the ankle, knee and hip. Joint angle and angular velocity values displayed clear extension and flexion phases within each crank cycle.

4.6 Discussion

This study demonstrated the effect of different aero handlebar positions on lower limb muscle activation patterns and kinematic variables under submaximal intensity. Our study was dedicated to alterations in handlebar positions while keeping the participants' preferred saddle time trial positions constant. Compared to other positions, the aero handlebar with the lowest height resulted in more GMax activity and hip extension angle. These findings supported our hypothesis that altering the aero handlebar position would affect the lower limb joint kinematics and muscle activity. Alterations of aero handlebar positions, which are the most critical adjustments when fitting a bicycle (Chiu et al., 2013), allows a cyclist to find the perfect TTP that is aerodynamically optimized during competitions.

4.6.1 Electromyography (EMG)

The results showed that the normalized intensity and timing of lower extremity EMG activity were significantly influenced by changing the handlebar position. Lowering the handlebars in TTP 5 cm down and TTP 5 cm forward resulted in lowering the sagittal torso angle as compared to TTP 5 cm up (41% and 35%, respectively), and therefore caused a significant alteration of the EMG patterns, compared to the elevated handlebars in TTP 30° and 5 cm and TTP 5 cm up. TTP 30° and 5 cm up showed the least GMax activity, while TTP 5 cm down with the lowest sagittal torso angle resulted in the greatest GMax activity. The normalized RMS EMG values tended to be lower for biarticular RF compared to the monoarticular muscle GMax for all the six positions. These findings are in close agreement with the previous findings of increasing the GMax activity in the time trial condition (Elmer et al., 2010; J. C. Martin & Brown, 2009). Moreover, the only significant difference in the biarticular muscle RF was for the preferred TTP versus TTP 30° and 5 cm. This can be related to the synergistic activation of RF as the hip extensor with other hip extensors as a single muscle group in the preferred TTP position. The corresponding changes for the VL

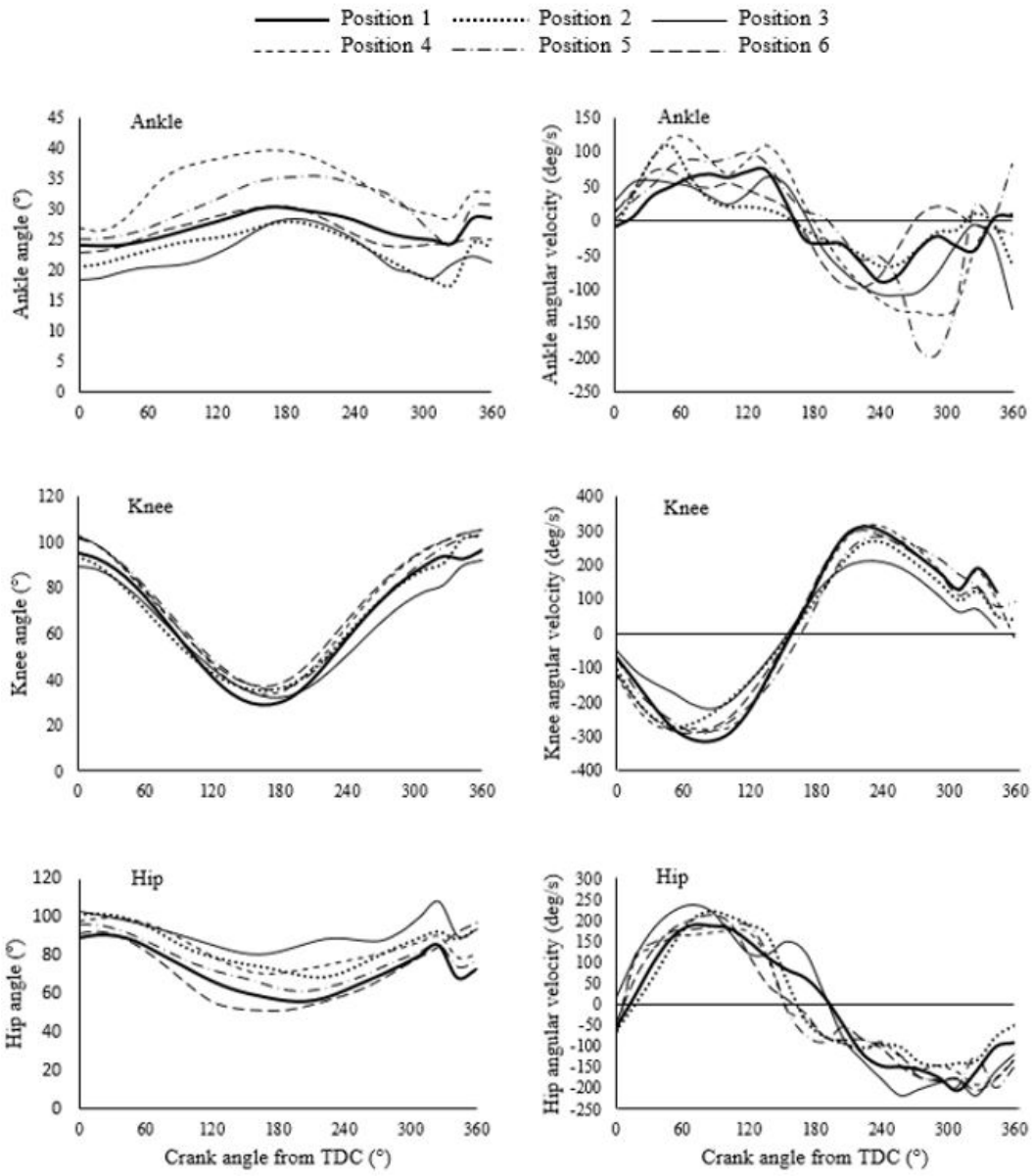

Figure 4.6 Mean curves of joint angles (left) and joint angular velocities (right). Hip and knee angles are 0 at full extension, and ankle angle is 0 in standard anatomical position (90° included angle). The positive direction was set for hip flexion, knee flexion and dorsiflexion for the ankle. Position 1, time trial position (TTP) 30° up; Position 2, TTP 30° and 5 cm up; Position 3, TTP 5 cm down; Position 4, TTP 5 cm up; Position 5, preferred TTP; Position 6, TTP 5 cm forward.

were of smaller magnitude for TTP 5 cm down versus TTP 5 cm up. Although the VM activity for TTP 5 cm down were generally lower than TTP 5 cm up, this difference was not consistent across all participants. The monoarticular knee extensors (VM, VL) may need help from the biarticular RF muscle to forcefully extend the knee joint. RF crosses the knee and hip joints to extend the knee and flex the hip simultaneously (Gregor et al., 1991). The sum RMS EMG of the four lower limb muscles was significantly decreased by 14.2% for TTP 30° and 5 cm up versus preferred TTP. The increased sum RMS EMG could be explained by the changes in the hip extensor RF. While the EMG activation of GMax is directly related to the sagittal torso angle, there is no such direct relationship for the RF. It has been seen in previous studies that the monoarticular muscles show a greater effect in muscle activity when changing position (Li & Caldwell, 1998), and therefore preferred TTP was less affected by changing the handlebar positions. While no other comparative study is available in the field of handlebar position alteration in TTPs, a few studies have been conducted on the effect of lowering the sagittal torso angle on the lower extremity muscle activity patterns, reporting increased muscle activation by lowering the sagittal torso angle (Dorel et al., 2009; Duc et al., 2008; Fintelman et al., 2016; Savelberg et al., 2003), which is consistent with our results for muscle activation patterns. However, since we altered the handlebar position and applied it during the TTPs, we cannot directly compare our results with those of the aforementioned studies.

Although the EMG timing patterns are similar among the six TTPs, changes in the handlebar position led to a later onset for GMax activation (Figure 4.4). In TTP 5 cm down and TTP 5 cm forward, the onset of GMax activation shifted later in the crank cycle, which may suggest that the cyclists changed their pedaling technique through the hip extension during the first (0° to 90°) and second (90° to 180°) quadrants, by lowering and moving forward the handlebar, respectively. Previous literature has shown that the greatest activity for GMax occurs from the beginning of pedaling the cycle through the second quadrant, while the hip is extending (Dorel et al., 2009; Gregor et al., 1991). Similarly, in this study, the GMax was activated from the middle of the first quadrant to a crank angle of about 120° during the second quadrant (Figure 4.2). Although GMax showed a greater normalized RMS EMG activity for TTP 5 cm down as compared to TTP 5 cm up, the EMG timing revealed a significant reduction in the burst duration of GMax for TTP 5 cm down. EMG offset occurred significantly later for VL and VM in TTP 5 cm down as compared to TTP 5 cm up, whereas the biarticular knee flexor RF appeared unchanged. The VL and VM were both activated from the middle of the fourth quadrant (270° to 360°) to the middle of the second quadrant, while the RF was active between approximately 300° until the end of the first quadrant. Later GMax onset on one side, and lower RF activity and unchanged onset

on the other side, suggest that the relative contribution of the hip and knee extensors to power production during the second quadrant in TTP 5 cm down changed in favour of hip extensors. These findings agree reasonably well with the previously reported effects of cyclist position changes on the onset and offset patterns of EMG timing (da Silva et al., 2016; Dorel et al., 2009; Fintelman et al., 2016). Our results confirmed the results of Fintelman et al. (2016), who reported that alterations in the torso angle would only affect the monoarticular muscles. Despite the changes of EMG activity, the effect of these changes on force production cannot be quantified, and therefore precisely predicting the joint moment changes associated with alteration in handlebar position remains difficult. Future studies using prediction of the force produced from the EMG activity (Olney & Winter, 1985; Pedersen et al., 1987; Redfield & Hull, 1986) may be of interest to provide additional information on the impact of manipulating handlebars position.

4.6.2 Kinematics

The kinematic assessments of different handlebar positions illustrate the importance of the characteristics of the lower limbs during cycling in different TTPs, and avoiding positions previously associated with injury. Moreover, optimizing handlebar position by matching the joint flexion angle to the optimal for power production is beneficial for cycling efficiency (Savelberg et al., 2003). To the best of our knowledge, this is the first study to evaluate the kinematic variables of the lower limb in different aero handlebar positions. Our results showed that the changes in the handlebar position highlighted a difference of 11.2°, 11.7° and 31.1° in the peak angle of ankle, knee and hip joints, respectively. There was a significant increase in peak values of angle and angular velocity of the ankle and the peak of the knee (Table 4.3), by moving the handlebar upwards, from TTP 5 cm down to TTP 5 cm up, while the ROM of both the ankle and knee decreased. Similar results were obtained by Heil et al. (1997); they reported the increase in kinematic variables in ankle, knee during pedaling with torso angle in the range of 20° to 30°. Sanderson et al. (2006) showed that changes in joint angles may cause muscles to operate in a more productive portion of length-tension curves. The increase of the peak knee angle and reduction of ROM with the upward movement of handlebars from TTP 5 cm down to TTP 5 cm up illustrate an increased extensor muscle VL and VM's length and reduced range of lengthening, respectively. These changes in the muscle length can be associated with the enlargement of muscle activity (Sanderson et al., 2006), which was confirmed by our EMG results. For the hip joint, the greater GMax activity in TTP 5 cm down could also be related to changes in joint kinematics, since the hip joint showed the higher peak hip flexion, which is estimated to be 31.1° between TTP 5 cm down

and TTP 5 cm up. We did not observe differences in hip joint ROM, which could be explained by the function of the biarticular RF muscle. The decline in the hip angle, which is caused by the increase of the sagittal torso angle, can affect the hip flexor RF, and therefore the hip ROM.

Our findings suggest that altering the handlebar positions affects the muscles' activity, kinematics of leg movements and their association. We observed that lowering the handlebar height during the first and second quadrants increased hip extensor muscle (GMax) activation. However, moving the handlebar in TTP 5 cm forward stretched the GMax (hip extensor) slightly and shortened the RF (hip flexor) effectively by this forward tilt, becoming less effective. Our results showed that although the long-term adaptation to the preferred TTP can be the optimal cycling position, hip extensors' increased contribution in TTP 5 cm down might outweigh a reduced contribution from hip flexor. Furthermore, changing the handlebar position forward and down increased the hip's peak angle, caused a deeper pedaling, and allowed the foot to pass over top dead center, leading to retaining the power drop. Cyclists could increase the pedal stroke's power, leading to greater pedaling efficiency when moving the aero handlebar downward since the power phase occurs when the hip extends (Baum & Li, 2003; Bijker et al., 2002). Therefore, it is believed that the TTP 5 cm down is the most beneficial performance-related positions among the investigated ones. All the tests were conducted under racing conditions, i.e., use of clip pedals, time trial posture and workload, which caused no joint over-flexion and over-extension. Using our results, researchers and bike fitters can avoid the excessively lower handlebar height.

4.7 Limits

The effects of handlebar position on EMG activity and kinematics can be more widely applied if both trained and novice cyclists are investigated. In addition, the effect of variation of pedaling cadence, which influences the EMG activity and kinematics variables (Baum & Li, 2003; Sanderson et al., 2006), has not been included. The alternations in the handlebar position were tested without changing the saddle height and orientation. This could impose a practical limitation on our results since cyclists and triathletes commonly modify the handlebar position and saddle height at the same level so that they maintain a relatively similar torso angle when handlebar position is changed. Although the markerless motion capture system was expected to perform reasonably well during the submaximal tests (Bonnechere et al., 2014; Choppin et al., 2014; Dutta, 2012), some limitations might be present. For instance, the Kinect might lose its reference point due to unknown reasons and therefore translate a slight accuracy error into incorrect joint center calculations. Thus, the markerless

system has yet to be further validated against the cycling kinematic gold standard data of a marker-based motion capture system.

The EMG activity was only collected from the right leg. Therefore, future research should record EMG from both lower limbs as well as the effective pedal force, which represents cyclists' pedaling technique (Menard et al., 2016; Mornieux et al., 2008), at varying aero handlebar adjustments. In addition, it is unclear if the lower limb joint kinematics is affected by the workload level. Further analysis of EMG and kinematic data, across a range of pedaling cadences and workload is essential to thoroughly assess the biomechanical responses of different handlebar positions.

4.8 Conclusion

This study investigated the lower limb kinematics and muscle activities during submaximal pedaling in various aero handlebar positions, using a markerless motion capture system. Results demonstrated that altering the aero handlebar position affected the pattern and timing of muscles crossing the hip (GMax, RF) and knee joints (VL and VM)) significantly. Lowering the handlebar down in TTP 5 cm modified EMG activity (increase GMax and decrease VL) and EMG timing (shifted onset for GMax and shifted offset for VL and VM) compared to the positions with the elevated handlebar. These modifications are strongly related to the changes of hip extension angle during the first and second quadrants, whereas the hip had the highest peak of angles and angular velocity when lowering the handlebar, caused an increase in the pedal stroke's power. It is not straightforward to establish whether an individual handlebar position is optimal; however, from the results, adapting to the TTP 5 cm down might likely improve the cycling performance with the greater contribution of GMax and extended hip angle.

4.9 Perspectives

This research indicated that altering the aero handlebar position during cycling influenced muscle activity and joint level kinematics, contributing to more insight into biomechanical adjustments of cyclist body position to altered cycling configurations. The present outcomes provide practical understanding to researchers, clinicians and coaches in search of an optimal handlebar position regarding the changes of muscle recruitment and kinematic parameters in different TTPs. Our investigation stands out from others due to our use of a feasible, applicable and affordable markerless motion capture system to examine the biomechanical performance of handlebar setup. Our study highlights the significance and potential of de-

tailed analysis of the handlebar position since we identified that lowering the handlebar height could improve the biomechanical cycling performance. Nevertheless, from an optimization perspective, considering the metabolic responses and aerodynamic aspects of handlebar alteration remains of primary importance to improve cycling performance during submaximal exercise and for a considerably longer period, which has a more pronounced effect on neuromuscular responses and performance parameters such as time to exhaustion and work-to-rest ratio.

4.10 Disclosure of interest

The authors declare no conflict of interest in relation to the research presented in this manuscript.

4.11 Acknowledgements

We thank all participants for devoting their time and energy to our study.

CHAPTER 5 ARTICLE 3: THE EFFECT OF DIFFERENT AERO HANDLEBAR POSITIONS ON AERODYNAMIC AND GAS EXCHANGE VARIABLES

This article represents a detailed aerodynamic analysis and metabolic functions of altering the time trial handlebar position. This analytical investigation on the existing modifications of the handlebar position proposes an overall optimized improvement to the cyclist performance.

My contribution to this study included the conceiving, planning the experiments (80%), along with performing the exercise bouts (90%), designing the model, developing the computational framework and the numerical simulations, analyzing the data (100%), writing the manuscript and its redaction.

This manuscript, "The effect of different aero handlebar positions on aerodynamic and physiological variables", has been submitted in the Journal of Biomechanics in October 2020 (Ghasemi, Curnier, Caru, Trépanier, et al., 2020).

Authors:

Mojtaba Ghasemi[1], Daniel Curnier[2], Maxime Caru[3], Jean-Yves Trépanier[1], Delphine Périé[1]

[1] Department of Mechanical Engineering, Polytechnique Montreal, Montreal, Canada
[2] Department of Kinesiology, University of Montreal, Montreal, Canada
[3] Laboratory of Pathophysiology of EXercise (LPEX), School of Kinesiology and Physical Activity Sciences, Faculty of Medicine, University of Montreal

5.1 Abstract

Adopting the time trial position (TTP) represents a notable improvement for cycling aerodynamic performance. Aero handlebars are designed to enable the cyclist to adopt a more aerodynamic TTP. However, it is unclear to what realistic extent the aero handlebar configuration affects the aerodynamics and physiological functioning. Thus this study aimed to investigate the effect of aero handlebar alterations on physiological parameters and aerodynamics of TTP. Seven male competitive cyclists and triathletes performed submaximal tests on a cycle ergometer at six different TTPs. Oxygen uptake, respiratory exchange ratio, minute ventilation and tidal volume were collected. Using the computational fluid dynamics (CFD) method, the detailed airflow patterns around the cyclist were investigated. The results were analyzed in terms of drag area, velocity and pressure distributions around the cyclist, surface pressure coefficient and surface wall shear stress. It was revealed that varying the aero handlebar position significantly influences the aerodynamic performance, while maximal values of all the physiological variables remained unchanged. Compared to the cyclist's preferred TTP, the frontal area, drag coefficient and drag area were reduced by 4.1%, 4.6% and 8.5%, respectively, when lowering the handlebar position by 5 cm, which overcomes the metabolic costs.

Keywords: Computational Fluid Dynamics (CFD), aero handlebar, Cycling position, Aerodynamic drag

5.2 Introduction

Aerodynamic drag is the most considerable resistive force cyclists experience, and its reduction is critical to improving cycling performance. At racing speeds of 54 km/h, the aerodynamic drag is approximately 90% of the total resistance (Debraux et al., 2011; P. E. Di Prampero, 2000; C. Kyle & Weaver, 2004; Lukes et al., 2004; J. C. Martin et al., 2006; Millet & Candau, 2002; Padilla et al., 2000). Many studies have been conducted to decrease the aerodynamic drag (M. N. Abdullah et al., 2015; Alam et al., 2014; Barry et al., 2015b; Chowdhury et al., 2010; Garcia-Lopez et al., 2008; Jobson et al., 2008; Mustary et al., 2014; Oggiano et al., 2009). Among these aerodynamic drag forces, the cyclist's body position accounts for about 70% (Alam et al., 2014; Defraeye, Blocken, Koninckx, Hespel, & Carmeliet, 2010a), highlighting the significance of body position when attempting to improve performance. Consequently, the decrement of aerodynamic drag requires a vast understanding of the cyclist's position and its drag area (AC_D), which is the product of the drag coefficient (C_D) and the frontal area (A).

Time trial position (TTP) is adopted by cyclists to improve their optimal performance, where the torso held very low to reduce the frontal area. Various studies have investigated the aerodynamic drag of the time trial position using the wind-tunnel tests (Garcia-Lopez et al., 2008; Grappe et al., 1997; Jobson et al., 2008; Lukes et al., 2005). However, few studies exist for the effect of aero handlebars, which may be essential adjustments when fitting a bicycle (C. Kyle, 1989; Lukes et al., 2005; Oggiano et al., 2008; Oggiano et al., 2009). Garcia-Lopez et al. (2008) reported a significant reduction in aerodynamic drag of about 14% when the height of the aero handlebars was lowered during riding in a TTP. Oggiano et al. (2008) found that changes in handlebar position (about 20 mm) reduced the aerodynamic drag more significantly compared to changes in seat position.

Although changing the cyclist position improved the aerodynamics, it affects the physiological responses and the peak power output (PPO) inconclusively (Dorel et al., 2009; Jobson et al., 2008). Previous investigations usually examine the physiological functioning of TTP as compared to other common positions with various torso angles, i.e., upright position and dropped position (Dorel et al., 2009; Fintelman et al., 2015; Origenes et al., 1993). An increase in oxygen consumption (VO_2) and heart rate in the cyclist's preferred time trial position has been reported compared to the upright position and dropped position under submaximal conditions (Evangelisti et al., 1995; Gnehm et al., 1997; Richardson & Johnson, 1994). Such responses to the lower torso angle positions indicated an increased metabolic cost associated with such positions (Candau et al., 1999; Jobson et al., 2008). On the contrary,

recent literature has concluded that there is no effect of the torso angle on the VO_2 and heart rate (Dorel et al., 2009). Nevertheless, the metabolic and physiological functioning of different aero handlebar positions with small differences in torso angle has not been examined in previous studies.

In addition to field tests and wind-tunnel measurements, the numerical simulation by computational fluid dynamics (CFD) could also be inquired to investigate aerodynamic drag (Barber et al., 2009; Blocken, 2014; Blocken & Toparlar, 2015; Crouch et al., 2017; Gardan et al., 2017; Mannion et al., 2018). CFD approaches have been demonstrated to be a powerful tool in sports aerodynamics, providing high-resolution data on the complex flow field. Changing the flow circumstances and the parameters involved in a time-efficient manner makes CFD a more feasible option for the parametric analysis of cycling aerodynamics. CFD simulations have been used extensively for investigating cyclists in different race positions or TTPs (Defraeye, Blocken, Koninckx, Hespel, & Carmeliet, 2010a; Defraeye et al., 2014; Griffith et al., 2014). However, to the best of our knowledge, a detailed analysis of altering the aero handlebar position effects on aerodynamics by either CFD simulations or wind-tunnel tests has not yet been published. Moreover, despite prior research examining the influences of different cycling position on physiological and aerodynamic variables, there are somewhat little studies investigating the influence of alteration of the aero handlebar on such parameters. Therefore, this paper aims to contribute to the understanding of the aerodynamics of different aero handlebar positions using CFD simulations, secondly to determine the effect of such positions on physiological parameters. Simulations were performed using a uniform velocity of 15 m/s, corresponding to the relative air movement due to cycling during time trial competition.

5.3 Methods

5.3.1 Experimental design

Seven male competitive time trial cyclists and triathletes volunteered to participate in the study. Participants reported to ride on average 286 ± 74 km a week and had used aero handlebars for 5.6 ± 2.4 years. The participant's physical characteristics were: age, 29.6 ± 7.5 years; height, 182.9 ± 7.4 cm; body mass, 73.6 ± 4.6; peak power output (PPO), 357.9 ± 53.5 W; peak oxygen consumption ($\dot{V}O_{2peak}$), 61.4 ± 11.3 mL.kg^{-1}.min^{-1}; heart rate, 183.6 ± 12.4 bpm. They had no physical, respiratory and cardiovascular impairment preventing them from a competitive cycling exercise. The study was approved by the Ethical Committee of Polytechnique Montreal on human research (reference no CER-1819-30) and conducted in

line with the Declaration of Helsinki, and all participants gave written informed consent at the beginning of the study. The tests were carried out with a cycle ergometer (Corival 906 900, LODE Medical Technology BV, Groningen, the Netherlands) equipped with an aero handlebar. Each participant visited the laboratory on two separate occasions. During the first session, participants completed an incremental cycling test to determine their VO_{2peak}, using a breath-by-breath system (Ultima CardiO_2, 790705-006, 12 lead ECG Test CPX, MedGraphics Cardiorespiratory Diagnostics, St. Paul, MI). The LODE ergometer and gas analyzer were calibrated before each test according to the manufacturers' recommendations. The test started with a 5-min unloaded warm-up. Then an incremental procedure started at 75 W for 3 min, and the load was increased every minute by 20 W until the participant was no longer able to maintain the cadence above 60 rpm. During the session, the PPO, $\dot{V}O_{2peak}$, heart rate, power output at the ventilatory threshold and peak respiratory exchange ratio were constantly recorded. The second visit consisted of six submaximal cycling exercises in different handlebar positions randomly. Aero handlebar positions were: (1) handlebar 30° up from the preferred position (TTP 30° up); (2) handlebar 30° and 5 cm up from the preferred position (TTP 30° and 5 cm up); (3) handlebar 5 cm down from the preferred position (TTP 5 cm down); (4) handlebar 5 cm up from the preferred position (TTP 5 cm up); (5) preferred TTP; (6) handlebar 5 cm forward from the preferred position (TTP 5 cm forward), as shown in Figure 5.1. All the bouts were at 75% of the determined gas exchange threshold (GET) with a duration of six minutes, followed by six minutes of passive recovery. All gas-exchange variables, i.e., oxygen uptake ($\dot{V}O_{2peak}$), respiratory exchange ratio (RER), minute ventilation (VE) and tidal volume (VT), were measured under similar environmental conditions (~ 25°C) and by one instructor to ensure repeatability and that the same method was applied, using the same measurement equipment. The detailed method can be found in (Ghasemi, Curnier, Caru, Pageaux, et al., 2020).

5.3.2 Geometry, computational domain and grid

The geometrical parameters of the cyclist were obtained by using the elliptical zone method, which divides the body into elliptical zones representative of body shapes and segment densities (Jensen, 1978). The segment measurement and acquisition of its length and width were conducted using the markerless motion capture system (Kinect, Microsoft Corp., USA).

The 3D body surfaces of the six desired TTPs were modeled in CAD software (CATIA V5, Dassault-Systèms, France), applying all the specific body characteristics of the cyclist collected from the Kinect. Obtaining a well-defined and controlled CAD model allows the geometry and its features to be readily defined, adjusted, and moved within a fully parame-

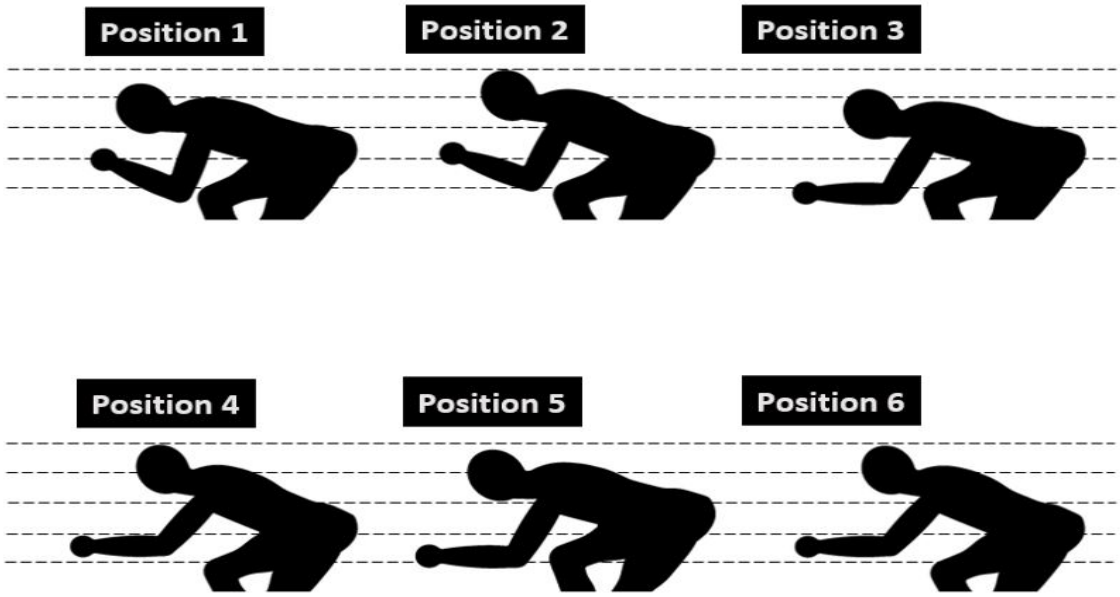

Figure 5.1 A sketch of the six aero handlebar positions: position 1, TTP 30° up; position 2, TTP 30° and 5 cm up; position 3, TTP 5 cm down; position 4, TTP 5 cm up; position 5, preferred TTP; position 6, TTP 5 cm forward. Dashed lines are depicted to provide a more visual presence of differences between the positions.

terized CAD model to test the effect of aero handlebar alternations, compared to a 3D scan. More detailed information on the geometry is available from Ghasemi et al. (2020). The cyclist had a height of 1.89 m and a weight of 70.3 kg. The cyclist geometry was simplified, specifically concerning the abdomen, chest and hands. The six TTPs were analyzed to provide a more comprehensive aerodynamic comparison.

The full-scale cyclist was then placed in a computational domain with size according to best practice guidelines (Zaidi et al., 2010). To minimize computation time, only the cyclist's body has been considered without including the bicycle. The size of the computational domain and the imposed boundary conditions are specified in Figure 5.1. The upstream, downstream and lateral distance of the domain faces to the model were 3.5 m, 11 m and 2.7 m, respectively. This resulted in a blockage ratio of approximately 2%. The grid generation was based on grid-generation guidelines for cycling aerodynamics (Tominaga et al., 2008). To evaluate the CFD model's numerical uncertainties and determine the adequate grid size, a grid convergence study was conducted using three different meshes, i.e., coarse (2.6×10^6 cells), medium (6.8×10^6 cells) and fine (16.2×10^6 cells) grids. The drag coefficient of the preferred TTP was determined as the target variable. Based on the method suggested by Roache (1994, 1997), the grid convergence index (GCI) can be defined as

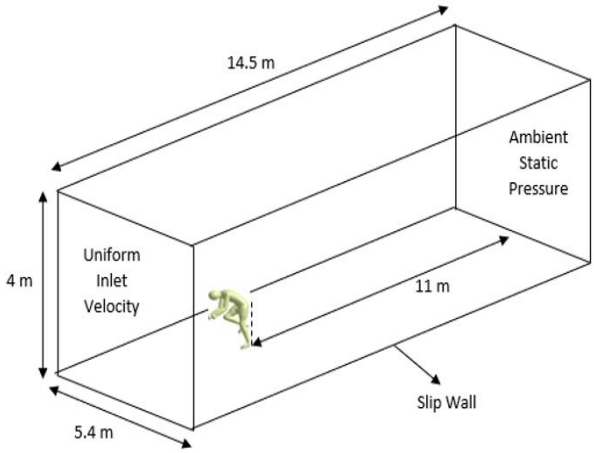

Figure 5.2 Computational domain, geometry and boundary conditions.

$$GCI = \frac{F_s \left|\varepsilon\right|}{r^p - 1} \tag{5.1}$$

Where F_s is the safety factor, ε the relative error between the fine and medium mesh, r the grid refinement ratio and p the order of accuracy. The safety factor is set to 1.25. GCI values of 0.96% and 0.11% were obtained for the medium and fine grids, respectively. The GCI value of medium mesh suggests that the resolution of the medium mesh is sufficient to predict the flow correctly, and hence no further mesh refinement is required. The grids used to produce the results contained 6.8×10^6 cells. An unstructured mixed grid was used, featuring very small prismatic cells within the boundary layer region of cyclist with the first layer height only 30 μm, and an average dimensionless wall unit y^* lower than 1 was generally attained in the boundary layer region. Based on the dimensionless wall unit y^*, this high-resolution grid was needed to fully resolve the thin boundary layer down to the viscous sublayer since the viscous sublayer at the surface is very thin. Note that the parameter y^* is used instead of y^+ to specify grid resolution requirements for cycling aerodynamic applications (Blocken & Toparlar, 2015; Defraeye, Blocken, & Carmeliet, 2010). Tetrahedral cells with an average cell size of about 0.04 m further away from the surface were used in other regions.

5.3.3 Boundary conditions

At the inlet of the fluid domain, a uniform velocity of 15 m/s was imposed, representing the average velocity during a no-wind time trial competition for an elite cyclist. Air turbulence intensity of 0.02% was considered. The simulation of the non-pedaling (static-legs) cyclist model was assumed with the assumption that the flow topology of a cyclist is consistent

across a static leg and rotating leg at the related phase of leg rotation (Crouch et al., 2016). For the ground, sides and upper surfaces of the field, a slip-wall boundary (symmetry) was applied. At the computational domain outlet, the free outflow condition (ambient static pressure) was imposed. A no-slip boundary condition with zero roughness was used on the cyclist surface.

5.3.4 Aerodynamic drag

Aerodynamic drag F_D (N) relates to the dimensionless drag coefficient C_D and the frontal area A (m^2), as demonstrated below, where ρ is the density of air (kg/m^3) and U is the approach flow wind velocity (m/s).

$$F_D = \frac{1}{2}\rho A C_D U^2 \tag{5.2}$$

Aerodynamic drag in cycling is often quantified by the drag area (AC_D), which is preferable to drag coefficient (C_D) since it does not require a precise determination of the frontal area (A).

5.3.5 CFD simulation

The CFD code ANSYS Fluent 18.1© was used to perform simulations for the six TTPs. The transition shear stress transport (SST) $k-\omega$ model was opted to solve the 3D steady Reynolds averaged Navier-Stokes equations (3D RANS), which is extensively considered to have the best overall performance and accuracy in previous studies for the aerodynamics of a single cyclist (Defraeye, Blocken, Koninckx, Hespel, & Carmeliet, 2010b; Langtry & Menter, 2009). The semi implicit method for pressure linked equations (SIMPLE) algorithm was used for pressure-velocity coupling with second-order discretization schemes. Pressure interpolation was second order. Gradients were computed with the least-squares cell-based method (Defraeye, Blocken, Koninckx, Hespel, & Carmeliet, 2010a). The governing equations were solved iteratively, while convergence was monitored. Convergence was obtained when residuals reached less than 10^{-5}.

5.3.6 Statistical analyses

A one-way repeated measures analysis of variance (IBM SPSS Statistics 26.0, Chicago, IL) was performed to compare all considered physiological parameters among the six TTPs. Prior to the test, the data were checked for normality and sphericity. When sphericity could not be

assumed, a Greenhouse–Geisser correction was applied. Post-hoc testing was performed with Bonferroni adjustments to detect the differences. The significance level was set at $P = 0.05$ and all the physiological data are presented as mean values ± SD.

5.4 Results

5.4.1 Physiological measures

Figure 5.3 shows the peak responses of VO_2, RER, VE and VT for the six submaximal positions. Although the differences were not significantly different between positions, VO_2 and VE were increased by 5.1% and 4.0% respectively, in TTP 5 cm down compared to the preferred TTP, while RER and VT remained unchanged. In addition, VO_2, VE and VT in TTP 5 cm forward were lower by 3.4%, 1.8% and 2.0%, respectively compared to TTP 5 cm down. Furthermore, VO_2, RER and VE showed an increase when participants pedalled at lower handlebar positions (TTP 5 cm down and TTP 5 cm forward).

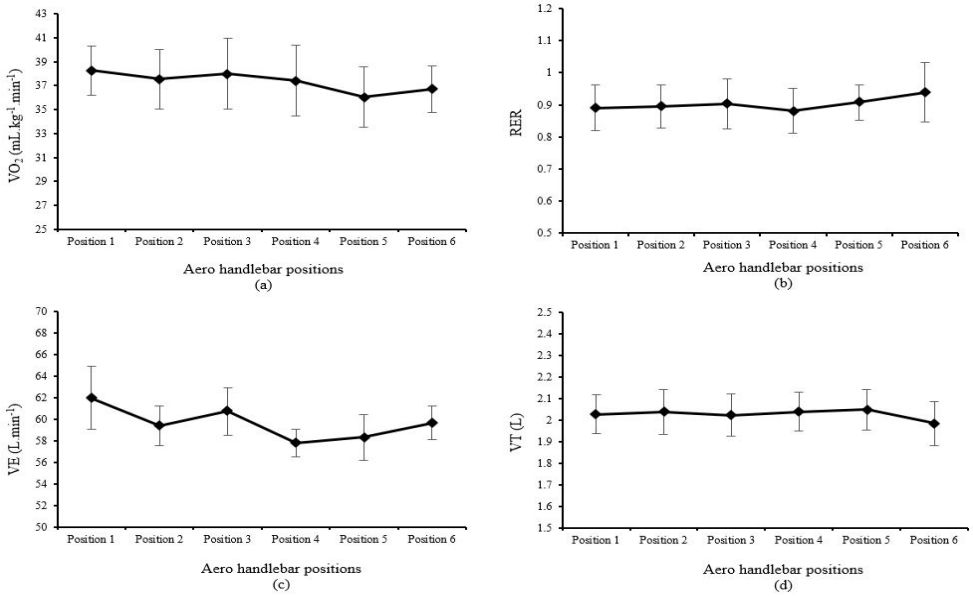

Figure 5.3 The peak responses of gas-exchange variables at different aero handlebar positions: position 1, TTP 30° up; position 2, TTP 30° and 5 cm up; position 3, TTP 5 cm down; position 4, TTP 5 cm up; position 5, preferred TTP; position 6, TTP 5 cm forward. (a) VO_2, oxygen uptake; (b) RER, respiratory exchange ratio; (c) VE, minute ventilation; (d) VT, tidal volume.

5.4.2 Modeling validation

The CFD results were compared with experimental and numerical results from Beaumont et al. (2018), Blocken et al. (2013) and Defraeye et al. (2010a) to validate the numerical procedure. Table 5.1 represents the drag area values along with data used for comparison. The drag area of the cyclist obtained from our CFD simulations are in close agreement with Beaumont et al. (2018) and Blocken et al. (2013) for a single cyclist without bicycle in TTP. Moreover, our results showed good consistency with values of wind-tunnel experiments and CFD obtained by Defraeye et al. (2010a), albeit a different inlet velocity of 10 m/s.

Table 5.1 Drag area of CFD simulations and wind-tunnel experiments (Experimental) for comparison with the current study.

Studies	AC_D (m^2)	Deviation (%)
Defraeye et al. (2010a) - CFD	0.142	0.0
Defraeye et al. (2010a) - Experimental	0.134	5.6
Blocken et al. (2013) - CFD	0.135	4.9
Blocken et al. (2013) - Experimental	0.134	5.6
Beaumont et al. (2018) - CFD	0.138	2.8
Current study - Preferred TTP	0.142	

Table 5.2 illustrates the drag area AC_D, drag coefficient C_D and the frontal area A, deduced from CAD software, for a cyclist without bicycle for the six different aero handlebar positions. The frontal area was smallest for TTP 5 cm down (0.329 m^2) and largest for TTP 30° and 5 cm up (0.361 m^2). Compared to preferred TTP, TTP 30° and 5 cm up and TTP 5 cm up showed larger frontal areas (5.0% and 2.2%, respectively), while the frontal areas of TTP 30° up, TTP 5 cm down and TTP 5 cm forward were smaller (0.3%, 4.1% and 0.9%, respectively) than preferred TTP. The drag coefficient was highest for TTP 30° up, followed by preferred TTP, and lowest for position TTP 5 cm down. The reduction of drag area in TTP 5 cm down was 8.5% as compared to preferred TTP. The drag area of TTP 30° and 5 cm up, which showed the largest frontal area, was the highest, and the drag area for TTP 5 cm down was the lowest. Compared to the preferred TTP, TTP 30° up, TTP 30° and 5 cm up and TTP 5 cm up showed a higher drag area (1.4%, 3.4% and 0.7%, respectively). It can be seen that the drag area for TTP 30° up was higher than TTP 5 cm up and preferred TTP, although it had a slightly lower frontal area. Lowering the frontal area could result in minimising the resistance force. Still, a decrease in a frontal area alone does not necessarily lead to a lower drag area.

Table 5.2 Drag area AC_D (m^2, drag coefficient C_D and frontal area A (m^2) for the six aero handlebar positions.

Positions	AC_D (m^2)	C_D	A (m^2)
TTP 30° up	0.144	0.421	0.342
TTP 30° and 5 cm up	0.147	0.407	0.361
TTP 5 cm down	0.130	0.395	0.329
TTP 5 cm up	0.143	0.405	0.353
Preferred TTP	0.142	0.414	0.343
TTP 5 cm forward	0.140	0.412	0.340

5.4.3 Analysis of velocity and pressure fields, surface pressure and wall shear stress

Figure 5.4 and 5.5 depict the velocity contours and the pressure coefficient C_p, respectively, in the vertical centerplane for all the six investigated positions. The legend in Figure 5.5 has been limited to the interval [– 0.5, 0.5] to highlight the pressure field changes better. It is evident that changes in handlebar position notably influenced both airstream and pressure distribution around the cyclist. The impact of aero handlebar alterations and the interactions between the vorticities generated by the arms and the cyclist's upper body is demonstrated.

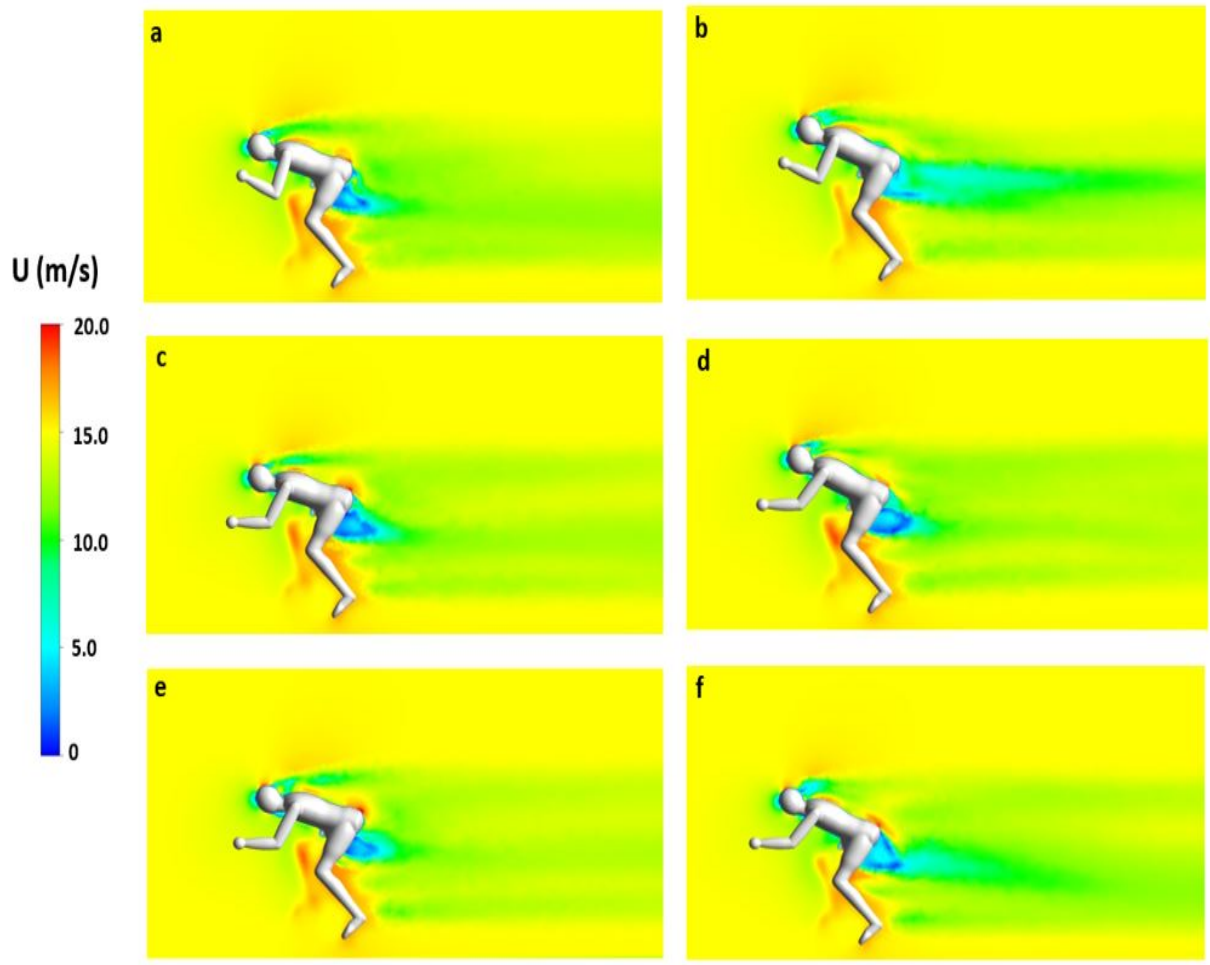

Figure 5.4 Contours of velocity in the vertica center plane for a cyclist in the six aero handlebar positions (cycling speed is 15 m/s): (a) TTP 30° up; (b) TTP 30° and 5 cm up; (c) TTP 5 cm down; (d) TTP 5 cm up; (e) preferred TTP; (f) TTP 5 cm forward.

Figure 5.4c indicates that the flow pattern is a lesser disturbance since a smaller wake was created. It is evident from Figure 5.5 that the low-pressure regions behind the cyclist resulted in high local velocities and an increase in total drag (Figure 5.4). The low-pressure regions (blue color) are regions where the flow is detached.

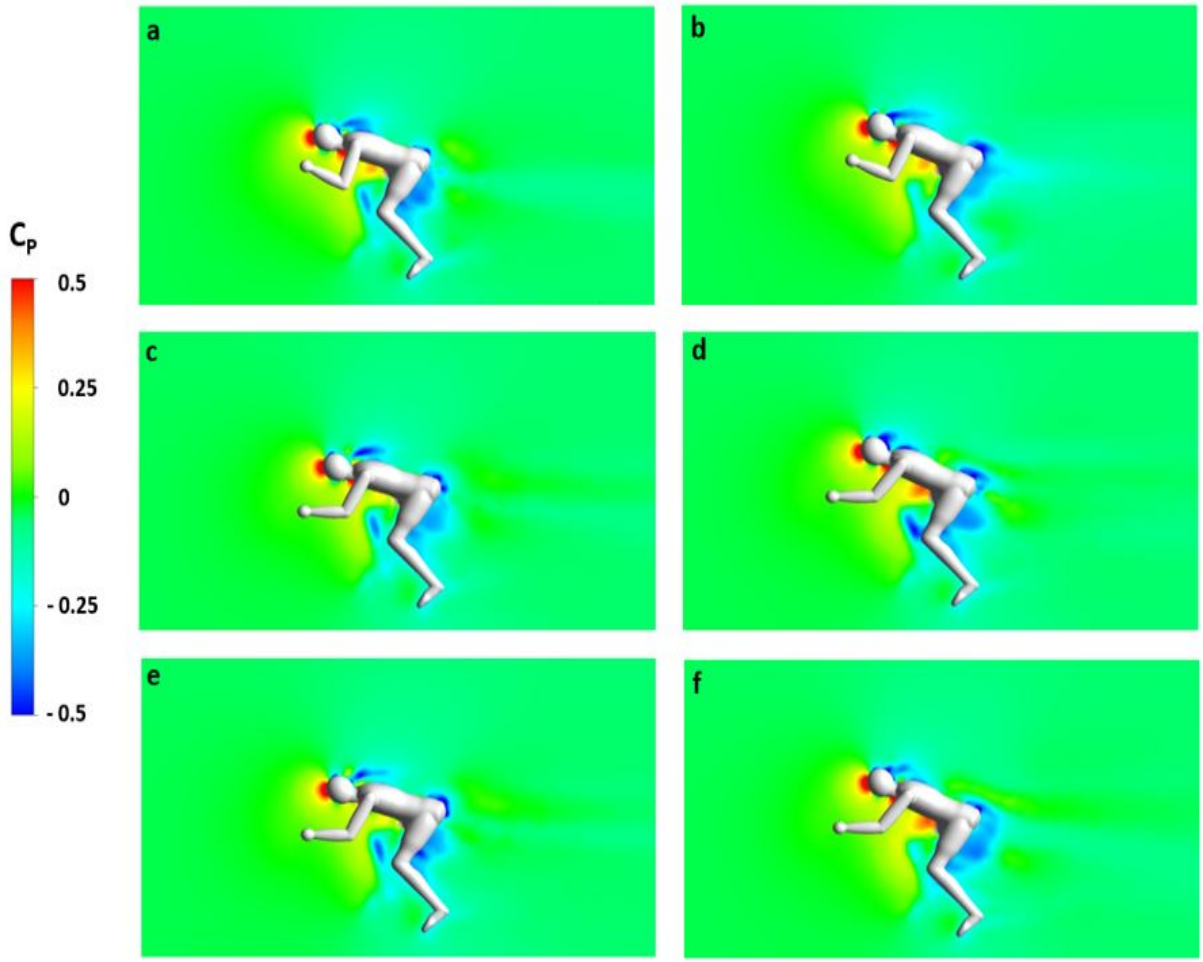

Figure 5.5 Contours of pressure coefficient C_p in the vertica center plane for a cyclist in the six aero handlebar positions (cycling speed is 15 m/s): (a) TTP 30° up; (b) TTP 30° and 5 cm up; (c) TTP 5 cm down; (d) TTP 5 cm up; (e) preferred TTP; (f) TTP 5 cm forward.

Figure 5.6 and Figure 5.7 represent the front, side and top views of the pressure coefficient C_p, and the wall shear stress distribution on the cyclist body for the six positions, respectively. It can be seen that the surface pressure coefficients are maximized at the zones perpendicular to the direct main flow and minimized at the areas that are not subject to direct flow impingement, i.e., the sides of arms, the bottom of the cyclist's torso, the shoulders and legs.

Lowering the handlebar in TTP 5 cm down relatively reduces the wall shear stresses in the back of the rider, as seen in Figure 5.7c, while TTP 30° and 5 cm up (5.7b) with the elevated handlebar resulted in maximizing the shear stresses.

5.5 Discussion

To the authors' best knowledge, a detailed aerodynamic analysis and monitoring the physiological responses of different aero handlebar positions have not yet been published. CFD analysis offers a very efficient platform to obtain higher resolution modeling of flow patterns, which provides greater insight into the sources of aerodynamic resistance forces. We conduct a detailed aerodynamic analysis of altering the time trial handlebar position, and the gas-exchange variables were collected continuously. The results are evaluated for the drag area and frontal area of the cyclist, the velocity and pressure fields, surface pressure and wall shear stress on the cyclist's body. A maximum deviation of 4.9% indicates a good agreement for the preferred TTP as compared to previous CFD investigations (Blocken et al., 2013). This deviation could be due to various CFD techniques and numerical simulations, different geometry and computational domain and diverse 3D model of cyclists that have been used for CFD calculations.

Manipulation of the handlebar position affected the physiological parameters insignificantly. In particular, lowering the aero handlebar in TTP 5 cm down did not limit the physiological functioning, which would suggest the aerodynamic gains of pedaling at the lowered handlebar. Our finding supports and complements previous observations that lowering the handlebar height leading to lowering the torso angle would not impair the physiological performances (Dorel et al., 2009; Franke et al., 1994; Heil et al., 1997). This trend of relatively unaffected physiological performances when changing the aero handlebar position could result from the limited range of torso angles applied during submaximal bouts. Berry et al. (1994) revealed that the lung volume, VE and VT are not significantly influenced by cyclist body position.

We found that the frontal area, drag coefficient and drag area of TTP can decrease by 8.9%, 2.9% and 11.6%, respectively, for lowering the aero handlebar height and orientation from TTP 30° and 5 cm up to TTP 5 cm down. The drag coefficients of TTP 30° and 5 cm up and TTP 5 cm up were closely similar. However, the frontal area of TTP 30° and 5 cm up was more significant than TTP 5 cm up and accordingly, the drag area of position TTP 30° and 5 cm up was higher than TTP 5 cm up. TTP 5 cm down and TTP 5 cm forward showed the least drag area as well as the frontal area. This confirms the earlier findings of the reduction of aerodynamic drag caused by decreasing the frontal area and, thus, a decrease in

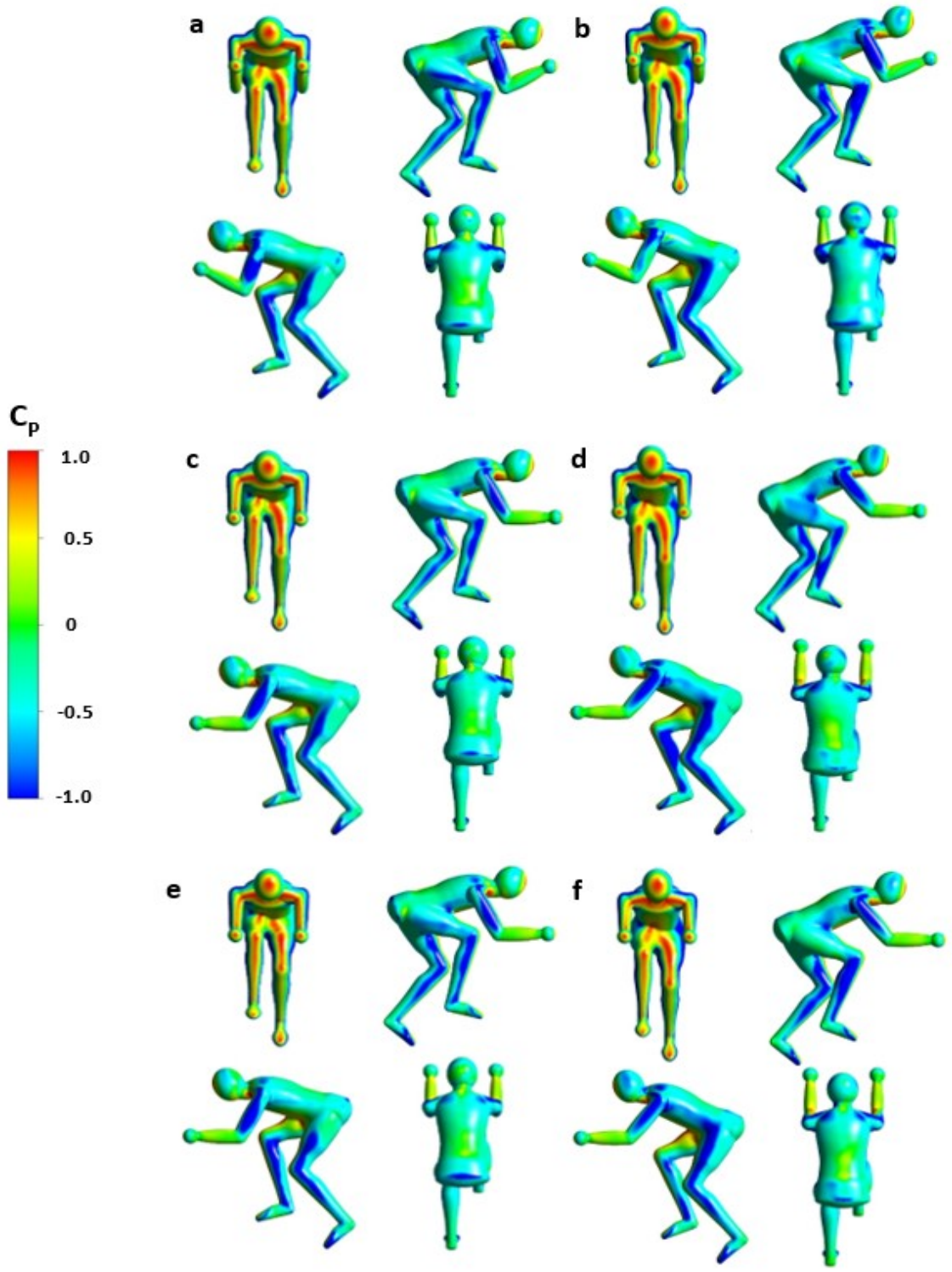

Figure 5.6 Front, sides and top views of the surface pressure coefficient C_p on the cyclist's body for the six aero handlebar positions. (a) TTP 30° up; (b) TTP 30° and 5 cm up; (c) TTP 5 cm down; (d) TTP 5 cm up; (e) preferred TTP; (f) TTP 5 cm forward.

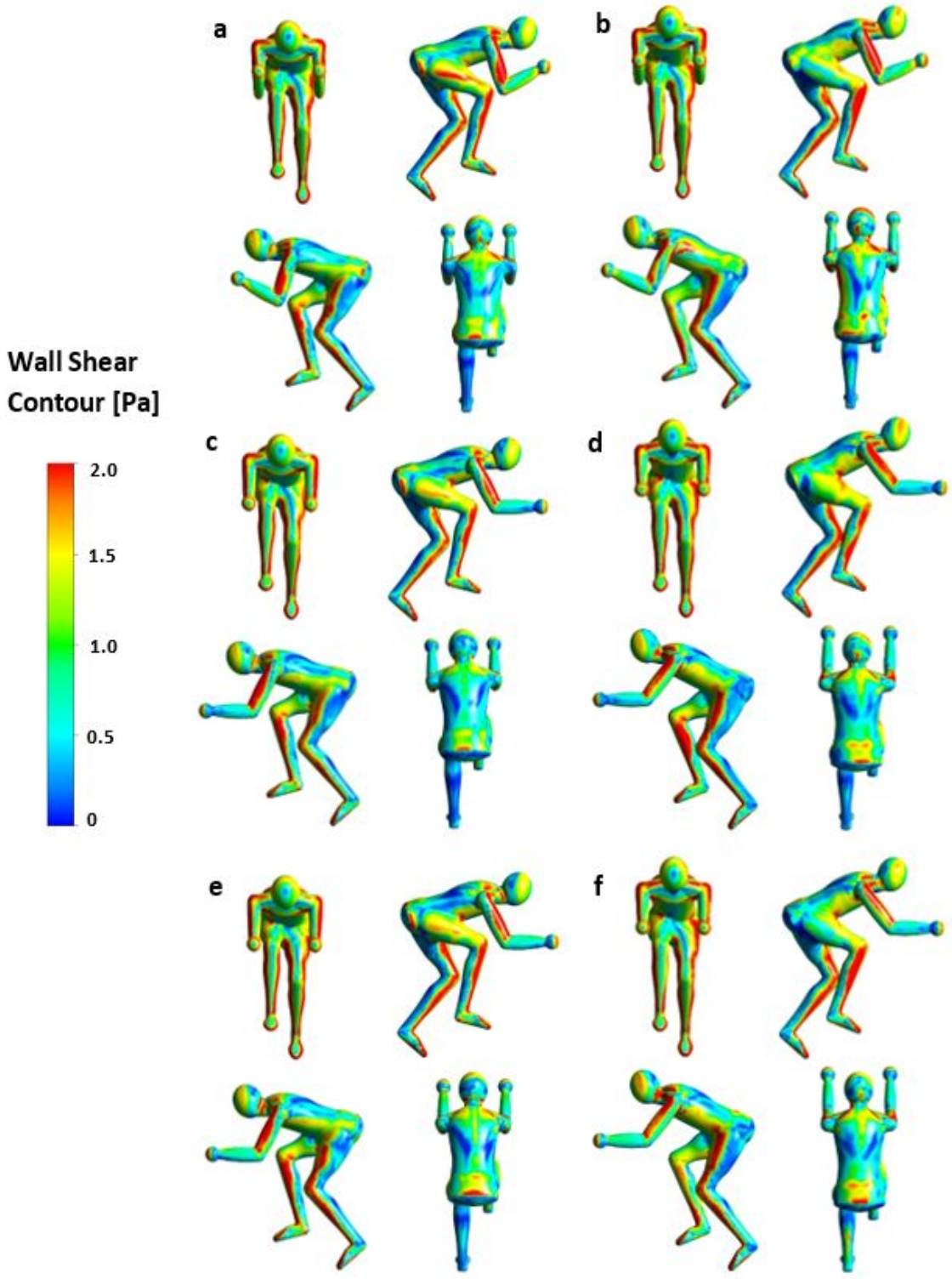

Figure 5.7 Front, sides and top views of the surface shear stress distribution on the cyclist's body for the six aero handlebar positions. (a) TTP 30° up; (b) TTP 30° and 5 cm up; (c) TTP 5 cm down; (d) TTP 5 cm up; (e) preferred TTP; (f) TTP 5 cm forward.

the torso angle (Blocken et al., 2013; Garcia-Lopez et al., 2008).Therefore, one can conclude that lowering the handlebar position reduces the drag area and is more effective than moving the handlebar forward. Compared to the preferred TTP, the drag area for TTP 30° up was 1.4% higher than preferred TTP, while TTP 5 cm up showed an increase of 0.7% in the drag area. This more significant increase is related to the increment of drag coefficient (0.414 vs 0.421 for TTP 30° up and 0.405 for TTP 5 cm up) since the growth in the frontal area of the cyclist in TTP 30° up was lower than for TTP 5 cm up, as compared to preferred TTP (0.343 m^2 vs 0.342 m^2 for TTP 30° up and 0.353 m^2 for TTP 5 cm up). This confirms the Beaumont et al. (2018) finding that lowering the frontal area alone may not necessarily lead to a reduction in aerodynamic drag.

For all the aero handlebar positions, the distribution of high-pressure areas is discovered on the front side of the cyclist, leading to the positive pressure coefficient (C_p) values. The low-pressure areas at the shoulders and bottom of the cyclist body are more noticeable for TTP 30° up and TTP 30° and 5 cm up, while in TTP 5 cm down, pressure gradients on the back of the cyclist are more limited. Large vortices often developed from these areas result in an increment in the drag area. Further, the areas with the increased wall shear stress correspond to zones where the flow separations appear (Beaumont et al., 2018), and therefore, in the areas in which low-pressure zones are generated (i.e., the areas with negative pressure gradients), the drag forces increase. In particular, the back of the cyclist in TTP 30° and 5 cm up and TTP 5 cm up (Figure 5.6b and 5.6d, respectively) may be observed as the areas with the increased drag forces in regions such as head, shoulders and bottom of the cyclist body. Moreover, comparing the distribution of shear stress shown in Figure 5.7 and the total drag force (17.9 N and 20.3 N for TTP 5 cm down and TTP 30° and 5 cm up, respectively) revealed that the force caused by pressure is much greater than caused by shear stress. Thus, the primary resistive force is the pressure force acting on the cyclist.

It is expected that the findings of the present study and its trends are independent of the anthropometric data of the investigated cyclist. However, future studies should consider less trained male cyclists and potentially female cyclists to assess the full extent of anthropometric parameters. Regarding the overall effort for performance evaluation and its optimization of pedaling in different aero handlebar positions, the joint level power, crank torque and pedal force of the cyclists associated with riding in various positions should be taken into account. Future studies should address the potential effects of different TTPs on all the involved parameters.

5.6 Conclusion

The present study focused on the physiological responses and aerodynamics of different aero handlebar positions using the CFD method. The aerodynamic drag of a cyclist with six different aero handlebar positions has been analyzed, while the shoulder angle and position of the hands were kept constant. We observed significant differences in aerodynamic drag and cyclist's frontal area when the handlebar position is altered. The low drag cases correspond to the position where the aero handlebar moved down and forward. TTP 5 cm down exhibited the least value of the drag area. This reduction, which was the combined result of a decrease in both the frontal area and drag coefficient, will likely outweigh the insignificant increase in metabolic costs at the investigated cycling intensity. Analysis of pressure distribution on and around the cyclist and the surface wall shear contours was used to highlight the aerodynamic effects of variations in the handlebar positions along with the location and the extent of vortices and flow separation zones. Results indicated that in the positions with the elevated handlebar, the low-pressure areas at the shoulders and bottom of the cyclist body are more significant, leading to higher C_D.

5.7 Conflict of Interest

The authors declare no conflict of interest in relation to the research presented in this manuscript.

5.8 Acknowledgements

We thank all participants for devoting their time and energy to our study.

CHAPTER 6 GENERAL DISCUSSION

The present dissertation addresses the performance and aerodynamic evaluation of the cyclist's position with a primary focus on the time trial position and its variations. The overall objective of this project was to establish and develop a set of tools for the performance evaluation of cyclist's positions. It consists of three parts. In the first part, we proposed and validated a parameterized quantitative technique for modeling cyclists in different positions using a markerless system. An evaluation was then performed to determine the influence of changing the time trial handlebar position on the physiological responses and kinematic variables of the lower extremities in six different positions while recording the muscle activation patterns of the lower limb. Finally, in the last part, a detailed CFD aerodynamic analysis of altering the time trial handlebar position was conducted to determine whether these alterations could induce cyclist performance. In this chapter, the significant outcomes of experiments and numerical simulations of the present dissertation are summarized with an emphasis on the limitations of these approaches and suggested prospects of future studies.

6.1 Summary of Works

One of the main contributions of the thesis is the development and validation of a set of parameterized tools to model a 3D digital manikin of professional cyclists at a static crank angle by using a markerless motion capture system. We have presented a fully parameterized and a low-cost framework to provide a 3D body surface leading to an efficient solution for modeling various positions and conditions of cyclists with different anthropometric measurements. This is in line with the first objective of the study and its hypothesis, i.e., to establish and progress an applicable system for conducting the aerodynamic analysis of cyclists in various cycling positions.

The parameterized Kinect-based technique can define the 3D generated model accurately. The comparison between our Kinect-based model and the scanner-based model showed a relatively small difference, which was insignificant, given the anthropometric data variations. Applying the markerless acquisition (Microsoft Kinect) sensor, particularly for capturing the cyclists' anthropometric data, combined with the elliptical zone method of a computer-aided design software, parametric surface modeling provided the opportunity to conduct CFD simulations. The reduced aerodynamic drag reflected the positive effect of lowering the sagittal torso angle. Moreover, The results demonstrated that the simulated and measured

drag areas were in close agreement with the previous studies.

It is now reasonably certain from the results presented that the parameterized modeling framework combined with CFD, which has proven to be one of the most useful and widely employed aerodynamic performance evaluation methods, is a valuable tool to evaluate the drag of different cyclist's positions. A substantial advantage of this method is that detailed information is obtained inexpensively and without complicated setup and technical expertise. Changing the position and modeling various body composition and cycling positions in CFD simulations require a re-generation of the mesh and time-efficiently adapted numerical calculation parameters. Therefore, the markerless motion capture system can provide the conclusive and comparable relative comparison of various cycling positions.

The use of the Kinect-based motion capture method, which acquires the motion data of the lower limb joints movement along with monitoring muscle recruitment and recording the physiological responses during pedaling enabled us to properly determine the influence of changing the time trial handlebar position on lower limb muscle activation patterns and kinematic variables under submaximal intensity. In general, the motion capture systems, including Kinect, contain errors through inaccuracies of tracking, digitizing, and post-processing of spatial, positional and orientational data. Limited evaluation of the 3D marker-based systems in the high-velocity motion, such as cycling, showed that errors due to soft tissue artifacts and errors in predicting lower joints' center locations are approximately 2 cm and 5°-10°, respectively (Bell et al., 1989; Fiorentino et al., 2017). Therefore, the inaccuracy of the 2D Kinect capturing while recording the sagittal plane is acceptable accuracy since it is similar to the accuracy of the 3D marker-based systems (Benoit et al., 2006). Moreover, previous studies showed that markerless motion tracking accuracy could be improved by decreasing the distance from the object and combining sensor data with fixed anatomy and range of motion (S. Han et al., 2013; Napoli et al., 2017), like the pedaling motion of a cyclist.

The angle, angular velocity, and range of motion (ROM) of the ankle, knee, and hip joint of the right lower limb were calculated. Results showed a significant increase in the peak of ankle and knee angles of TTP 5 cm up compared with TTP 5 cm down, while the peak value of the hip angle of TTP 5 cm down was greater than TTP 5 cm up. Although ankle ROM in TTP 5 cm up was greater than TTP 5 cm down, no significant differences were observed in the knee and hip ROM. The variability of joint ROM could be related to the cyclists' anthropometric, and therefore, the recommendations for alterations of cyclist's position, including the handlebar, should be applied using individual preferred TTP as we have addressed in our adjustments. These findings illustrate the emphasis of kinematic evaluation and its adjustment given that the excessive joint angles are related to injury risk and cycling

performance (R. Bini et al., 2011), and avoid positions previously associated with injury risk.

One goal of this study was to clarify whether the handlebar position would alter the lower limb muscle patterns. Investigating, comparing, and analyzing the cause-effect relationships of biomechanical parameters of the lower extremity that affect the performance of the cyclist were performed. Our results suggest that altering the handlebar position affects the activity of muscles, kinematics of leg movement, and the association between them. This relates closely with lowering the handlebar and the change of pedaling technique through the hip and knee extension. These findings are of importance because of prevalent bike fitting approaches, which can reflect changes in cyclist kinematics during cycling at a given position.

From the results, it is concluded that a cyclist may activate the muscles and move more effectively when the handlebars are lower or move forward since hip flexor and extensor changes are expected given the increase in hip flexion angle. Moving forward is less efficient since the GMax slightly stretched and RF effectively shortened by this forward tilt, becoming less effective. The GMax and RF are two dominant muscles that produce the most considerable amount of torque in cycling. Furthermore, changing the handlebar position forward and down increased the hip ROM, leading to a deeper pedaling and allowing the foot to pass over TDC. The latter can prevent the hip from lateral movement from side to side and therefore retain the drop in power. The higher the handlebar, the less flexion the hip will have at TDC. That is why the position with the handlebar 5 cm down from the preferred position is considered the most beneficial performance-related time trial position among the investigated ones. Hence, our second objective, which was investigating the muscle functionality and kinematics of lower limbs during pedaling in different time trial positions, is achieved.

Finally, we conducted a detailed aerodynamic analysis of altering the time trial handlebar position while collecting the gas-exchange variables. The drag area TTP 5 cm down was the least value while TTP 30° and 5 cm up showed the largest one. Although moving the handlebar upward increased the frontal area, results indicated that this increment of the frontal area might not necessarily increase the drag area due to the drag coefficient changes.

For the TTP 30° up and TTP 30° and 5 cm up, the drag area increased by the low-pressure regions observed at the shoulders and bottom of the cyclist body and the increased wall shear stress caused by the zones where the flow separations appear. CFD results have also shown that in terms of drag area, lowering the handlebar position is more effective than moving it forward, which is relative to the attempt for the overall improvement of cycling performance as well as the third objective of this project. Altering the handlebar position did not affect physiological responses including oxygen uptake, respiratory exchange ratio, minute ventilation and tidal volume, suggesting that the aerodynamic gains of pedaling at

the lowered handlebar outweigh the metabolic costs.

The complexity of cycling performance evaluation provides continuing challenges and opportunities in various aspects. The markerless motion capture system combined with the elliptical zone method proved to be very applicable, feasible, effective and affordable, resulted in an accurate enough 3D manikin for the aerodynamic analysis. This study has shown that CFD holds extensive leverages, which can lead to whole-flow field data and, therefore, produce enormous detailed insight into the cyclist position's aerodynamic behavior and performance. Analyzing different time trial handlebar positions has shown that although moving the handlebar down have not affected the physiological performances significantly, it could reduce the drag area and improve the produced power through the increased GMax activity and hip extension angle while pedaling.

6.2 Limitations and future research

Although the accuracy of the acquisition of the markerless sensor was evaluated and considered to be acceptable, it has been shown that capturing the motions using more than one Kinect simultaneously can improve accuracy through specific approaches, such as the multi-Kinect trilateration approach (L. Yang et al., 2015). Furthermore, emphasis on more sophisticated algorithms for reducing the noise of depth data and captured sequences would simplify the reconstruction, allowing surfaces to converge higher resolution data quicker.

The focus of this investigation was directed towards the performance of muscle activities, kinematics and aerodynamics in trained cyclists. We did not analyze the performance of novice cyclists, which could provide more extensive insight into the involved parameters. A further limitation relates to the effect of pedaling cadence manipulation during cycling in different positions that have not been considered. Although cadence was not interrupted due to concerns regarding its interference with the biomechanical performance, cyclists were instructed to maintain the predetermined cadence using a visual display mounted in front of them. However, previous studies indicated that the lower limb muscle activation patterns and contractions could vary with cadence variations (Baum & Li, 2003; Marsh & Martin, 1995; Sanderson et al., 2006). Therefore, the covariate effect of various range of pedaling cadences on different handlebar positions' biomechanical performance could be beneficial in future studies. Also, it is suggested to collect EMG of both right and left legs while recording the kinetic data, including the effective force on the seat and handlebar, as well as kinematics.

Although collecting the high-resolution pedal force data provides a means of directly evaluating each lower segment's force production, pedal forces were not recorded in this study.

The 2D and 3D pedal forces can be measured using strain gauges or piezoelectric elements implemented in the pedal (Broker & Gregor, 1990). However, the shoe clip is restricted to the built-on pedal system that restricted the use of standard pedal cleats commonly used in cycling, forcing participants to change their pedal-shoe interface and readjust the foot position (Drouet et al., 2008; Wangerin et al., 2007). Therefore, future studies should perform tests on the ergometer mounted on the force plate to allow the 3D pedal force measurement while cyclists using their own shoe and pedal system.

Another limitation encountered in practical operation is that the saddle position and inclination were kept constant while altering the handlebar positions to consider the relationship of different parts of the bike frame. However, cyclists and triathletes commonly modify the handlebar position and saddle adjustment simultaneously to improve cycling comfort. Further research should evaluate the cofounding effect of the handlebar position on the saddle height and tilt angle and their biomechanical performance interactions.

The CFD simulations applied for different time trial handlebar positions were based on the same cyclist's parameterized 3D body model. Our intention was to eliminate anthropometric bias in comparing the various positions. Although the obtained aerodynamic parameters, i.e., the frontal area, drag coefficient and drag area, will vary for individuals, it is expected that the patterns resulted from the CFD analysis will be consistent between different cyclists. Finally, the CFD simulations were conducted with the assumption of static legs, which was based on earlier research that showed the flow topology of a pedaling cyclist, averaged over one pedaling revolution, is similar to that of the same cyclist with the crank at the related phase of leg rotation (Crouch et al., 2016). Nevertheless, the effect of high pedaling frequency is predicted to be similar for all the submaximal tested positions. Future research should pay more attention to these limitations to improve our numerical model.

CHAPTER 7 CONCLUSION AND RECOMMENDATIONS

To date, a considerable body of research has sought to understand the effects of cyclists' positioning on cycling performance. However, the biomechanical and aerodynamic outcomes of altering the handlebar position have not been sufficiently specified. The present work is designed to be the first to consider the handlebar position effects on the performance extensively. In particular, this thesis was dedicated to examining cyclists' performance in various time trial positions using a markerless motion capture system. Although both Kinect sensors and elliptical zone techniques have been used separately in clinical and biomechanical applications, this is the first time combining these methods is attempted. This study demonstrates that the parameterized modeling framework developed and validated as part of this thesis has the potential to provide reliable, applicable, and affordable data for conducting a further aerodynamic analysis of cycling position.

The biomechanical evaluation of muscle recruitments in various handlebar positions showed that changing the aero handlebar position influenced the pattern and timing of monoarticular muscles of the hip and knee (GMax and VL). Furthermore, the hip extension angle increased when lowering the handlebar; however, the knee and ankle angles declined. Although we cannot directly conclude on implications for performance, reducing the handlebar position seems beneficial.

Finally, from the CFD simulations of six different handlebar positions, it was clearly shown that there were significant differences in aerodynamic drag and cyclist's frontal area when the handlebar position altered. The lowered handlebar position exhibited the least value of the drag area, which exceed the metabolic cost of respiratory work. This reduction resulted from a decrease in both frontal area and drag coefficient related to the limited pressure gradients on the back of the cyclist. Results have also shown that lowering the handlebar position is more effective than moving it forward in terms of drag area.

The findings provide practical understanding to researchers, clinicians and coaches regarding muscle recruitment when altering the handlebar. Lowering the handlebar position has proven to have likely a moderately positive effect on the biomechanical performance as well as gain aerodynamic benefit.

BIBLIOGRAPHY

Abdullah, M., Muda, M., Mustapha, F., & Shamsudin, M. (2017). Aerodynamics analysis for an outdoor road cycling helmet and air attack helmet. *International Journal of Materials, Mechanics and Manufacturing*, *5*(1), 46–50.

Abdullah, M. N., Mustapha, F., Muda, M., Arrifin, M., Rafie, A., & Shamsudin, M. (2015). Simulating bio-composite cycling helmet performance through fea and cfd approaches. *Malaysian Journal of Movement, Health & Exercise*, *4*(1).

Alam, F., Chowdhury, H., Elmir, Z., Sayogo, A., Love, J., & Subic, A. (2010). An experimental study of thermal comfort and aerodynamic efficiency of recreational and racing bicycle helmets. *Procedia Engineering*, *2*(2), 2413–2418.

Alam, F., Chowdhury, H., Wei, H. Z., Mustary, I., & Zimmer, G. (2014). Aerodynamics of ribbed bicycle racing helmets. *Procedia engineering*, *72*, 691–696.

Alexander, E. J., & Andriacchi, T. P. (2001). Correcting for deformation in skin-based marker systems. *Journal of biomechanics*, *34*(3), 355–361.

Amarantini, D., & Martin, L. (2004). A method to combine numerical optimization and emg data for the estimation of joint moments under dynamic conditions. *Journal of biomechanics*, *37*(9), 1393–1404.

Barber, S., Chin, S., & Carré, M. (2009). Sports ball aerodynamics: A numerical study of the erratic motion of soccer balls. *Computers & Fluids*, *38*(6), 1091–1100.

Barry, N., Burton, D., Sheridan, J., Thompson, M., & Brown, N. A. (2015a). Aerodynamic drag interactions between cyclists in a team pursuit. *Sports Engineering*, *18*(2), 93–103.

Barry, N., Burton, D., Sheridan, J., Thompson, M., & Brown, N. A. (2015b). Aerodynamic performance and riding posture in road cycling and triathlon. *Proceedings of the Institution of Mechanical Engineers, Part P: Journal of Sports Engineering and Technology*, *229*(1), 28–38.

Bartlett, R., Wheat, J., & Robins, M. (2007). Is movement variability important for sports biomechanists? *Sports biomechanics*, *6*(2), 224–243.

Baum, B. S., & Li, L. (2003). Lower extremity muscle activities during cycling are influenced by load and frequency. *Journal of Electromyography and Kinesiology*, *13*(2), 181–190.

Beaumont, F., Taiar, R., Polidori, G., Trenchard, H., & Grappe, F. (2018). Aerodynamic study of time-trial helmets in cycling racing using cfd analysis. *Journal of biomechanics*, *67*, 1–8.

Bell, A. L., Brand, R. A., & Pedersen, D. R. (1989). Prediction of hip joint centre location from external landmarks. *Human movement science*, *8*(1), 3–16.

Belluye, N., & Cid, M. (2001). Approche biomécanique du cyclisme moderne, données de la littérature. *Science & sports*, *16*(2), 71–87.

Benoit, D. L., Ramsey, D. K., Lamontagne, M., Xu, L., Wretenberg, P., & Renström, P. (2006). Effect of skin movement artifact on knee kinematics during gait and cutting motions measured in vivo. *Gait & posture*, *24*(2), 152–164.

Berger, K., Ruhl, K., Schroeder, Y., Bruemmer, C., Scholz, A., & Magnor, M. A. (2011). Markerless motion capture using multiple color-depth sensors. *VMV*, 317–324.

Berry, M., Pollock, W., Van Nieuwenhuizen, K., & Brubaker, P. (1994). A comparison between aero and standard racing handlebars during prolonged exercise. *International journal of sports medicine*, *15*(01), 16–20.

Bijker, K., De Groot, G., & Hollander, A. (2002). Differences in leg muscle activity during running and cycling in humans. *European journal of applied physiology*, *87*(6), 556–561.

Bini, R., Hume, P. A., & Croft, J. L. (2011). Effects of bicycle saddle height on knee injury risk and cycling performance. *Sports Medicine*, *41*(6), 463–476.

Bini, R. R., Hume, P. A., Lanferdini, F. J., & Vaz, M. A. (2014). Effects of body positions on the saddle on pedalling technique for cyclists and triathletes. *European journal of sport science*, *14*(sup1), S413–S420.

Bini, R. R., Hume, P. A., Lanferdini, F. J., & Vaz, M. A. (2013). Effects of moving forward or backward on the saddle on knee joint forces during cycling. *Physical Therapy in Sport*, *14*(1), 23–27.

Bini, R. R., Rossato, M., Diefenthaeler, F., Carpes, F. P., dos Reis, D. C., & Moro, A. R. P. (2010). Pedaling cadence effects on joint mechanical work during cycling. *Isokinetics and Exercise Science*, *18*(1), 7–13.

Bixler, B., Pease, D., & Fairhurst, F. (2007). The accuracy of computational fluid dynamics analysis of the passive drag of a male swimmer. *Sports biomechanics*, *6*(1), 81–98.

Bixler, B., & Riewald, S. (2002). Analysis of a swimmer's hand and arm in steady flow conditions using computational fluid dynamics. *Journal of biomechanics*, *35*(5), 713–717.

Blake, O., Champoux, Y., & Wakeling, J. (2012). Muscle coordination patterns for efficient cycling. *Medicine & Science in Sports & Exercise*, *44*(5), 926–938.

Blocken, B. (2014). 50 years of computational wind engineering: Past, present and future. *Journal of Wind Engineering and Industrial Aerodynamics*, *129*, 69–102.

Blocken, B. (2018). Les over rans in building simulation for outdoor and indoor applications: A foregone conclusion? *Building Simulation*, *11*(5), 821–870.

Blocken, B., Defraeye, T., Koninckx, E., Carmeliet, J., & Hespel, P. (2013). Cfd simulations of the aerodynamic drag of two drafting cyclists. *Computers & Fluids*, *71*, 435–445.

Blocken, B., & Toparlar, Y. (2015). A following car influences cyclist drag: Cfd simulations and wind tunnel measurements. *Journal of Wind Engineering and Industrial Aerodynamics*, *145*, 178–186.

Blocken, B., van Druenen, T., Toparlar, Y., & Andrianne, T. (2019). Cfd analysis of an exceptional cyclist sprint position. *Sports Engineering*, *22*(1), 10.

Boehnen, C., & Flynn, P. (2005). Accuracy of 3d scanning technologies in a face scanning scenario. *Fifth International Conference on 3-D Digital Imaging and Modeling (3DIM'05)*, 310–317.

Bonnechere, B., Jansen, B., Salvia, P., Bouzahouene, H., Omelina, L., Moiseev, F., Sholukha, V., Cornelis, J., Rooze, M., & Jan, S. V. S. (2014). Validity and reliability of the kinect within functional assessment activities: Comparison with standard stereophotogrammetry. *Gait & posture*, *39*(1), 593–598.

Borg, G. (1998). *Borg's perceived exertion and pain scales.* Human kinetics.

Broker, J. P., & Gregor, R. J. (1990). A dual piezoelectric element force pedal for kinetic analysis of cycling. *Journal of Applied Biomechanics*, *6*(4), 394–403.

Brown, D. A., Kautz, S., & Dairaghi, C. (1996). Muscle activity patterns altered during pedaling at different body orientations. *Journal of biomechanics*, *29*(10), 1349–1356.

Brownlie, L., Ostafichuk, P., Tews, E., Muller, H., Briggs, E., & Franks, K. (2010). The wind-averaged aerodynamic drag of competitive time trial cycling helmets. *Procedia Engineering*, *2*(2), 2419–2424.

Burke, E. (2003). *High-tech cycling.* Human Kinetics.

Candau, R. B., Grappe, F., Menard, M., Barbier, B., Millet, G. Y., Hoffman, M. D., Belli, A. R., & Rouillon, J. D. (1999). Simplified deceleration method for assessment of resistive forces in cycling. *Medicine and science in sports and exercise*, *31*, 1441–1447.

Capelli, C., Rosa, G., Butti, F., Ferretti, G., Veicsteinas, A., & di Prampero, P. E. (1993). Energy cost and efficiency of riding aerodynamic bicycles. *European journal of applied physiology and occupational physiology*, *67*(2), 144–149.

Casey, M., & Wintergerste, T. (2000). Ercoftac special interest group on quality and trust in industrial cfd-best practice guidelines. *European research community on flow, turbulence and combustion*, 123.

Casper, R. M., Jacobs, A. M., Kenney, E. S., & McMaster, I. B. (1971). On the use of gamma ray images for the determination of human body segment mass parameters. *Quantitative Imagery in the Biomedical Sciences I*, *26*, 49–58.

Chabroux, V., Barelle, C., & Favier, D. (2012). Aerodynamics of cyclist posture, bicycle and helmet characteristics in time trial stage. *Journal of applied biomechanics*, *28*(3), 317–323.

Chang, Y.-J., Chen, S.-F., & Huang, J.-D. (2011). A kinect-based system for physical rehabilitation: A pilot study for young adults with motor disabilities. *Research in developmental disabilities*, *32*(6), 2566–2570.

Chapman, A. R., Vicenzino, B., Blanch, P., Knox, J. J., Dowlan, S., & Hodges, P. W. (2008). The influence of body position on leg kinematics and muscle recruitment during cycling. *Journal of Science and Medicine in Sport*, *11*(6), 519–526.

Chen, G., Li, J., Wang, B., Zeng, J., Lu, G., & Zhang, D. (2016). Reconstructing 3d human models with a kinect. *Computer Animation and Virtual Worlds*, *27*(1), 72–85.

Chin, L. M., Kowalchuk, J. M., Barstow, T. J., Kondo, N., Amano, T., Shiojiri, T., & Koga, S. (2011). The relationship between muscle deoxygenation and activation in different muscles of the quadriceps during cycle ramp exercise. *Journal of applied physiology*, *111*(5), 1259–1265.

Chiu, M.-C., Wu, H.-C., & Tsai, N.-T. (2013). The relationship between handlebar and saddle heights on cycling comfort. *International Conference on Human Interface and the Management of Information*, 12–19.

Choppin, S., Lane, B., & Wheat, J. (2014). The accuracy of the microsoft kinect in joint angle measurement. *Sports Technology*, *7*(1-2), 98–105.

Choppin, S., & Wheat, J. (2013). The potential of the microsoft kinect in sports analysis and biomechanics. *Sports Technology*, *6*(2), 78–85.

Chowdhury, H., & Alam, F. (2014). An experimental study on aerodynamic performance of time trial bicycle helmets. *Sports Engineering*, *17*(3), 165–170.

Chowdhury, H., Alam, F., & Subic, A. (2010). Aerodynamic performance evaluation of sports textile. *Procedia Engineering*, *2*(2), 2517–2522.

Clarkson, S., Wheat, J., Heller, B., Webster, J., & Choppin, S. (2013). Distortion correction of depth data from consumer depth cameras. *3D Body Scanning Technologies, Long Beach, California, Hometrica Consulting*, 426–437.

Clauser, C. E., McConville, J. T., & Young, J. W. (1969). *Weight, volume, and center of mass of segments of the human body* (tech. rep.). Antioch Coll Yellow Springs OH.

Coyle, E., Feltner, M., Kautz, S., Hamilton, M., Montain, S., Baylor, A., Abraham, L., & Petrek, G. (1991). Physiological and biomechanical factors associated with elite

endurance cycling performance. *Medicine and science in sports and exercise*, *23*(1), 93–107.

Cram, J. R. (2003). The history of surface electromyography. *Applied psychophysiology and biofeedback*, *28*(2), 81–91.

Crouch, T. N., Burton, D., LaBry, Z. A., & Blair, K. B. (2017). Riding against the wind: A review of competition cycling aerodynamics. *Sports Engineering*, *20*(2), 81–110.

Crouch, T. N., Burton, D., Thompson, M. C., Brown, N. A., & Sheridan, J. (2016). Dynamic leg-motion and its effect on the aerodynamic performance of cyclists. *Journal of Fluids and Structures*, *65*, 121–137.

Crouch, T. N., Burton, D., Brown, N. A. T., Thompson, M. C., & Sheridan, J. (2014). Flow topology in the wake of a cyclist and its effect on aerodynamic drag. *Journal of Fluid Mechanics*, *748*, 5–35.

Dabnichki, P., & Avital, E. (2006). Influence of the postion of crew members on aerodynamics performance of two-man bobsleigh. *Journal of Biomechanics*, *39*(15), 2733–2742.

Dal Monte, A., Leonardi, L., Menchinelli, C., & Marini, C. (1987). A new bicycle design based on biomechanics and advanced technology. *Journal of Applied Biomechanics*, *3*(3), 287–292.

da Silva, J. C. L., Tarassova, O., Ekblom, M., Andersson, E., Rönquist, G., & Arndt, A. (2016). Quadriceps and hamstring muscle activity during cycling as measured with intramuscular electromyography. *European journal of applied physiology*, *116*(9), 1807–1817.

Davidson, C. M., De Vito, G., & Lowery, M. M. (2016). Effect of oral glucose supplementation on surface emg during fatiguing dynamic exercise. *2016 38th Annual International Conference of the IEEE Engineering in Medicine and Biology Society (EMBC)*, 3498–3502.

Davies, C. (1980). Effect of air resistance on the metabolic cost and performance of cycling. *European journal of applied physiology and occupational physiology*, *45*(2-3), 245–254.

Debraux, P., Grappe, F., Manolova, A. V., & Bertucci, W. (2011). Aerodynamic drag in cycling: Methods of assessment. *Sports Biomechanics*, *10*(3), 197–218.

Dedieu, P., Pelaez, M., Poirier, E., & Zanone, P.-G. (2020). Effects of saddle height on muscular pattern and interlimb coordination in cycling. *Journal of Physical Education and Sport*, *20*(1), 222–228.

Defraeye, T., Blocken, B., & Carmeliet, J. (2010). Cfd analysis of convective heat transfer at the surfaces of a cube immersed in a turbulent boundary layer. *International Journal of Heat and Mass Transfer*, *53*(1-3), 297–308.

Defraeye, T., Blocken, B., Koninckx, E., Hespel, P., & Carmeliet, J. (2010a). Aerodynamic study of different cyclist positions: Cfd analysis and full-scale wind-tunnel tests. *Journal of biomechanics*, *43*(7), 1262–1268.

Defraeye, T., Blocken, B., Koninckx, E., Hespel, P., & Carmeliet, J. (2010b). Computational fluid dynamics analysis of cyclist aerodynamics: Performance of different turbulence-modelling and boundary-layer modelling approaches. *Journal of biomechanics*, *43*(12), 2281–2287.

Defraeye, T., Blocken, B., Koninckx, E., Hespel, P., & Carmeliet, J. (2011). Computational fluid dynamics analysis of drag and convective heat transfer of individual body segments for different cyclist positions. *Journal of biomechanics*, *44*(9), 1695–1701.

Defraeye, T., Blocken, B., Koninckx, E., Hespel, P., Verboven, P., Nicolai, B., & Carmeliet, J. (2014). Cyclist drag in team pursuit: Influence of cyclist sequence, stature, and arm spacing. *Journal of biomechanical engineering*, *136*(1).

Dempster, W. T. (1955). *Space requirements of the seated operator, geometrical, kinematic, and mechanical aspects of the body with special reference to the limbs* (tech. rep.). Michigan State Univ East Lansing.

Dempster, W. T., & Gaughran, G. R. (1967). Properties of body segments based on size and weight. *American journal of anatomy*, *120*(1), 33–54.

de Pauw, K., Roelands, B., Cheung, S. S., De Geus, B., Rietjens, G., & Meeusen, R. (2013). Guidelines to classify subject groups in sport-science research. *International journal of sports physiology and performance*, *8*(2), 111–122.

Deschenes, M. R., Kraemer, W. J., McCoy, R. W., Volek, J. S., Turner, B. M., & Weinlein, J. C. (2000). Muscle recruitment patterns regulate physiological responses during exercise of the same intensity. *American Journal of Physiology-Regulatory, Integrative and Comparative Physiology*, *279*(6), R2229–R2236.

Di Prampero, P., Cortili, G., Mognoni, P., & Saibene, F. (1979). Equation of motion of a cyclist. *Journal of Applied Physiology*, *47*(1), 201–206.

Di Prampero, P. E. (2000). Cycling on earth, in space, on the moon. *European journal of applied physiology*, *82*(5-6), 345–360.

Dorel, S., Couturier, A., & Hug, F. (2008). Intra-session repeatability of lower limb muscles activation pattern during pedaling. *Journal of Electromyography and Kinesiology*, *18*(5), 857–865.

Dorel, S., Couturier, A., & Hug, F. (2009). Influence of different racing positions on mechanical and electromyographic patterns during pedalling. *Scandinavian journal of medicine & science in sports*, *19*(1), 44–54.

Drouet, J.-M., Champoux, Y., & Dorel, S. (2008). Development of multi-platform instrumented force pedals for track cycling (p49). *The engineering of sport 7*, 263–271.

Duc, S., Bertucci, W., Pernin, J., & Grappe, F. (2008). Muscular activity during uphill cycling: Effect of slope, posture, hand grip position and constrained bicycle lateral sways. *Journal of Electromyography and Kinesiology*, *18*(1), 116–127.

Durkin, J. L., Dowling, J. J., & Andrews, D. M. (2002). The measurement of body segment inertial parameters using dual energy x-ray absorptiometry. *Journal of biomechanics*, *35*(12), 1575–1580.

Dutta, T. (2012). Evaluation of the kinect™ sensor for 3-d kinematic measurement in the workplace. *Applied ergonomics*, *43*(4), 645–649.

Elmer, S., Barratt, P., Korff, T., & Martin, J. (2010). Joint-specific power production during submaximal and maximal cycling. *ISBS-Conference Proceedings Archive*.

Ericson, M. (1986). On the biomechanics of cycling. a study of joint and muscle load during exercise on the bicycle ergometer. *Scandinavian journal of rehabilitation medicine. Supplement*, *16*, 1–43.

Espitia-Contreras, A., Sanchez-Caiman, P., & Uribe-Quevedo, A. (2014). Development of a kinect-based anthropometric measurement application. *2014 IEEE Virtual Reality (VR)*, 71–72.

Evangelisti, M. I., Verde, T. J., Andres, F. F., & Flynn, M. G. (1995). Effects of handlebar position on physiological responses to prolonged cycling. *The Journal of Strength & Conditioning Research*, *9*(4), 243–246.

Fern'ndez-Baena, A., Susín, A., & Lligadas, X. (2012). Biomechanical validation of upper-body and lower-body joint movements of kinect motion capture data for rehabilitation treatments. *2012 fourth international conference on intelligent networking and collaborative systems*, 656–661.

Ferrer-Roca, V., Roig, A., Galilea, P., & Garc'ıa-López, J. (2012). Influence of saddle height on lower limb kinematics in well-trained cyclists: Static vs. dynamic evaluation in bike fitting. *The Journal of Strength & Conditioning Research*, *26*(11), 3025–3029.

Fintelman, D., Sterling, M., Hemida, H., & Li, F. (2015). The effect of time trial cycling position on physiological and aerodynamic variables. *Journal of sports sciences*, *33*(16), 1730–1737.

Fintelman, D., Sterling, M., Hemida, H., & Li, F.-X. (2016). Effect of different aerodynamic time trial cycling positions on muscle activation and crank torque. *Scandinavian journal of medicine & science in sports*, *26*(5), 528–534.

Fintelman, D., Sterling, M., Hemida, H., & Li, F.-X. (2014). The effect of crosswinds on cyclists: An experimental study. *Procedia Engineering*, *72*, 720–725.

Fiorentino, N. M., Atkins, P. R., Kutschke, M. J., Goebel, J. M., Foreman, K. B., & Anderson, A. E. (2017). Soft tissue artifact causes significant errors in the calculation of joint angles and range of motion at the hip. *Gait & posture*, *55*, 184–190.

Franke, W., Betz, C., & Humphrey, R. H. (1994). Effects of rider position on continuous wave doppler responses to maximal cycle ergometry. *British journal of sports medicine*, *28*(1), 38–42.

Frigo, C., & Shiavi, R. (2004). Applications in movement and gait analysis. *Electromyography: Physiology, engineering, and noninvasive applications. Hoboken (NJ): John Wiley & Sons, Inc*, 381–402.

Gabel, M., Gilad-Bachrach, R., Renshaw, E., & Schuster, A. (2012). Full body gait analysis with kinect. *2012 Annual International Conference of the IEEE Engineering in Medicine and Biology Society*, 1964–1967.

Galna, B., Barry, G., Jackson, D., Mhiripiri, D., Olivier, P., & Rochester, L. (2014). Accuracy of the microsoft kinect sensor for measuring movement in people with parkinson's disease. *Gait & posture*, *39*(4), 1062–1068.

Garcia-Lopez, J., Rodriguez-Marroyo, J., Juneau, C.-E., Peleteiro, J., Martínez, A., & Villa, J. (2008). Reference values and improvement of aerodynamic drag in professional cyclists. *Journal of sports sciences*, *26*(3), 277–286.

Gardan, N., Schneider, A., Polidori, G., Trenchard, H., Seigneur, J.-M., Beaumont, F., Fourchet, F., & Taiar, R. (2017). Numerical investigation of the early flight phase in ski-jumping. *Journal of biomechanics*, *59*, 29–34.

Gardano, P., & Dabnichki, P. (2006). On hydrodynamics of drag and lift of the human arm. *Journal of Biomechanics*, *39*(15), 2767–2773.

Ghasemi, M., Curnier, D., Caru, M., Pageaux, B., Trépanier, J.-Y., & Périé, D. (2020). The effect of different aero handlebar positions on muscle activity and kinematics of lower limb [Manuscript submitted for publication]. *Journal of Sports Sciences*.

Ghasemi, M., Curnier, D., Caru, M., Trépanier, J.-Y., & Périé, D. (2020). The effect of different aero handlebar positions on aerodynamic and physiological variables activity and kinematics of lower limb [Manuscript submitted for publication]. *Journal of Biomechanics*.

Ghasemi, M., Curnier, D., Trépanier, J.-Y., Koenig, H., Pietro, E., & Périé, D. (2020). Fully parameterized body anthropometry for the aerodynamic analysis of cyclist position using the cfd method [Manuscript submitted for publication]. *Part P: Journal of Sports Engineering and Technology*.

Gibertini, G., Campanardi, G., Grassi, D., & Macchi, C. (2008). Aerodynamics of biker position. *BBAA VI International Colloquium on: Bluff Bodies Aerodynamics & Applications*, 20–24.

Gibertini, G., & Grassi, D. (2008). Cycling aerodynamics. *Sport aerodynamics* (pp. 23–47). Springer.

Gnehm, P., REICHENBACH, S., ALTPETER, E., WIDMER, H., & HOPPELER, H. (1997). Influence of different racing positions on metabolic cost in elite cyclists. *Medicine & Science in Sports & Exercise*, *29*(6), 818–823.

Grappe, F., Candau, R., Busso, T., & Rouillon, J. (1998). Effect of cycling position on ventilatory and metabolic variables. *International journal of sports medicine*, *19*, 336–341.

Grappe, F., Candau, R., Belli, A., & Rouillon, J. D. (1997). Aerodynamic drag in field cycling with special reference to the obree's position. *Ergonomics*, *40*(12), 1299–1311.

Gregor, R. J., Broker, J. P., & Ryan, M. M. (1991). 4 the biomechanics of cycling. *Exercise and sport sciences reviews*, *19*(1), 127–170.

Griffith, M. D., Crouch, T., Thompson, M. C., Burton, D., Sheridan, J., & Brown, N. A. (2014). Computational fluid dynamics study of the effect of leg position on cyclist aerodynamic drag. *Journal of Fluids Engineering*, *136*(10).

Gross, A. C., Kyle, C. R., & Malewicki, D. J. (1983). The aerodynamics of human-powered land vehicles. *Scientific American*, *249*(6), 142–153.

Han, J., Shao, L., Xu, D., & Shotton, J. (2013). Enhanced computer vision with microsoft kinect sensor: A review. *IEEE transactions on cybernetics*, *43*(5), 1318–1334.

Han, S., Achar, M., Lee, S., & Peña-Mora, F. (2013). Empirical assessment of a rgb-d sensor on motion capture and action recognition for construction worker monitoring. *Visualization in Engineering*, *1*(1), 1–13.

Hanna, R., Ujihashi, S., & Haake, S. (2002). Can cfd make a performance difference in sport. *The engineering of sport*, *4*, 17–30.

Heil, D., Derrick, T., & Whittlesey, S. (1997). The relationship between preferred and optimal positioning during submaximal cycle ergometry. *European journal of applied physiology and occupational physiology*, *75*(2), 160–165.

Hermens, H. J., Freriks, B., Disselhorst-Klug, C., & Rau, G. (2000). Development of recommendations for semg sensors and sensor placement procedures. *Journal of electromyography and Kinesiology*, *10*(5), 361–374.

Holliday, W., Fisher, J., Theo, R., & Swart, J. (2017). Static versus dynamic kinematics in cyclists: A comparison of goniometer, inclinometer and 3d motion capture. *European Journal of Sport Science*, *17*(9), 1129–1142.

Houtz, S., & Fischer, F. J. (1959). An analysis of muscle action and joint excursion during exercise on a stationary bicycle. *JBJS*, *41*(1), 123–131.

Hsu, W.-L., Krishnamoorthy, V., & Scholz, J. P. (2006). An alternative test of electromyographic normalization in patients. *Muscle & Nerve: Official Journal of the American Association of Electrodiagnostic Medicine*, *33*(2), 232–241.

Hug, F., Bendahan, D., Le Fur, Y., Cozzone, P. J., & Grelot, L. (2004). Heterogeneity of muscle recruitment pattern during pedaling in professional road cyclists: A magnetic resonance imaging and electromyography study. *European journal of applied physiology*, *92*(3), 334–342.

Hug, F., Decherchi, P., Marqueste, T., & Jammes, Y. (2004). Emg versus oxygen uptake during cycling exercise in trained and untrained subjects. *Journal of Electromyography and Kinesiology*, *14*(2), 187–195.

Hug, F., & Dorel, S. (2009). Electromyographic analysis of pedaling: A review. *Journal of electromyography and Kinesiology*, *19*(2), 182–198.

Jensen, R. K. (1978). Estimation of the biomechanical properties of three body types using a photogrammetric method. *Journal of biomechanics*, *11*(8-9), 349–358.

Jeukendrup, A. E., & Martin, J. (2001). Improving cycling performance. *Sports Medicine*, *31*(7), 559–569.

Jobson, S. A., Nevill, A. M., George, S. R., Jeukendrup, A., & Passfield, L. (2008). Influence of body position when considering the ecological validity of laboratory time-trial cycling performance. *Journal of sports sciences*, *26*(12), 1269–1278.

Jorge, M., & Hull, M. (1986). Analysis of emg measurements during bicycle pedalling. *Journal of biomechanics*, *19*(9), 683–694.

Jux, C., Sciacchitano, A., Schneiders, J. F., & Scarano, F. (2018). Robotic volumetric piv of a full-scale cyclist. *Experiments in Fluids*, *59*(4), 74.

Katović, D., Gruić, I., Bušić, A., Bronzin, T., Pažin, K., Bolčević, F., Medved, V., & Mišigoj-Duraković, M. (2016). Development of computer system for digital measurement of human body: Initial findings. *icSPORTS 2016-4th International Congress on Sport Sciences Research and Technology Support*.

Knox, J. J., & Hodges, P. W. (2005). Changes in head and neck position affect elbow joint position sense. *Experimental brain research*, *165*(1), 107–113.

Knutson, L. M., Soderberg, G. L., Ballantyne, B. T., & Clarke, W. R. (1994). A study of various normalization procedures for within day electromyographic data. *Journal of electromyography and kinesiology*, *4*(1), 47–59.

Kyle, C. R., & Burke, E. (1984). Improving the racing bicycle. *Mechanical engineering*, *106*(9), 34–45.

Kyle, C. (1989). The aerodynamics of handlebars and helmets. *Cycling Science*, *1*(1), 22–25.

Kyle, C. (1991). The effect of crosswinds upon time trials. *Cycling Sci*, *3*(3-4), 51–6.

Kyle, C., & Weaver, M. (2004). Aerodynamics of human-powered vehicles. *Proceedings of the Institution of Mechanical Engineers, Part A: Journal of Power and Energy*, *218*(3), 141–154.

Lakens, D. (2013). Calculating and reporting effect sizes to facilitate cumulative science: A practical primer for t-tests and anovas. *Frontiers in psychology*, *4*, 863.

Langtry, R. B., & Menter, F. R. (2009). Correlation-based transition modeling for unstructured parallelized computational fluid dynamics codes. *AIAA journal*, *47*(12), 2894–2906.

Laplaud, D., Hug, F., & Grélot, L. (2006). Reproducibility of eight lower limb muscles activity level in the course of an incremental pedaling exercise. *Journal of Electromyography and Kinesiology*, *16*(2), 158–166.

Leardini, A., Chiari, L., Della Croce, U., & Cappozzo, A. (2005). Human movement analysis using stereophotogrammetry: Part 3. soft tissue artifact assessment and compensation. *Gait & posture*, *21*(2), 212–225.

Lecrivain, G., Slaouti, A., Payton, C., & Kennedy, I. (2008). Using reverse engineering and computational fluid dynamics to investigate a lower arm amputee swimmer's performance. *Journal of Biomechanics*, *41*(13), 2855–2859.

Li, L. (2004). Neuromuscular control and coordination during cycling. *Research quarterly for exercise and sport*, *75*(1), 16–22.

Li, L., & Caldwell, G. E. (1998). Muscle coordination in cycling: Effect of surface incline and posture. *Journal of Applied Physiology*, *85*(3), 927–934.

Lukes, R., Chin, S., & Haake, S. (2005). The understanding and development of cycling aerodynamics. *Sports engineering*, *8*(2), 59–74.

Lukes, R., Hart, J., Chin, S., & Haake, S. (2004). The aerodynamics of mountain bicycles: The role of computational fluid dynamics. *The Engineering of Sport*, 104–110.

Ma, Y., Kwon, J., Mao, Z., Lee, K., Li, L., & Chung, H. (2011). Segment inertial parameters of korean adults estimated from three-dimensional body laser scan data. *International Journal of Industrial Ergonomics*, *41*(1), 19–29.

MacIntosh, B. R., Neptune, R. R., & Horton, J. F. (2000). Cadence, power, and muscle activation in cycle ergometry. *Medicine and science in sports and exercise*, *32*(7), 1281–1287.

Mannion, P., Toparlar, Y., Blocken, B., Clifford, E., Andrianne, T., & Hajdukiewicz, M. (2018). Analysis of crosswind aerodynamics for competitive hand-cycling. *Journal of Wind Engineering and Industrial Aerodynamics*, *180*, 182–190.

Marsh, A. P., & Martin, P. E. (1995). The relationship between cadence and lower extremity emg in cyclists and noncyclists. *Medicine and science in sports and exercise*, *27*(2), 217–225.

Martin, J. C., & Brown, N. A. (2009). Joint-specific power production and fatigue during maximal cycling. *Journal of biomechanics*, *42*(4), 474–479.

Martin, J. C., Gardner, A. S., Barras, M., & MARTIN, D. T. (2006). Modeling sprint cycling using field-derived parameters and forward integration. *Medicine & Science in Sports & Exercise*, *38*(3), 592–597.

Martin, J. C., Milliken, D. L., Cobb, J. E., McFadden, K. L., & Coggan, A. R. (1998). Validation of a mathematical model for road cycling power. *Journal of applied biomechanics*, *14*(3), 276–291.

Martin, J. C., & Nichols, J. A. (2018). Simulated work loops predict maximal human cycling power. *Journal of Experimental Biology*, *221*(13), jeb180109.

Martin, P. E., Mungiole, M., Marzke, M. W., & Longhill, J. M. (1989). The use of magnetic resonance imaging for measuring segment inertial properties. *Journal of biomechanics*, *22*(4), 367–376.

Massion, J., Alexandrov, A., & Frolov, A. (2004). Why and how are posture and movement coordinated? *Progress in brain research* (pp. 13–27). Elsevier.

Meile, W., Reisenberger, E., Mayer, M., Schmölzer, B., Müller, W., & Brenn, G. (2006). Aerodynamics of ski jumping: Experiments and cfd simulations. *Experiments in fluids*, *41*(6), 949–964.

Menard, M., Domalain, M., Decatoire, A., & Lacouture, P. (2016). Influence of saddle setback on pedalling technique effectiveness in cycling. *Sports biomechanics*, *15*(4), 462–472.

Millet, G., & Candau, R. (2002). Facteurs mécaniques du coût énergétique dans trois locomotions humaines. *Science & sports*, *17*(4), 166–176.

Mirka, G. A. (1991). The quantification of emg normalization error. *Ergonomics*, *34*(3), 343–352.

Mornieux, G., Stapelfeldt, B., Gollhofer, A., & Belli, A. (2008). Effects of pedal type and pull-up action during cycling. *International journal of sports medicine*, *29*(10), 817–822.

Mustary, I., Chowdhury, H., Loganathan, B., Alharthi, M., & Alam, F. (2014). Aerodynamic efficiency and thermal comfort of road racing bicycle helmets. *19th Australasian Fluid Mechanics Conference, Melbourne, Australia*.

Napoli, A., Glass, S., Ward, C., Tucker, C., & Obeid, I. (2017). Performance analysis of a generalized motion capture system using microsoft kinect 2.0. *Biomedical Signal Processing and Control*, *38*, 265–280.

Nguyen, C. V., Izadi, S., & Lovell, D. (2012). Modeling kinect sensor noise for improved 3d reconstruction and tracking. *2012 second international conference on 3D imaging, modeling, processing, visualization & transmission*, 524–530.

Norton, J., Donaldson, N., & Dekker, L. (2002). 3d whole body scanning to determine mass properties of legs. *Journal of biomechanics*, *35*(1), 81–86.

Oggiano, L., Leirdal, S., Sætran, L., & Ettema, G. (2008). Aerodynamic optimization and energy saving of cycling postures for international elite level cyclists. *The engineering of sport*, *7*, 597–604.

Oggiano, L., Troynikov, O., Konopov, I., Subic, A., & Alam, F. (2009). Aerodynamic behaviour of single sport jersey fabrics with different roughness and cover factors. *Sports Engineering*, *12*(1), 1–12.

Olney, S. J., & Winter, D. A. (1985). Predictions of knee and ankle moments of force in walking from emg and kinematic data. *Journal of biomechanics*, *18*(1), 9–20.

Origenes, M., Blank, S. E., Schoene, R. B., et al. (1993). Exercise ventilatory response to upright and aero-posture cycling. *Medicine and science in sports and exercise*, *25*(5), 608–612.

Padilla, S., Mujika, I., Angulo, F., & Goiriena, J. J. (2000). Scientific approach to the 1-h cycling world record: A case study. *Journal of applied physiology*, *89*(4), 1522–1527.

Pearsall, D., Reid, J., & Ross, R. (1994). Inertial properties of the human trunk of males determined from magnetic resonance imaging. *Annals of biomedical engineering*, *22*(6), 692–706.

Pedersen, D., Brand, R., Cheng, C., & Arora, J. (1987). Direct comparison of muscle force predictions using linear and nonlinear programming.

Raasch, C. C., & Zajac, F. E. (1999). Locomotor strategy for pedaling: Muscle groups and biomechanical functions. *Journal of neurophysiology*, *82*(2), 515–525.

Redfield, R., & Hull, M. (1986). Prediction of pedal forces in bicycling using optimization methods. *Journal of biomechanics*, *19*(7), 523–540.

Richardson, R. S., & Johnson, S. C. (1994). The effect of aerodynamic handlebars on oxygen consumption while cycling at a constant speed. *Ergonomics*, *37*(5), 859–863.

Roache, P. J. (1994). Perspective: A method for uniform reporting of grid refinement studies.

Roache, P. J. (1997). Quantification of uncertainty in computational fluid dynamics. *Annual review of fluid Mechanics*, *29*(1), 123–160.

Rodrigues, T. B., Catháin, C. Ó., Devine, D., Moran, K., O'Connor, N. E., & Murray, N. (2019). An evaluation of a 3d multimodal marker-less motion analysis system. *Proceedings of the 10th ACM Multimedia Systems Conference*, 213–221.

Rouboa, A., Silva, A., Leal, L., Rocha, J., & Alves, F. (2006). The effect of swimmer's hand/forearm acceleration on propulsive forces generation using computational fluid dynamics. *Journal of Biomechanics*, *39*(7), 1239–1248.

Rutberg, J. (2008). Wind tunnel vision.

Sanders, R. H., Chiu, C.-Y., Gonjo, T., Thow, J., Oliveira, N., Psycharakis, S. G., Payton, C. J., & McCabe, C. B. (2015). Reliability of the elliptical zone method of estimating body segment parameters of swimmers. *Journal of sports science & medicine*, *14*(1), 215.

Sanders, R. H., Wilson, B. D., & Jensen, R. K. (1991). Accuracy of derived ground reaction force curves for a rigid link human body model. *Journal of Applied Biomechanics*, *7*(4), 330–343.

Sanderson, D. J., & Amoroso, A. T. (2009). The influence of seat height on the mechanical function of the triceps surae muscles during steady-rate cycling. *Journal of Electromyography and Kinesiology*, *19*(6), e465–e471.

Sanderson, D. J., Martin, P., Honeyman, G., & Keefer, J. (2006). Gastrocnemius and soleus muscle length, velocity, and emg responses to changes in pedalling cadence. *Journal of Electromyography and Kinesiology*, *16*(6), 642–649.

Savelberg, H. H., Van de Port, I. G., & Willems, P. J. (2003). Body configuration in cycling affects muscle recruitment and movement pattern. *Journal of Applied Biomechanics*, *19*(4), 310–324.

Scarano, F., Terra, W., & Sciacchitano, A. (2019). Investigation of the drag crisis on the leg of a cycling mannequin by means of robotic volumetric piv. *Proceedings of the 15th International Conference on Fluid Control, Measurements and Visualization, Napoles, Italy*, 27–30.

Schmitz, A., Ye, M., Shapiro, R., Yang, R., & Noehren, B. (2014). Accuracy and repeatability of joint angles measured using a single camera markerless motion capture system. *Journal of biomechanics*, *47*(2), 587–591.

Seth, A., Sherman, M., Reinbolt, J. A., & Delp, S. L. (2011). Opensim: A musculoskeletal modeling and simulation framework for in silico investigations and exchange. *Procedia Iutam*, *2*, 212–232.

Sheets, A. L., Corazza, S., & Andriacchi, T. P. (2010). An automated image-based method of 3d subject-specific body segment parameter estimation for kinetic analyses of rapid movements. *Journal of biomechanical engineering*, *132*(1).

Shotton, J., Sharp, T., Kipman, A., Fitzgibbon, A., Finocchio, M., Blake, A., Cook, M., & Moore, R. (2013). Real-time human pose recognition in parts from single depth images. *Communications of the ACM*, *56*(1), 116–124.

Silberman, M. R., Webner, D., Collina, S., & Shiple, B. J. (2005). Road bicycle fit. *Clinical Journal of Sport Medicine*, *15*(4), 271–276.

Sims, B. W., & Jenkins, P. E. (2011). Aerodynamic bicycle helmet design using a truncated airfoil with trailing edge modifications. *ASME 2011 International Mechanical Engineering Congress and Exposition*, 453–462.

Smisek, J., Jancosek, M., & Pajdla, T. (2013). 3d with kinect. consumer depth cameras for computer vision. *Advances in Computer Vision and Pattern Recognition*, 3–25.

Spoelstra, A., de Martino Norante, L., Terra, W., Sciacchitano, A., & Scarano, F. (2019). On-site cycling drag analysis with the ring of fire. *Experiments in Fluids*, *60*(6), 90.

Sprigings, E., Burko, D., Watson, L., & Laverty, W. (1987). An evaluation of 3 segmental methods used to predict the location of the total-body cg for human airborne movements. *Journal of Human Movement Studies*, *13*(2), 57–68.

Taati, B., Campos, J., Griffiths, J., Gridseth, M., & Mihailidis, A. (2012). Towards a real-time, configurable, and affordable system for inducing sensory conflicts in a virtual environment for post-stroke mobility rehabilitation: Vision-based categorization of motion impairments. *The 9th International Conference on Disability, Virtual Reality and Associated Technologies. International Society for Virtual Rehabilitation*, 239–244.

Takaishi, T., Yamamoto, T., Ono, T., Ito, T., & Moritani, T. (1998). Neuromuscular, metabolic, and kinetic adaptations for skilled pedaling performance in cyclists. *Medicine and science in sports and exercise*, *30*, 442–449.

Tanaka, H., Monahan, K. D., & Seals, D. R. (2001). Age-predicted maximal heart rate revisited. *Journal of the american college of cardiology*, *37*(1), 153–156.

Terra, W., Sciacchitano, A., & Scarano, F. (2016). Evaluation of aerodynamic drag of a full-scale cyclist model by large-scale tomographic-piv. *International workshop on non-intrusive optical flow diagnostics, Delft*, 25–26.

Terra, W., Sciacchitano, A., & Scarano, F. (2018). A novel approach for skin suit aerodynamic optimization using local momentum deficit. *Multidisciplinary Digital Publishing Institute Proceedings*, *2*(6), 222.

Tominaga, Y., Mochida, A., Yoshie, R., Kataoka, H., Nozu, T., Yoshikawa, M., & Shirasawa, T. (2008). Aij guidelines for practical applications of cfd to pedestrian wind environment around buildings. *Journal of wind engineering and industrial aerodynamics*, *96*(10-11), 1749–1761.

Tordi, N., Perrey, S., Harvey, A., & Hughson, R. L. (2003). Oxygen uptake kinetics during two bouts of heavy cycling separated by fatiguing sprint exercise in humans. *Journal of Applied Physiology*, *94*(2), 533–541.

Underwood, L., Schumacher, J., Burette-Pommay, J., & Jermy, M. (2011). Aerodynamic drag and biomechanical power of a track cyclist as a function of shoulder and torso angles. *Sports Engineering*, *14*(2-4), 147–154.

Wangerin, M., Schmitt, S., Stapelfeldt, B., & Gollhofer, A. (2007). Inverse dynamics in cycling performance. *Advances in medical engineering* (pp. 329–334). Springer.

Wicke, J., & Lopers, B. (2003). Validation of the volume function within jensen's (1978) elliptical cylinder model. *Journal of Applied Biomechanics*, *19*(1), 3–12.

Xu, X., & McGorry, R. W. (2015). The validity of the first and second generation microsoft kinect™ for identifying joint center locations during static postures. *Applied ergonomics*, *49*, 47–54.

Yang, J. F., & Winter, D. (1984). Electromyographic amplitude normalization methods: Improving their sensitivity as diagnostic tools in gait analysis. *Archives of physical medicine and rehabilitation*, *65*(9), 517–521.

Yang, L., Zhang, L., Dong, H., Alelaiwi, A., & El Saddik, A. (2015). Evaluating and improving the depth accuracy of kinect for windows v2. *IEEE Sensors Journal*, *15*(8), 4275–4285.

Ye, M., Wang, X., Yang, R., Ren, L., & Pollefeys, M. (2011). Accurate 3d pose estimation from a single depth image. *2011 International Conference on Computer Vision*, 731–738.

Yu, C.-Y., Lo, Y.-H., & Chiou, W.-K. (2003). The 3d scanner for measuring body surface area: A simplified calculation in the chinese adult. *Applied ergonomics*, *34*(3), 273–278.

Yu, C.-Y., Lin, C.-H., & Yang, Y.-H. (2010). Human body surface area database and estimation formula. *Burns*, *36*(5), 616–629.

Zaidi, H., Fohanno, S., Taiar, R., & Polidori, G. (2010). Turbulence model choice for the calculation of drag forces when using the cfd method. *Journal of biomechanics*, *43*(3), 405–411.

Zdravkovich, M., Ashcroft, M., Chisholm, S., & Hicks, N. (1996). Effect of cyclist's posture and vicinity of another cyclist on aerodynamic drag. *The engineering of sport*, *1*, 21–28.

Zhang, X., Lee, S.-W., & Braido, P. (2004). Towards an integrated high-fidelity linkage representation of the human skeletal system based on surface measurement. *International Journal of Industrial Ergonomics*, *33*(3), 215–227.